DYNAMIC NATURE OF VOLCANIC PHENOMENA: 2001-02 ERUPTION PROCESSES AT ETNA AND STROMBOLI, ITALY

A DISSERTATION SUBMITTED TO THE GRADUATE DIVISION OF THE UNIVERSITY OF HAWAI'I IN PARTIAL FULFILLMINT OF THE REQUIREMENTS FOR THE DEGREE OF

DOCTOR OF PHILOSOPHY

IN

GEOLOGY AND GEOPHYSICS

AUGUST 2006

By
Nicole C. Lautze

Thesis Committee:

Bruce Houghton, Chairperson
Sarah Fagents
Michael Garcia
Andrew Harris
David Muenow

El trabajo más productive es el que sale de las manos de un hombre contento
-Victor Pauchet

Excava el pozo antes de que tengas sed.
-proverbio chino

We can't solve problems by using the same kind of thinking we used when we created them.
-Einstein

ACKNOWLEDGEMENTS

Many individuals have played a role in making this route towards the PhD an exciting and fulfilling experience-- both scientifically and personally.

First, I am grateful to Bruce for being an inspiring, energetic, and dedicated advisor. The breadth of knowledge and experience I have gained by working with Bruce is immeasurable, as is my gratitude.

Second, a big thank you to my committee. Thanks especially: to Sarah, for consistently positive encouragement (was huge); to Mike, for providing counsel on innumerable occasions, and patiently reviewing various fellowship applications (much appreciated); to Andy, for skillful guidance with the Etna study, and for many helpful suggestions related to the Stromboli work; and to Dr. Muenow, for consistently offering a calm voice of support.

I wholly appreciate the camaraderie and technical support offered by Matt Patrick, Julia Sable and Nancy Adams, and officemates: John Bailey and Jim Gharib (first), and Deb Eason and Eric Bergmanis (current). Their smiling patience with my many little questions spared many headaches and saved countless hours.

Thanks to *YOGA* and to the pool, and to yoga friends and pool friends (and other friends), which kept me healthy and balanced and happy over the past 5 years.

An extended thanks to Andy Harris, John Bailey, Maurizio Ripepe and John Dehn for including me during their work on Stromboli and Etna in 2001. This was my exhilarating first visit to these volcanoes and first up-close and personal with lava.

I continue to thank my undergraduate mentors—Jon Davidson and David Paige—for not letting me get distracted by the 'real world' and urging me on to grad school. Thanks to Jon for noticing both my affinity toward volcanoes and how easily I get cold; in sum, that Hawaii suits me.

How to thank a fantastic family? Thanks to Jon (brother) and Kimberly (sister) for valuing our genetic connection and for making me smile. Underlying everything thanks to mom and dad—for being a truly unconditional pillar of support since day one... and for making me smile too.

I thank the National Weather Service and the National Science Foundation for providing fellowships which funded me for the extent of this dissertation. I also acknowledge the University of Hawai'i's Graduate Division and Graduate Student Organization, whose travel grants facilitated incredible and culturally-enriching experiences, and the establishment of connections that carry into the future...

The work was supported by NSF grant EAR-0207734.

ABSTRACT

This dissertation identifies and explains fluctuations in eruption at the persistently active basaltic volcanoes of Etna (Sicily, Italy) in 2001 and Stromboli (Aeolian Islands, Italy) in 2002. In the Etna chapter, ~72 hours of ground-based gas puff frequency and lava flow velocity data are considered alongside ~8 months of satellite-based effusion rate data. The data suggest oscillations in the shallow supply of magma on timescales of both hours and months.

The Stromboli chapters use microtextural analysis of lapilli samples to identify the presence of three physically distinct magma types (low density, LD; transitional textures, TT; high density, HD) with contrasting vesicle textures. Quantitative vesicularity data indicate that the textures are linked via an ongoing, time-dependant evolution involving increasing degrees of coalescence and outgassing from LD to TT to HD magma. Fine-scale mingling of end-member magma types implies dynamic shallow processes that are linked with the passage of gas slugs through the shallow conduit during Strombolian explosions. New LD magma rises with gas slugs; mingling with HD occurs during and immediately following slug ascent.

A similar textural diversity is documented in six samples from a 2-hour sequence of similar explosions and one explosion ~24 hours later. This indicates that Stromboli's shallow magma is physically complex at the instant of a single explosion, and that, with minor variation, such physical complexity is likely to persist through sequences of similar explosions (on timescales of hours to days). In comparison, contrasts in the textural properties of ejecta from three periods of more markedly contrasting explosion intensity (May, September/October, December) suggests a feedback between changing rheology of shallow magma and explosion processes (over periods of weeks to months).

This thesis uses a variety of methods to highlight and explain changes in the pattern of observed eruption. Ground- and satellite- based thermal remote sensing data suggest oscillations in the shallow supply rate of magma at Etna in 2001. Microtextural analyses of ejecta from Stromboli in 2002 imply a link between the physical properties of shallow magma and explosion style. This dissertation therefore highlights fine-scale shallow processes that contribute to the dynamic nature of volcanic eruptions.

TABLE OF CONTENTS

LIST OF TABLES

LIST OF FIGURES

Chapter 1: Introduction

Chapter 2: Pulsed lava effusion at Mount Etna during 2001

Chapter 3: Physical mingling of magma and complex eruption dynamics in the shallow conduit at Stromboli volcano, Italy

Chapter 4: Linking explosion intensity and magma rheology during 2002 at Stromboli volcano

Chapter 5: Single explosions at Stromboli in 2002: use of lapilli microtextures to map a Strombolian fragmentation zone

CHAPTER 1. Introduction

1.1 Overview

This dissertation seeks to identify and explain some characteristics of relatively mild, effusive and explosive styles of eruptive activity typically observed at basaltic volcanoes. In Chapter 2, thermal remote sensing data are used to recognize short-term oscillations in the rate of lava effusion and degassing during persistent effusive activity at Mount Etna volcano (Italy) in 2001. Such oscillations are linked to probable variations in the supply rate of magma to Etna's summit area. Chapters 3 through 5 focus on explaining variations in the typical pattern of mildly explosive (Strombolian) activity at Stromboli volcano (Italy) during 2002. These studies use the vesicularity textures of ejecta to identify three texturally distinct magmas that are linked via contrasting residence times in the shallow conduit. Data suggest the existence of a rheological feedback between the physical characteristics of shallow magma and eruption vigor at Stromboli during three periods in 2002.

As a preface, I note that the timing of my work on Etna and Stromboli was fortuitous, in that it occurred during a period of heightened eruptive activity at both volcanoes. Etna experienced two significant flank eruptions during July - August 2001 (Behncke and Neri, 2003; Calvari and Pinkerton 2004; Taddeucci et al., 2004; chapter 2) and from October 2002 to January 2003 (Neri et al., 2005; Monaco et al., 2005). Stromboli exhibited an unusually wide range of activity during December 2002 to 2003 (see citations below). This included an extended effusive period (Calvari et al., 2005; Ripepe et al., 2005a), a volcanogenic tsunami (Bonaccorso et al., 2003; Tinti et al., 2003), and a major paroxysm (Calvari et al., 2006; Rosi et al., 2006). Though these events resulted in costly damage, minor injuries, and major inconvenience, no serious injuries or deaths occurred (Calvari et al., 2006). The resultant heightened state of affairs in recent years at both

volcanoes-- manifested as direct involvement by Italy's Civile Protezione, and the major expansion of monitoring efforts by the Instituto Nazionale di Geofisica e Volcanologia (INGV; Ripepe et al., 2005a; Calvari et al., 2005, 2006; Rosi et al., 2006)-- contributed an additional element of timeliness to my work.

1.2 Etna and Stromboli volcanoes

1.2.1 Tectonic setting and magma composition

Stromboli and Etna are spaced ~120 km apart within a tectonic setting dominated by weak convergence between the African and European plates, and secondarily by eastward migration of the Tyrrhenian-Appenines subduction system (Figure 1.1; Schiano et al., 2004). Predominantly calc-alkaline magma is erupted in the Aeolian Islands, whereas Na-alkaline magma dominates at Etna (Schiano et al., 2004). This variety of magma compositions implies the existence of a fine-scale and complex geodynamical setting between the two volcanoes (e.g. localized mantle evolution and/or plate dynamics; Schiano et al., 2004). The Aeolian Islands are thought to represent typical examples of island arc magmatism related to subduction of the oceanic Ionian slab, while the Na-alkaline affinity of Etna is inferred to be inherited from intraplate mantle sources of a controversial nature (Schiano et al., 2004; Monaco et al., 2005). Various interpretations regarding Etna include: extensional tectonics, mantle diapirism/hot spot, or rollback motion of the Ionian slab (Schiano et al., 2004, and references therein; Monaco et al., 2005 and references therein). See Figure 1.1 for further description of this complex setting.

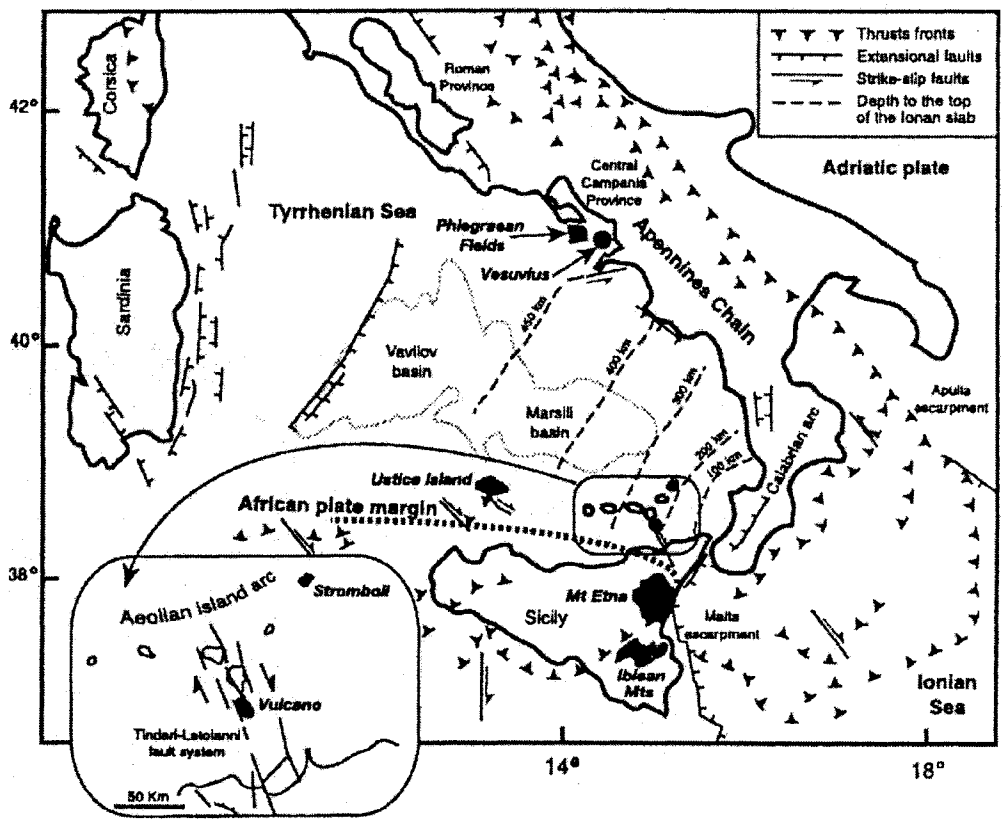

Figure 1.1 Schematic tectonic map of southern Italy. Note the existence of a compressional regime between the African plate (which includes Etna) and European plates. This is complicated by subduction of the Ionian microplate beneath the Tyrrhenian microplate, which occurs between the Apulia escarpment and the Malta escarpment. Note also, thinning of the Ionian microplate that occures along a NE/SW trend from south of Vesuvius toward Etna. Finally, note the presence of a NNW/SSE trending strike-slip fault system that transects the Aeolian Islands (see inset). Figure 1 of Shiano et al. (2004).

1.2.2 Mount Etna

Mount Etna (Sicily, Italy; Figure 1.1) is a composite volcano whose base measures ~60 x 40 km and whose summit lies at 3320 m above sea level (Coltelli et al., 2000; Chester et al., 1985). Etna is the largest and most productive volcano in Europe (Coltelli et al., 2000), with a record of more or less continuous eruption since ~1500 B.C. (Chester et al., 1985). Eruptive activity over the last 180 ka is characterized by alternating effusive and explosive emission of Na-alkaline magma (Gillot et al., 1994). Subaerial activity at Etna has migrated among four different eruptive centers, which have been grouped into four major stratigraphic units (Gillot et al., 1994): Ancient Alkaline Centers (180-100 ka), Trifoglietto (80-60 ka), Ancient Mongibello (35-14 ka) and Recent Mongibello (14 ka to Present). While lava effusion has volumetrically dominated throughout this time, Etna's explosive history over the past 100 ka includes a spectrum from low intensity (fire fountaining and Strombolian activity) to subplinian (Coltelli et al., 2000) to a single identified Plinian eruption in 122 B.C. (Coltelli et al., 1998).

Two patterns of effusive activity are exhibited at Etna (Wadge et al., 1975; Guest and Murray, 1979; Romano and Sturiale, 1982; Chester et al, 1985; Harris et al., 2000). *Persistent activity* is localized at the summit craters (see Figure 2.1) and is characterized by low effusion rate (~0.1-0.5 m^3s^{-1}; Guest and Murray, 1979) with steady output (Harris et al., 2000). *Flank eruptions* occur generally along the volcano's rift systems and are characterized by higher effusion rates (~10 m^3; Guest and Murray, 1979). Harris et al. (2000) demonstrate that such events show an effusion rate trend of rapid increase to a peak, followed by slower decline.

In recent years, public awareness regarding eruption hazard at Etna has increased, largely due to expanded media coverage resulting from monitoring and outreach efforts by the INGV (Alparone et al., 2004; Coltelli, 2006). The currently dominant problems posed by eruption at

Etna involve air travel, long-propagating lava flows, and inconvenient and costly ash cleanup (Branca and del Carlo, 2005; Coltelli, 2006).

1.2.3 Stromboli volcano

Stromboli is the northernmost island of the Aeolian Island arc, a chain of seven islands and many seamounts ~30 km north of Sicily in the Tyrrhenian Sea (Figure 1.2; Rosi, 1980; Barberi et al., 1993; Falsaperla et al., 1999). Subaerially, the island comprises a conical composite volcano with a diameter ranging from 2.4 to 5 km (Rosi et al., 1980; Keller et al., 1993; see Figure 5.1). The entire edifice rises from a depth of ~2000 m below sea level (b.s.l.) to an elevation of 924 m a.s.l (Barberi et al., 1993; Hornig-Kjarsgaard et al., 1993). The oldest subaerial rocks on the island are ~100 ka, though the Strombolicchio neck, located 1.7 km NE of Stromboli Island and belonging to the same submarine edifice is 204 +/- 25 ka (Figure 1.2; Hornig-Kjarsgaard et al., 1993; Gillot and Keller, 1993).

Seven main periods of effusive and explosive activity characterize the magmatic history of the subaerial portion of Stromboli's edifice (Rosi, 1980; Hornig-Kjarsgaard et al., 1993). The transition from one period to another is usually associated with a change in magma composition (Francalanci et al, 1993; Hornig-Kjarsgaard et al., 1993). The seven recognized periods, their duration, and the dominant magma composition are: Paleostromboli I (61 – 100 ka; high-K calc-alkaline basalt), Paleostromboli II (55 – 64 ka; calc-alkaline basalt), Paleostromboli III (35 – 55 ka; high-K calc-alkaline basalt), Scari (~35 ka; transitional shoshonite), Vancori (13 – 25 ka; shoshonite), Neostromboli (6 – 13 ka; shoshonite), and Recent (Present – 6 ka; shoshonite, high-K, calc-alkaline basalt; Rosi et al., 1980; Gillot and Keller, 1993; Keller et al., 1993; Francalanci et al., 1993; Hornig-Kjarsgaard et al., 1993). Eight edifice collapses of variable nature (crater,

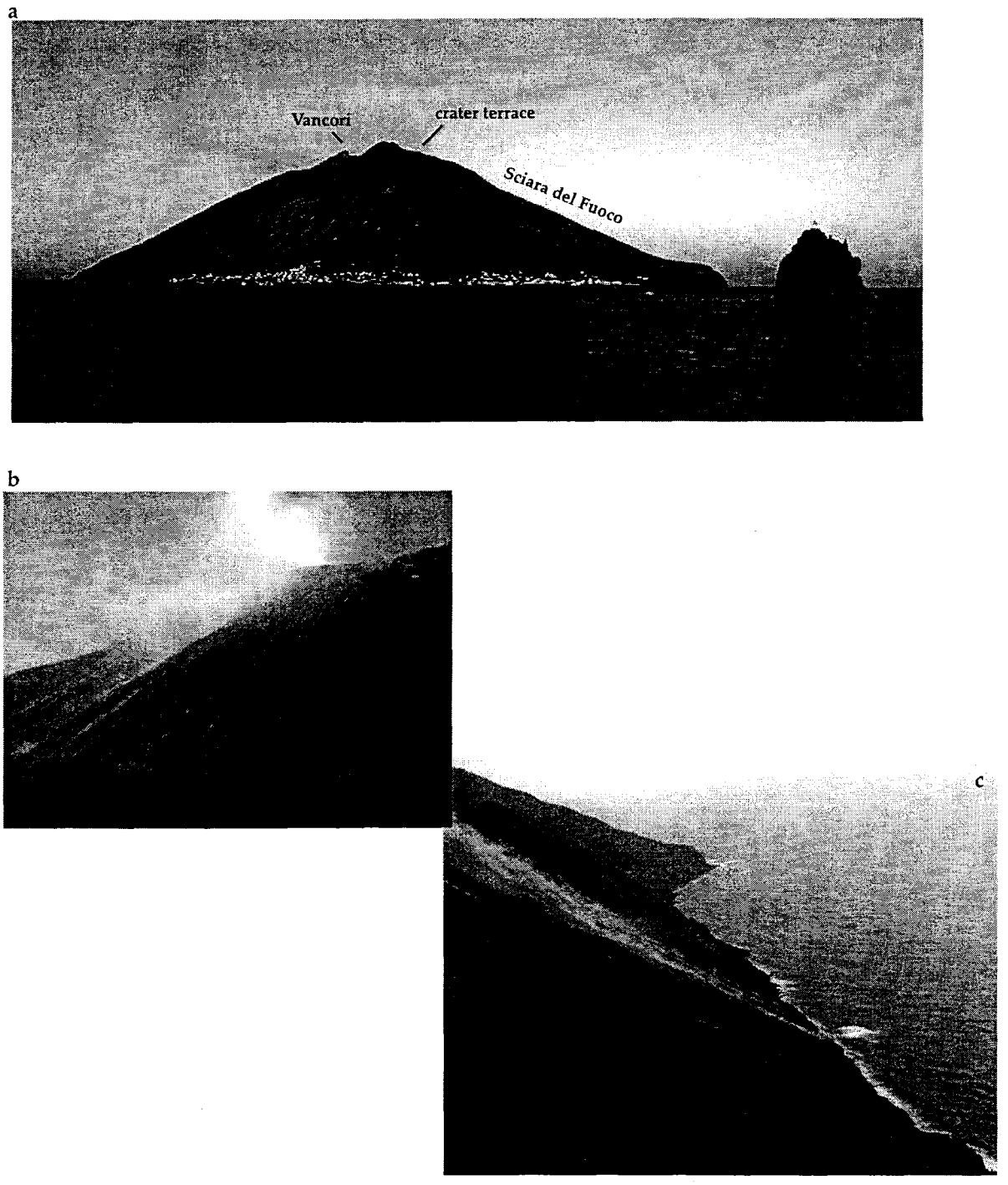

Figure 1.2 Photos of Stromboli volcano. *a*: Stromboli volcano from the NE. View of Stromboli village (island foreground) and Strombolicchio (small island on right of image). *b:* Sciara del Fuoco from the west. *c:* Sciara del Fuoco from the NE. Note the cloud of dust and splash of water resulting from ejecta rolling down the Sciara. *a: taken by J. Alean; b: taken by B. Houghton in Sept 2003; c: taken by N. Lautze in June 2004.*

caldera, flank, and sector) have alternated with these constructional phases (Kokelaar and Romagnoli, 1994; Tibaldi, 2003).

The NW flank of Stromboli is dominated by a collapse scar (the Sciara del Fuoco, Figure 1.2), which resulted from one or more sector collapses (Kokelaar and Romagnoli, 1994; Bertagnini and Landi, 1996; Tibaldi, 2003). The active crater terrace lies at 800 m a.s.l., and typical activity is sufficiently mild that ejecta falls in the vicinity of the craters or is efficiently funneled down the Sciara and into the sea (Figure 1.2). Two small villages exist on the island (see figure 5.1). Stromboli village is home to ~400 permanent residents, and at times up to thousands of tourists (Barberi et al., 1993). Ginostra is home to ~40 people and sits on the southwest corner of the island. Both towns and especially Ginostra is at risk of fallout from Stromboli's paroxysmal events, such as occurred in 1930 and 2003 (Barberi et al., 1993; Calvari et al., 2006; Rosi et al., 2006).

1.5 Dissertation outline

Chapter 2 of the dissertation uses thermal remote sensing data to identify minutes- to months-long pulsations in effusion rate and degassing during January to July 2001 at Mt. Etna. Satellite-based data reveal four 23-to-57 day pulses that occur along an increasing trend leading into the 2001 flank eruption. Three days of field-based data for effusion rate and degassing during persistent activity in May 2001 show hours-and-minutes long oscillations. There is some evidence of positive correlation among these shorter-term data, which may indicate changes in the supply rate of magma to Etna's shallow system. This chapter has been modified slightly from the study as published in 2004 in the *Journal of Volcanology and Geothermal Research* (vol. 137).

Chapter 3 provides a microtextural description of Strombolian ejecta collected in September 2002. Within a sample of ejecta from multiple explosions at Stromboli over a ~24 hour period during September 2002, two texturally distinct magmas, bubble-rich and bubble-poor, are identified and described. The sharp and fine-scale occurrence of mingling between the end member magmas gives insight into shallow conduit processes occurring at Stromboli. This work was published in *Geology* in May 2005 (vol. 33, no. 5).

Chapter 4 analyzes the textures in ejecta from Stromboli during three periods in 2002 (May, September/October, December), each characterized by different styles and intensities of activity. On the basis of variability in the ejecta textures, it is inferred that the shallow magma had different degassing histories and rheologies. Calculations regarding the viscosity of the identified magmas suggest a feedback link to the power of explosion. This chapter is in press in *Bulletin of Volcanology*.

Chapter 5 examines textures of lapilli from single explosions at Stromboli, and explores the diversity of the fragmentation zone during a single Strombolian explosion. This study documents that the fragmentation zone at the point of a single explosion is texturally diverse, and identifies a sensitive correlation between the abundance of bubble-rich magma ejected and the power of explosions over ~24 hours.

Chapter 6 links the main concepts of the dissertation and states some ideas regarding future directions. Where warranted, an extended contributions and acknowledgments section has been added to each chapter (beyond what has been included in published or submitted manuscripts).

CHAPTER 2. Pulsed lava effusion at Mount Etna during 2001

Abstract. Effusion rate and degassing data collected at Mt. Etna volcano (Italy) in 2001 show variations occurring on time scales of hours to months. We use both long- and short-term data sets spanning January to August to identify these variations. The long data sets comprise a satellite- and ground-based time series of effusion rates, the latter include field-based effusion rate and degassing data collected from May 29 to 31.

The satellite-derived effusion rates for January through August reveal 4 volumetric pulses that are characterized by increasing mean effusion rate values, and lead up to the 2001 flank eruption. Peak effusion rates during these 23 to 57 day pulses were 1.2 m^3s^{-1} in Pulse 1 (1 January to 4 March), 1.1 m^3s^{-1} in Pulse 2 (5 March to 21 April), 4.2 m^3s^{-1} in Pulse 3 (24 April to 18 June), 8.8 m^3s^{-1} in Pulse 4 (23 June to 16 July), and 22.2 m^3s^{-1} during the flank eruption (17 July to 9 August). Rank order analysis of the satellite data shows that effusion rate values during the 2001 flank eruption define a statistically different trend than Etna's persistent activity from January 1 to July 17. Data prior to the flank eruption obey a power law relationship that may define an effusion rate threshold of ~3-5 m^3 s^{-1} for Etna's typical persistent activity.

Our short-term data coincide with the satellite-derived peak effusion period of Pulse 3. Degassing (at-vent puff frequency) shows a general increase from May 29 to 31, with hour-long variations in both puff frequency and lava flow velocity (effusion rate). We identify five 3 to 14 hour degassing periods that contain 26 shorter (19 to 126 minute-long) oscillations. This variation shows some positive correlation with effusion rate measurements during the same time period. If a relationship between puff frequency and effusion rate is valid, we propose that their short-term variation is the result of changes in the supply rate of magma to the near-vent conduit system. Therefore, these short-term data provide some evidence that the clear weeks- to months-

long variation in Etna's effusive activity (January to August, 2001) was overprinted by a minutes- to hour- scale oscillation in shallow supply.

2.1 Introduction

That mass flux rates can vary over timescales of days to months during episodic, effusive basaltic eruptions is well known. Wadge (1981) showed that on such time scales, mass fluxes during a basaltic eruption often reach a maximum value after a short period of waxing flow. The release of elastic strain then causes the mass eruption rate to fall more slowly than it rose. However during persistent basaltic eruptions, magma supply and mass flux rates are generally assumed to be broadly constant. Allard et al. (1994) estimated that persistent degassing and mild explosive and effusive activity at Stromboli (Italy) has been maintained by a mass flux of 0.01-0.02 $km^3\ yr^{-1}$ for over ~2000 years. Harris et al. (2000) identified a similar, generally steady effusion rate characterizing persistent summit activity at Mount Etna (Italy) from 1980-1995. There is mounting evidence, however, that this activity shows considerable short-term variation (Swanson et al., 1979; Tilling et al., 1987)

Recent experiments on Stromboli volcano (Italy) indicate that mass flux to persistently active basaltic systems may proceed in a pulsatory manner. At Stromboli, Ripepe et al. (2002) recorded positively correlated variations in degassing and explosive activity, with 5-40 minute phases characterized by either vigorous or weak degassing. Ripepe et al. (2002) suggest that this is consistent with variations in the rate at which the shallow system is supplied by gas-rich magma. At Erta Ale (Ethiopia), however, cyclic variations in the surface activity of a basaltic lava lake (~1-2 hours) can be accommodated within a model in which supply is constant, and surface variation is caused by convective instabilities within the lake itself (Harris et al., 2002).

An ideal way to identify variations in mass flux at persistently active volcanic systems is to make detailed effusion rate measurements over hours to months. Here we achieve this through an examination of the persistent effusive activity at Etna that preceded the flank eruption during July to August 2001. In an effort to characterize the time-varying nature of persistent basaltic activity, this paper presents: i) a satellite- and ground- based effusion rate time series at Etna from January through August 2001, and ii) effusion rate and degassing data collected at Etna during a field experiment May 29-31, 2001.

2.2 Etna's activity during 2001

This section presents a qualitative description of Etna's activity in 2001. It is intended as a narrative leading into the quantitative description of pulsatory effusive activity that ensues. We note that this description includes explosive activity, which is not incorporated in the later data.

The current structure of Etna volcano consists of four summit craters and fissure systems that trend northeast and south (Figure 2.1). Persistent activity from January to July 17 was concentrated at Southeast Crater (SEC). Through April, activity was primarily effusive, and characterized by low, but generally increasing, effusion rates of 1 to 3 m^3s^{-1}. Strombolian activity commenced during the first half of May, and was accompanied by heightened effusion rates (up to a maximum of 12 $m^3 s^{-1}$), which persisted through the second half of June. Episodic fire fountaining events in May, June and July were followed by a flank eruption during July 17 to August 9. This was followed by a hiatus in activity that lasted until March 2002. We review the activity in more detail below.

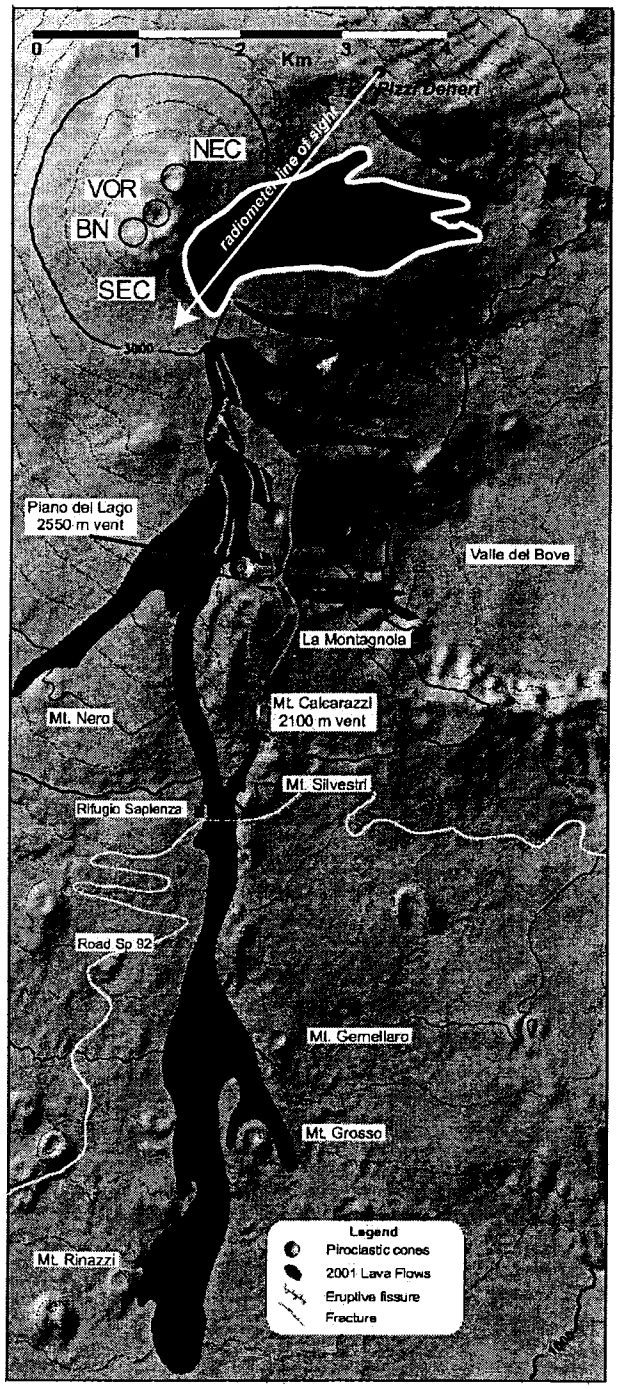

Figure 2.1 Map of Etna showing the location of the main volcanic centers [Northeast crater (NEC), Voragine (VOR), Bocca Nuova (BN), Southeast crater (SEC)] and flows (in gray) associated with the 2001 flank eruption. Also note the approximate location of the flow field active during our field experiment May 29-31 to NE of SEC (black with white outline; identified using a Landsat ETM+ image for July 13, 2001), and the location of Pizzi Deneri with the line of sight from the puff monitoring IR-thermometer to the SEC as indicated (figure modified from Eos article by Calvari et al., 2001).

2.2.1 Last months of 2000 – April, 2001

Activity at Etna during late 2000 and the initial months of 2001 consisted of episodic Strombolian and ash explosions from Bocca Nuova (BN) and SEC, and lava emission from the N flank of SEC. BN exhibited intermittent, low-intensity emission of gas and lithic ash at a consistently increasing frequency through January. Strombolian activity, juvenile ash emissions, and strong degassing occurred at BN throughout February, increasing slightly through March and April.

Strombolian activity at SEC commenced on January 15, peaked three days later, and stopped by January 21. Lava emission from a fissure at an elevation of 3080 m on the N flank of SEC began January 21 and proceeded discontinuously through late April. Effusive activity from additional vents at 3100 m and 3150 m on the N flank of SEC commenced during early February. The 3100 m flow continued for several days, and the 3150 m flow persisted until the end of February. Effusive activity escalated during March and April, with an increase in effusion rate at the 3080 m vent, and the opening of an effusive vent on SEC's east flank on April 8 (Andronico et al., in prep.). Still, effusion rate throughout the period was generally less than 1 $m^3 s^{-1}$, and increased to 2-3 $m^3 s^{-1}$ only on April 27 (Andronico et al., in prep.). Degassing at SEC was observed to increase during the last days of April.

2.2.2 May – July 17, 2001

Between May and mid-July, variable but heightened effusive activity at SEC was accompanied by an increase in the frequency of explosive events and the onset of fire fountain episodes. Activity at BN was inconsequential.

In the first days of May, weak spattering from the north fissure of SEC formed hornitos around the vents, and amplified effusion rates peaked at 10-12 $m^3 s^{-1}$ on May 3 (Andronico et al., in prep.). Strombolian activity from the summit of SEC (not witnessed since January 21) resumed

on May 7, and the first fire fountain event of the year occurred May 9. A vent at 3150 m opened with an effusion rate of 2.5-4.5 $m^3 s^{-1}$ on May 18 (Andronico et al., in prep.). Heightened activity during the final days of May was marked by the occurrence of Strombolian activity also at North-East Crater (NEC), a sharp increase in Strombolian activity at SEC on May 28, and effusion rates from the N base of SEC increasing to 6-8 $m^3 s^{-1}$ during May 29-30 (Andronico et al., in prep.).

Fourteen paroxysmal episodes occurred between June 1 and July 17, mostly from a vent on the N flank of SEC. During such events, continuous fire fountaining persisted for up to 1 hour, and was accompanied by degassing at all of the summit craters and lava effusion from SEC's N flank fissure. The fire fountaining generally fed short-lived (hour- to day- long) lava flows. The episodes were preceded by a 5-11 hour increase in Strombolian and effusive activity.

On July 13, the final paroxysm of this period occurred with a seismic swarm and the opening of fissures along SEC's S flank.

2.2.3 2001 Flank Eruption (July 17- August 9)

A flank eruption began at 07:00 (local time) on July 17, at a fissure at 2950 m extending south from the base of the SEC. Vents farther to the south at 2700 m and 2100 m opened during July 17-18, and a fourth vent was established at 2550 m during July 19. Minor vents opened to the northeast of the SEC during July 20-23, but by July 19 and for the majority of the eruption, activity had become concentrated along a ~7 km long, ~N-S trending field of fissures on the south flank (Figure 2.1). The dominant effusive centers at 2700 m and 2100 m were consistently active throughout the eruption. Flows from the 2100 m fissure extended ~3.5 km southward to the 1350 m contour by July 19, causing authorities to declare a state of emergency. This vent ultimately produced the longest (6.5 km), and volumetrically largest (18-24 x 10^6 m^3 bulk volume) lava flow

of the eruption. On July 22, fast moving flows from the 2700 m fissure destroyed several ski lifts and approached the tourist complex at the Refugio Sapienza. Flows from 2950 m and 2550 m were shorter, extending a maximum distance of 2-3 km by the end of July.

Major explosive activity was focused at the 2550 m vent. Phreatomagmatic eruptions produced thick ash clouds from its opening on July 19 through July 24. Between July 24 and 25, there was a shift to fire fountaining activity, which rapidly formed the main cone of the eruption. In the last days of July there was a return to ash-dominant emission. The effusion rate at the 2100 m fissure began to decline by August 1, and was followed by a similar decrease at the 2900 m and 2700 m vents within the following days. Activity at 2550 m ceased on August 6, and the last emission of lava was observed at the 2100 m vent on August 9.

The 24 day-long flank eruption emplaced a ~4.7 km^2 lava flow field on Etna's south flank (Figure 2.1), with a preliminary estimated bulk volume of 48 x 10^6 m^3 and a time-averaged lava effusion rate of 24 m^3 s^{-1} (Calvari et al., 2001). Corrected for a vesicularity of 22±12 % (after Harris et al., 2000), this gives a DRE volume of 32-43 x 10^6 m^3 for effusive activity, and a mean lava effusion rate of 15-21 m^3s^{-1}.

2.2.4 Post-2001 Flank Eruption

The months following the 2001 flank eruption through March 2002 were strikingly quiet and marked the longest non-eruptive interval at Etna since 1995. No fresh magma appeared in the summit craters and activity was typified solely by fumarolic activity and occasional collapse at the four summit craters.

Between March and September 2002, sporadic Strombolian activity resumed at NEC and BN. Etna then returned to a state of calm from September 22 through October 26. A seismic swarm that began late in the evening of October 26, 2002 forewarned the onset of a new flank

eruption on October 27. This eruption continued until January 28, 2003. It exhibited a number of phases distinguished by variations in eruption style, and involved activity at both Etna's south and northeast fissure systems.

2.3 Data and methods

Our data set consists of: i) lava effusion rate values for January-August 2001 that are derived from satellite and ground-based methods, and ii) effusion rate and degassing data obtained during a field experiment May 29-31, 2001. We use the latter data to track variation on timescales of minutes to days, and as a check on day- to month-long trends apparent in the longer time series.

2.3.1 Long-term effusion rates, January – August, 2001

2.3.1.1 Satellite-based methods

Thermal data from the Advanced Very High Resolution Radiometer (AVHRR) flown aboard NOAA satellite series were used to obtain DRE effusion rate estimates following methodologies given in Harris et al. (1997a, 1997b, 2000). AVHRR provides up to 4 images per day of Etna, though images with cloud cover are unusable (Harris et al., 1997b). Thermal data were received at the University of Dundee and processed in real time at the Plymouth Marine Laboratory (U.K.). Calibrated data were transferred from Plymouth to the Hawaii Institute of Geophysics and Planetology, where hot spot products were posted on the web (http://hotspot.higp.hawaii.edu/etna/ and http://goes.higp.hawaii.edu/cgi-bin/imageview). During the 2001 flank eruption, this system enabled scientists at the Istituto Nazionale di Geofisica e Vulcanologia - Sezione di Catania (INGV-CT) to view AVHRR-derived effusion rate values within 6 hours of data reception. Together with ground-based measurements collected by

INGV-CT, these data were used during the eruption for hazard assessment and civil protection purposes.

For this study, all AVHRR images obtained for the period January 1 to August 9, 2001 were manually scrutinized for image quality, cloud cover, and the presence or absence of a thermal anomaly in Etna's summit region. A total of 207 cloud-free images with anomalous thermal radiance due to volcanic activity were identified.

Effusion rate values for each image were obtained by summing estimates of the radiative, convective, and conductive heat loss for each anomalous pixel. Calculation of these heat losses requires the area (A_{lava}) and surface temperature (T_{lava}) of the lava in each pixel (Harris et al., 1997a; 1997b; 2000). When possible, these values were attained using the dual-band method of Dozier (1981) and Rothery et al. (1988). The dual-band method yields the fraction of a pixel occupied by hot lava (p) and the lava surface temperature (T_{lava}) by using two bands of AVHRR thermal data (R_3 and R_4) that are each corrected for surface emissivity, atmospheric transmissivity, upwelling, and solar reflection, and the following equations:

$$R_3 = p\, L_3(T_{lava}) + (1-p)\, L_3(T_b) \quad (1a)$$

$$R_4 = p\, L_4(T_{lava}) + (1-p)\, L_4(T_b) \quad (1b)$$

L_x is the Planck function for a blackbody at wavelength x and temperature T, and T_b is the approximate pixel background temperature. The value of T_b was obtained from the nearest, non-anomalous pixel. Equations 1a and 1b can then be solved for p and T_{lava}. Multiplying p by the AVHRR pixel area of 10^6 m^2 yields A_{lava}.

In some cases, AVHRR band 3 (R_3) was saturated, and therefore the single-band method described in Harris et al. (1997a) and Harris et al. (1997b) was used. In this method, assuming a range for T_{lava} allows p to be calculated from Equation 1b. Effusion rate (ER) is now calculated as

a function of lava area according to the equation $ER = x A_{lava}$ (in which x is a thermally-defined constant; Wright et al. 2001).

AVHRR band 3 saturation occurs at a pixel-integrated temperature of ~50 ºC (Harris et al., 1996). Assuming a lava surface temperature of 500 – 1000 ºC against a background of 0 – 25 ºC, R_3 will reach saturation when the lava area reaches $10^2 - 10^3$ m^2 ($p = 10^{-4} - 10^{-3}$). AVHRR band 4, on the other hand, will not saturate until the lava area reaches 1-4 x 10^4 m^2 ($p = 10^{-2} - 4 \times 10^{-2}$). No pixels saturated in band 3 were observed during January through April, which is consistent with the low level of effusive activity during this time. From May 1 through August 9 however, band 3 was saturated in all cloud-free images and thus the single band method was applied. The effusion rate values calculated from AVHRR images are presented as 'satellite-derived' in Figure 2.2.

2.3.1.2 Ground-based methods

Ground-based estimates were made in one of two ways. Prior to the 2001 flank eruption values were obtained following the methodology of Calvari et al. (2002). This approach uses measurements of a lava channel width (w), depth (d), and maximum velocity of flow in the channel (V_{max}) (and assumes a semi-circular channel geometry) to obtain instantaneous bulk volume effusion rates (ER) from $ER = 0.67 V_{max} w d$. During the 2001 flank eruption, values were obtained using the method given in Calvari et al. (1994), wherein the area (A) and thickness (d) of flow units emplaced during a known period of time (t) are used to calculate bulk mean effusion rates (ER) from $ER = A d / t$. We corrected all values for vesicularity of 22±12 % to convert from bulk to DRE values (Harris et al., 2000). These data are presented as 'ground-based' in Figure 2.2.

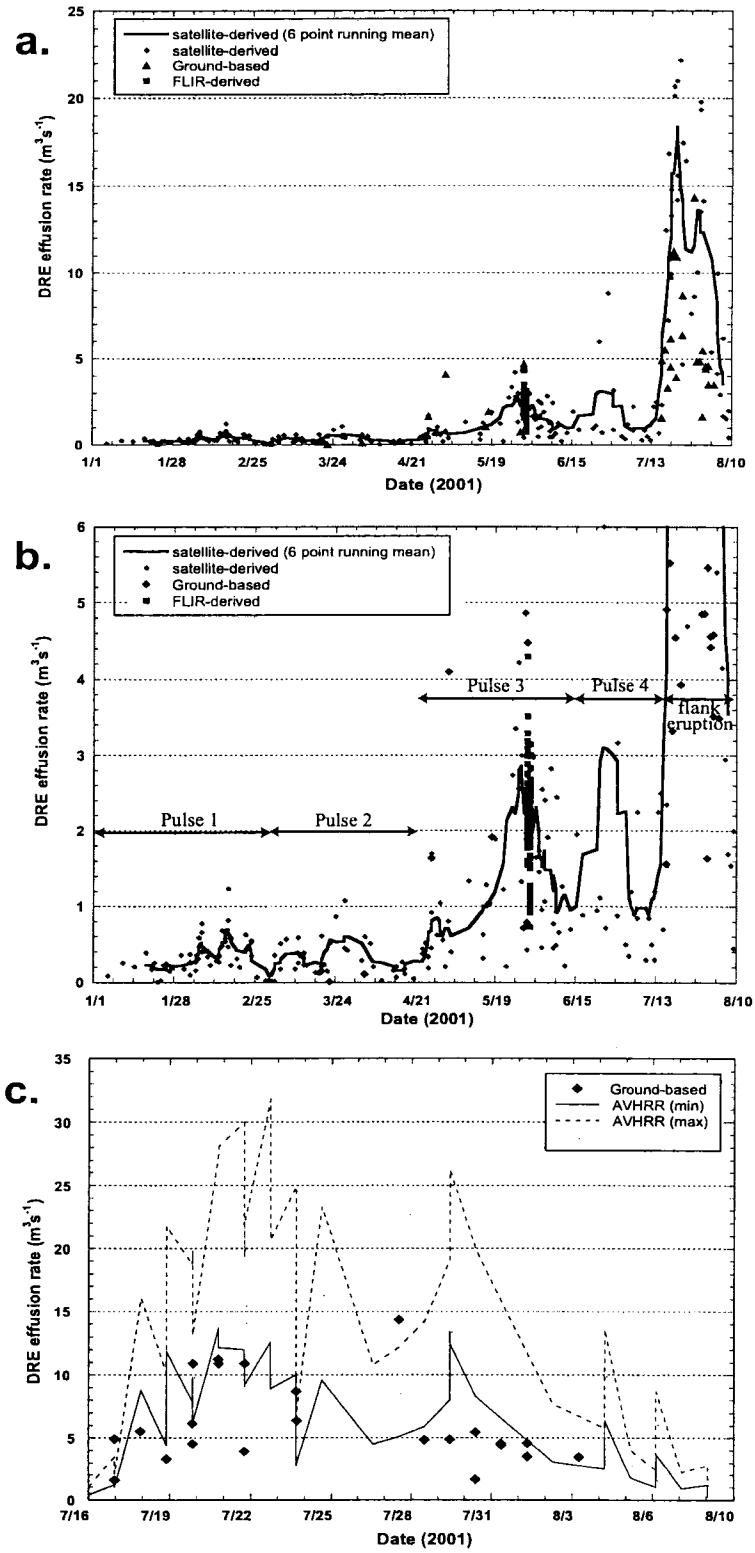

Figure 2.2 Complete effusion rate database, including satellite-derived, ground-based, and FLIR-derived data: (a) entire range of effusion rate values for January 1 to August 9, 2001 (b) detail of the effusion rate range from 0 to 6 m^3s^{-1} for January 1 to August 9, 2001 with arrows indicating the 4 identified effusion rate pulses preceding the 2001 flank eruption (c) detail of the 2001 flank eruption.

2.3.2 Short-term effusion rates and degassing, May 29-31, 2001

2.3.2.1 Effusion rate calculations from channel-fed activity

Lava effusion from a vent on the NE flank of SEC fed a compound flow field throughout the duration of our field experiment (see Figure 2.1 for approximate location). A well-established master channel ~1.5 m deep and ~3 m wide fed multiple 'a'a flows that extended no more than 2 km from the vent and contributed to a ~1 km wide flow field extending northwards from the SEC. Flow in the channel was not stable, with 10 to 30 minute surges in effusion breaking 1 to 3 hour periods of steady-to-waning flow. During each surge, an increase in effusion rate developed over some minutes, causing channel overfill and the formation of short-lived flow units that extended a few tens of meters.

To track changes in the flow velocity in the master channel, a Forward Looking Infra-Red (FLIR) thermal imager was aimed onto the channel surface ~250 m down-flow from the vent. The FLIR collected images at a rate of 1 image every 10 seconds from approximately 14:45 to 18:30 on May 30 and 12:00 to 13:45 and 15:00 to 17:00 on May 31. We obtained flow velocities by tracking the transit of pieces of crust in at least 3 consecutive images. Given these channel dimensions and measured flow velocities, bulk effusion rate values were calculated following the method of Calvari et al. (2002), and DRE values were attained by correcting for a vesicularity of 22%. These data are presented as 'FLIR-derived' in Figure 2.2.

2.3.2.2 Degassing from SEC, May 29-31, 2001

During our field experiment, persistent degassing from the summit of SEC occurred as a discrete burst, or puff, every few seconds (Figure 2.3). The model of Ripepe et al. (2002) explains puffs as caused by the ascent of bubble bands in the conduit. Each band generates a pulse in gas emission, or puff, upon reaching the free lava surface in the conduit. Ripepe et al. (2002) infer

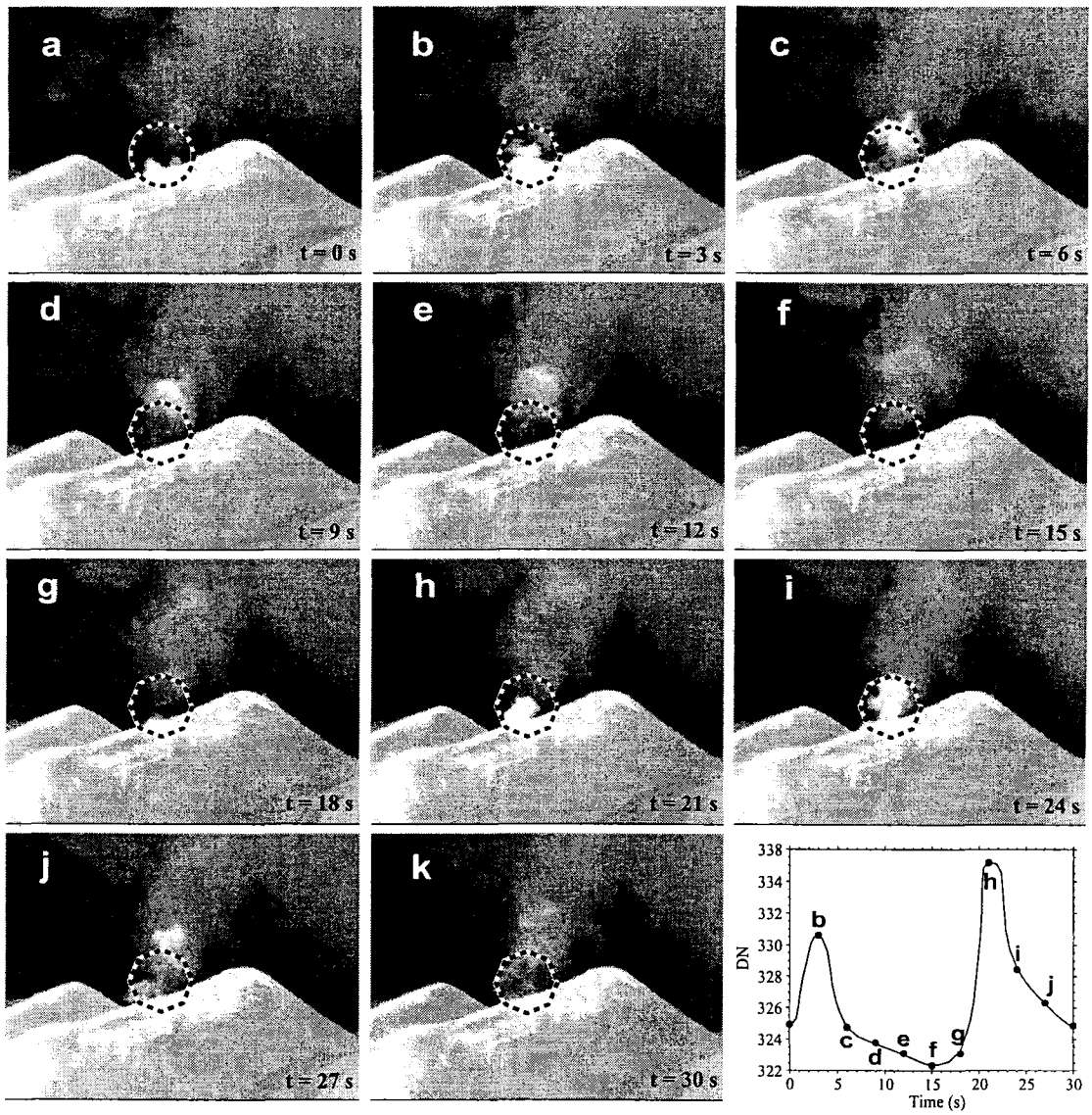

Figure 2.3 Time series of FLIR thermal images that shows two gas puffs rising from SEC. The dashed circle represents the approximate field of view of the thermal infrared radiometer. The inset graph shows a schematic time series of IR-thermometer data (DN = digital number). Letters in individual images correspond to points shown on inset.

that periods of rapid degassing are associated with a high puff frequency (high frequency of bubble band rise), and periods of low degassing are associated with a low puff frequency.

Following the approach of Ripepe et al. (2002), we pointed an Omega OS 554, 8-14 μm, thermal infrared (IR) thermometer at the SEC summit to monitor the frequency and relative temperature (amplitude) of the puffing. The radiometer was placed at Pizzi Deneri, a distance of ~2.5 km from the SEC summit (Figure 2.1), and targeted using the thermal signal of puffs (i.e. the summit was scanned until a good, oscillating signal was obtained). Given this distance and the one degree field of the sensor, the recorded thermal radiance covered a ~45 m circular field of view (FOV) that was centered on the plume, but included portions of the cone and sky (Figure 2.3). Excellent visibility and low wind speed throughout our data collection period made for optimal observation conditions.

With the integrated thermal radiance converted to temperature, gas puffs are expressed as oscillations in the temperature record (Figure 2.4). Data were collected continuously at a 18 x 10^{-3} s sampling interval beginning at 21:10 on May 29 and ending at 16:40 on May 31, except during a ~3 hour power failure during the morning of May 30. Three sample data sets showing variation in puff frequency and apparent amplitude are shown in Figure 2.4.

The thermal signal of puffs may show a diurnal variation (Figure 2.5). If so, it can be explained by variation in the temperature of the volcanic edifice, combined with the relatively low temperature of the gas plume. Ground surface temperatures ranged from below freezing at night, to 60º C during the day. A reasonable FOV comprised of 40% cone at either 0 or 60°C and 60% sky at -18° C, will yield approximate FOV integrated temperatures of -10°C and 21°C, respectively. A FOV with 10% gas (puff) at 75°C, 40% cone at either 0 or 60°C, and 50% sky at -18°C will yield FOV integrated temperatures of 3 and 31°C, respectively. Thus, the magnitude of the same puff appears as 13 C when the cone is relatively cold (i.e. during nighttime hours), and

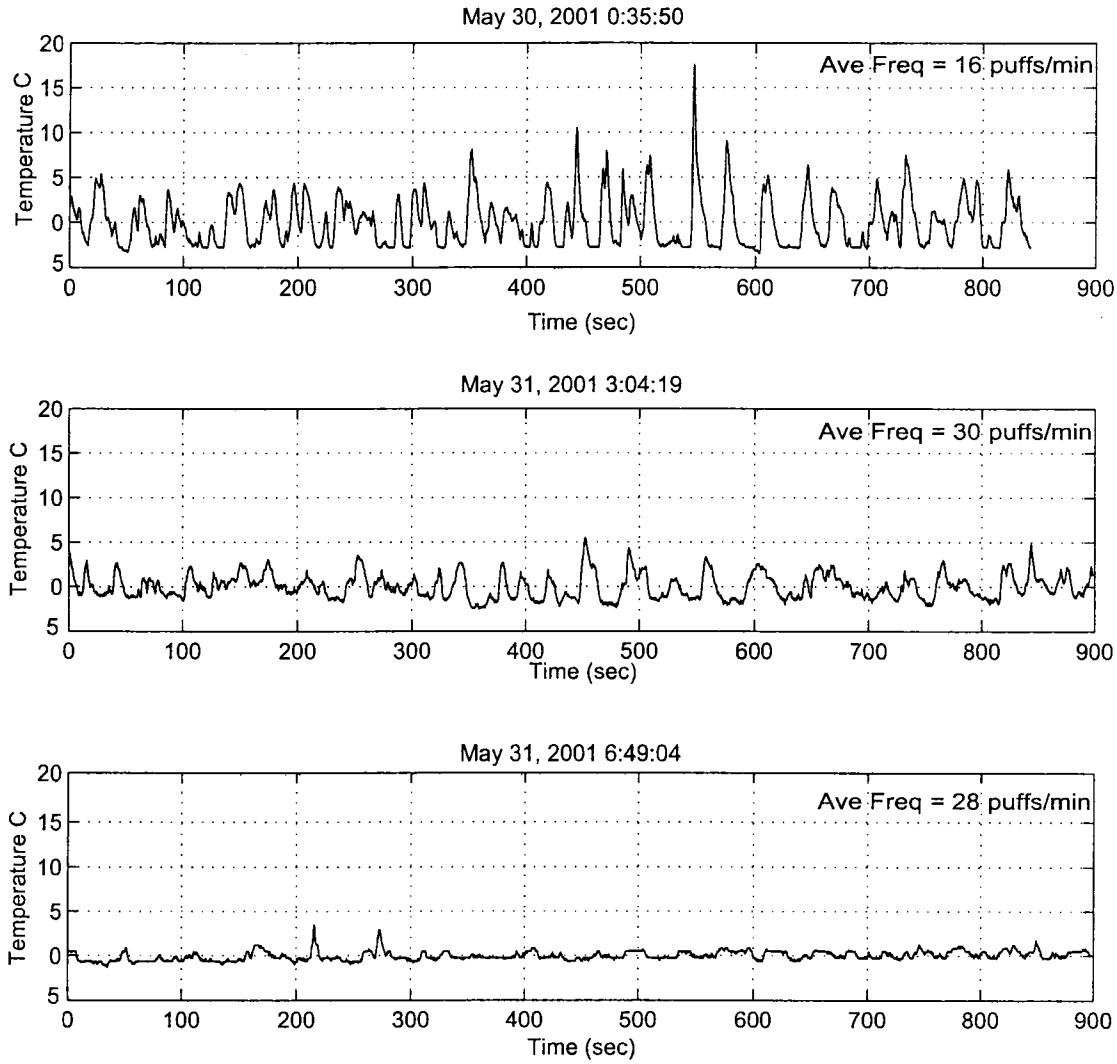

Figure 2.4 Three ~15 minute IR-thermometer data sets obtained for SEC puffing. Each spike represents a single gas puff through the IR-thermometer field of view. Note the lack of correlation between the apparent puff amplitude and average puff frequency.

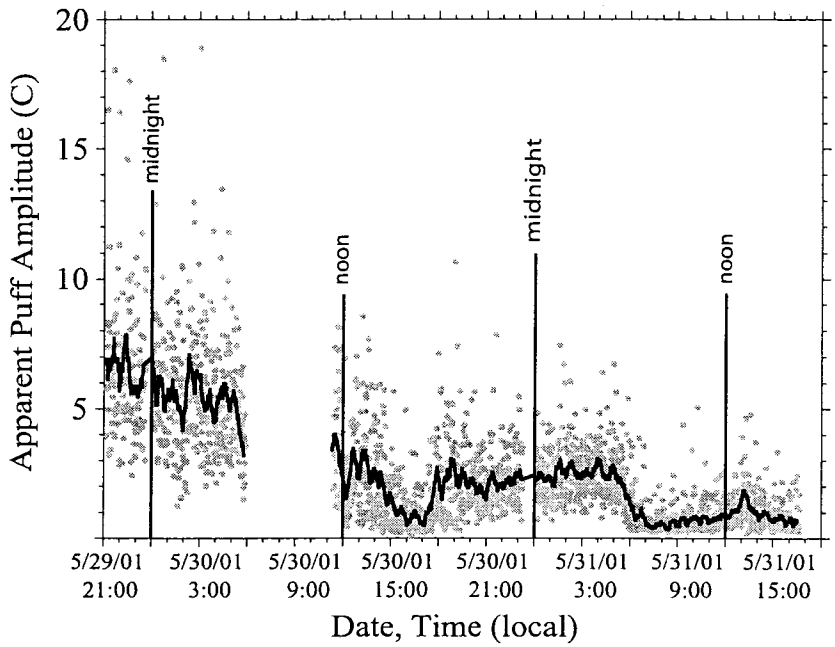

Figure 2.5 Plot of apparent puff amplitude versus time, with points representing the maximum puff amplitude per minute. The solid line is a 20-minute running mean through the data. Note the apparent diurnal effect, for example between 18:00 on May 30 and 06:00 on May 31

10º C when the cone is relatively warm. Figure 2.5 shows a time series of apparent puff amplitude (measured as the maximum per-minute relative to the FOV integrated temperature, or maximum per-minute amplitude of a spike as shown in Figure 2.4). Note that puffs appear to be higher amplitude during the nighttime hours from May 30 to 31, and decrease during the daylight hours on May 31. Though our data lends evidence that a diurnal variation affects the apparent thermal amplitude of puffs, our time series is too short to state this definitively. We expect a longer time series would confirm this to be true. Therefore, our analysis of variation in degassing rate (section 2.4.2) incorporates only puff frequency (number of puffs per minute), as given in Figure 2.6. This parameter should be unaffected by non-volcanic, diurnal influences.

2.3.3 Effusion rate data and validation

The full long-term effusion rate database is given in Figure 2.2. Effusion rate values derived from all methods show relatively good agreement. On May 30, 49 FLIR-derived effusion rate measurements made between 14:45 and 18:38 (local time) give a mean and standard deviation of 2.5 and 0.5 m^3s^{-1}, with a range of 1.5 to 4.3 m^3s^{-1}. These compare with average satellite-based values of 2.4 m^3s^{-1} at 00:46 on May 29, and 3.2 m^3s^{-1} and 2.7 m^3s^{-1} at 00:36 and 12:12 on May 30.

In addition, six AVHRR effusion rate values obtained between March 18 and 21 that average 0.24 m^3s^{-1} with a range of 0.12 to 0.61 m^3s^{-1} compare with a ground-derived effusion rate of 0.19 m^3s^{-1} measured March 20. Another good comparison occurs between March 16 and 22 when three AVHRR-derived effusion rate values averaging 1.45 m^3s^{-1} with a range of 1.22 to 1.89 m^3s^{-1} compare with a ground-derived estimate of 1.33 m^3s^{-1} on May 17 and 2.45 m^3s^{-1} on May 18. Also, ground-based and satellite-derived effusion rate trends during the 2001 flank event are similar (Figure 2.2c).

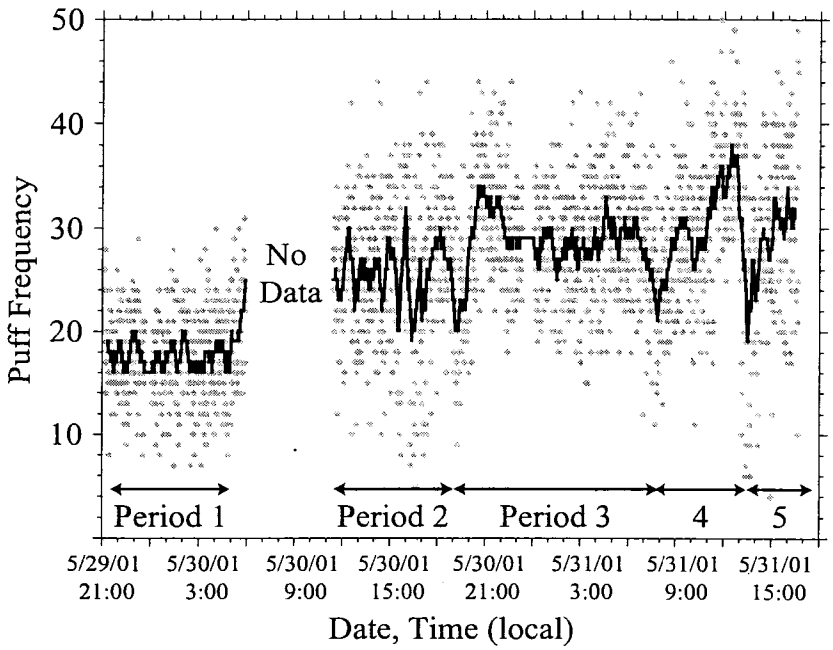

Figure 2.6 Plot of puff frequency versus time. Points represent the number of puffs per minute, and the solid line is a 20-minute running mean through this data. Five puffing periods are identified on the basis of having a characteristic and relatively persistent puff frequency, and/or being bounded by a major decrease in the puffing frequency.

2.4 Results and Discussion

2.4.1 Long-term effusion rates: oscillations in the erupted flux, January – August 2001

Our AVHRR-derived effusion data for January to August 2001 indicates that the flank eruption of July to August 2001 was preceded by a series of building phases. We identify 4 pulses that follow an increasing trend (Figure 2.2b, Table 2.1). Volumes shown in Table 2.1 were obtained by integrating the AVHRR effusion rate values within each pulse through time. This gives a satellite-derived DRE volume for the 2001 flank eruption lava flows of 19.8±7.7 x 10^6 m^3, which is lower than the ground-based DRE volume of 37.5±5.5 x 10^6 m^3 for effusive activity. The use of anomalously high or low effusion rate values can introduce significant error into volume estimates derived from satellite-based data (Harris et al., 2000). We therefore emphasize that a time series of effusion rates is more valuable for showing trends in effusion than for obtaining accurate volume estimates, though relative volumes can still be insightful.

2.4.1.1 Pulses prior to the 2001 flank eruption

Pulse 1 had a duration of ~57 days, was characterized by relatively low effusion rates (0.01 to 1.2 m^3s^{-1}), and produced ~1.3 x 10^6 m^3 of lava, as calculated using satellite thermal data. This pulse coincides with the onset of Strombolian eruptions and variation in effusive activity observed at SEC during January and February 2001. Note that Pulse 1 includes effusion rate spikes on February 7, 16 and 24 (Figure 2.2b).

After a decreasing effusion rate trend during February 24 through March 4, we identify a second pulse beginning on March 5. Pulse 2 persisted for ~46 days, was also characterized by relatively low effusion rates (0.01-1.1 m^3s^{-1}), and is volumetrically indistinguishable from Pulse 1. This pulse included two phases (March 5 -19 and March 20-April 23) and a single effusion rate

Table 2.1 Effusion Rate Pulses Summary

Pulse No.	Onset Date (2001)	End Date (2001)	Duration (days)	Peak Date	Peak E_r ($m^3 s^{-1}$)	Volume (x 10^6 m^3)	Mean E_r ($m^3 s^{-1}$)	σE_r ($m^3 s^{-1}$)
1	1 January	4 March	57	16 Feb	1.2	1.3	0.4	0.2
2	5 March	21 April	46	28 Mar	1.1	1.3	0.3	0.2
3	24 April	18 June	55	27 May	4.2	6.3	1.4	1.0
4	23 June	16 July	23	28 June	8.8	4.2	1.7	2.0
5	17 July	9 August	23	23 July	22.2	19.8	10.9	6.6

spike (March 28), subsequent to which our data show declining effusion rates for ~25 days until the onset of Pulse 3 (April 24).

Pulse 3 persisted for ~55 days through June 18. Due to the cloud-caused scarcity of data from May 4 to 25, it is not possible to determine whether Pulse 3 comprised two spikes occurring on April 27 and May 26, or if their appearance is an artifact introduced by the poor sampling rate during this interval. Pulse 3 had higher effusion rates than the previous two pulses, consistent with heightened activity observed at the SEC during this time.

Pulse 4 began June 23, reached a single peak on June 28, and persisted ~23 days until the onset of the 2001 flank eruption. This fourth pulse continued the trend of increasing peak and mean effusion rate values (Table 2.1).

2.4.1.2 *The 2001 flank eruption*

The 2001 flank eruption lasted 23 days and involved the largest satellite-derived volume, and highest peak and mean effusion rates in 2001 (Table 2.1). Our time series indicates that the eruption may have comprised two effusive phases that were separated by a reduction in effusive activity (but an increase in explosive activity) during July 24-27 (Figure 2.2c). The first episode showed waxing lava effusion rates to a peak of 22.2±9.6 m^3s^{-1} on July 23, followed by decreasing values to July 27. A second peak of 19.8±6.4 m^3s^{-1} was reached on July 30, subsequent to which satellite-derived effusion rates steadily declined through to the eruption's conclusion (Figure 2.2c).

We note that the lull in effusion during July 24-27 coincides with a change in eruption style at the 2550 m vent. Activity changed from ash-rich subplinian activity to fire fountaining on July 24, and then returned to ash emission on July 27-28. Therefore, the satellite-derived values for

lava effusion may under-represent the true net mass flux (effusive + explosive) during this interval.

2.4.1.3 Rank order analysis of the satellite-derived effusion rate time series.

We perform a rank order analysis of the satellite-derived effusion rate data to examine if it would have been possible to identify the change in Etna's eruptive state represented by the 2001 flank eruption. Building on Sornette et al. (1996), Pyle (1998) showed that for volcanic factors such as erupted volume and caldera size, a power law function defined by rank order statistics could be derived. Such a plot allows the largest (N) number of events (above a given threshold) to be used to predict the likely magnitude of the next largest occurrence of the same phenomena. Rothery et al. (2001) applied this method to 1.6 μm radiance data from the Along Track Scanning Radiometer (ATSR) for vents and flows at Etna. We follow their logic by plotting a time series of thermal data at an active volcanic system. Here, we consider each AVHRR-derived effusion rate value as an event, and give the highest value of effusion rate the rank of 1, with increasing rank number given in decreasing order of effusion rate. Any point that falls off of a linear extension through a given power law distribution would indicate a change in the state of the system. The AVHRR-derived effusion rate time series defines an exponentially increasing trend prior to the 2001 flank eruption (Figure 2.2). Plotting these data in rank order shows a power-law dependency of event frequency on event magnitude, wherein the time series has a high frequency of low effusion rate values and low frequency of higher effusion rate values (Figure 2.7).

Figure 2.7 shows two rank-order plots of the AVHRR-derived effusion rate time series for 2001. The lower curve is the subset of data from January 1 though July 17 with a trend line plotted through events ranked 4-23. The upper curve includes data from January 1 through

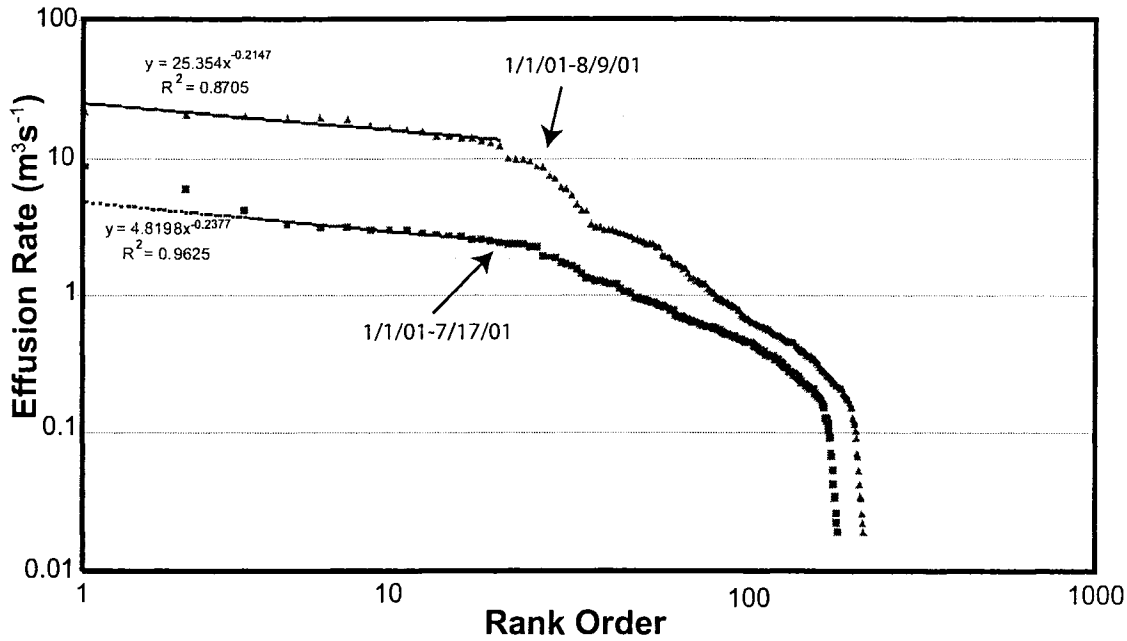

Figure 2.7 Log-log rank order plot of AVHRR-derived effusion rate data. The upper curve includes all data for Jan 1 to Aug 9; the lower curve includes only data prior to the 2001 flank eruption (Jan 1 to Jul 17). Solid lines are trends through events ranked 1-17 for the upper curve, and events ranked 3-23 for the lower curve. Equations shown are the power law function describing either trend line, with their associated R^2 value. The top 21 ranked effusion rate values on the upper curve are from the 2001 flank eruption, and note that they define a distribution statistically different than that of the lower curve.

August 9, 2001. The top 21 ranked events on this curve occur during the 2001 flank eruption and define a statistically different power law distribution. The shown trend line is plotted through events ranked 1-17.

Pyle (1998) uses maximum likelihood statistics to show that the function described by N number of events larger than a chosen threshold size, together with the magnitude of the currently ranked number one (largest) event ($Z_1^{current}$), can be used to predict the most likely magnitude of the next largest event (Z_1^{next}) according to $Z_1^{next} = [(2\mu+1)/(\mu+1)]^{(1/\mu)} Z_1^{current}$. In this equation, $\mu = -(1/b)$, b is the exponent of the power law function, and there is a relative error in μ of $\sim N^{(-1/2)}$. Applying this method to the data ranked 1-20 (i.e. N = 20) in the January 1 to July 17 data gives the function:

$$y = 7.0377x^{-0.3886} (R^2 = 0.9126)$$

and predicts a next-highest effusion rate of 10.9 ± 0.6 m^3s^{-1}. Because the three highest ranked data points appear to fall off the trend defined by the data ranked 4-23 (Figure 2.7), we also carry out an analysis using N = 20, but excluding the 3 highest ranked data points (i.e. using data ranked 4-23). This yields the function:

$$y = 4.8198^{-0.2377} (R^2 = 0.9625)$$

and predicts a next highest magnitude of 4.2 ± -0.9 m^3s^{-1}.

Of the 35 AVHRR-derived effusion rates attained during the 2001 flank eruption, the top 17 ranked events fall above the former predicted magnitude of 10.9 m^3s^{-1} and the top 27 ranked events fall above the latter value of 4.2 m^3s^{-1}. Therefore, if we consider the distribution defined by persistent activity at Etna from January 1 to July 17 as background, the statistical distribution of the 2001 flank eruption would, in fact, indicate a change in the volcano's eruptive state from persistent low level activity. Further, given the sharp increase in AVHRR-derived effusion rate values at the onset of the 2001 flank eruption (i.e. to 12.5 m^3s^{-1} on July 18 and 16.8 m^3s^{-1} on July 19,

see Figure 2.2), the change in Etna's activity could have been identified almost immediately using either function given above.

Petrological data supports the change in state represented by the 2001 flank eruption. Two distinct compositions of magma were erupted during this flank event—porphyritic Hawaiite at vents above 2600m (similar to magma commonly erupted in past centuries and in months preceding the 2001 flank eruption), and unusual porphyritic alkali basalt at vents below 2600m (Calvari et al., 2001). The addition of a second and unique composition of magma further indicates the volcano had undergone a change from its more typical persistent eruptive behavior.

The rank order analysis yields the unexpected finding that our highest ranked events may define an effusion rate threshold for both Etna's persistent state of activity (particularly if we exclude events ranked 1-3), and the 2001 flank eruption. Notice that the both linear trends in Figure 2.7 are relatively flat. Considering the January 1 to July 17 subset of data, for events ranked 4-23, $Z_1^{current} = 3.3\ m^3s^{-1}$ and, as stated above, the predicted $Z_1^{next} = 4.2 \pm 0.9\ m^3s^{-1}$, a difference of only 22%. Considering the upper curve and using N = 17 (which includes only data for the 2001 flank eruption) yields the function shown on Figure 2.7. For the 2001 flank eruption then, $Z_1^{current} = 22.2\ m^3s^{-1}$ and $Z_1^{next} = 26.0 \pm 0.1 m^3s^{-1}$, a difference of only 15%. Identification of an approximate threshold to effusion rates for Etna's persistent activity would be universally useful in characterizing this state of the volcanic system. It would be worthwhile to conduct a similar analysis using an even longer time series from this common style of activity to check the effusion rate limit of the system we may have identified. Our data indicate a range of ~3-5 m^3s^{-1} as this maximum limit for Etna's (non-anomalous) persistent style of activity.

Although episodic flank eruptions at Etna tend to vary in scope and intensity, identification of an approximate maximum effusion rate value for the 2001 flank eruption may provide a starting point for characterizing this state of the system. Our data indicate a potential maximum

threshold for flank eruptions at Etna in the range of 25-30 m^3s^{-1}. Plotted together in rank order, similar satellite-derived effusion rate data from more flank eruptions would provide insight into whether or not there is consistency in peak effusion rates among multiple events of this nature at Etna.

2.4.2 Degassing and channel-based effusion rate results: short term oscillations in the erupted flux, May 29-31, 2001

The puff frequency data presented in Figure 2.6 show trends on two time scales: a) a steady, increasing trend over the measurement period, and b) an hours to minutes oscillation over-printed on the more general trend. The steady increase in puff frequency from May 29 to 31 is broadly consistent with reports of heightened activity over the month of May (as discussed in Section 2.2.2). It is also consistent with the satellite-derived peak of Pulse 3 (May 26 – June 1; Figure 2.2b) and ground-based high of ~5 m^3s^{-1} for the months of May and June 2001 (Figure 2.8).

Our data indicate that a relationship between degassing and effusion rate may exist. For example, satellite-derived and average FLIR-derived effusion rate values both decreased from May 30 to May 31 (3.2 to 2.8 $m^3 s^{-1}$ and 4.3 to 3.4 $m^3 s^{-1}$, respectively; Figure 2.8), while puff frequency followed a generally increasing trend. If waning shallow supply of magma drives the decline in effusion, it is possible that the degassing response lags behind the effusion rate response, with a decrease in puff frequency manifesting itself 1-2 days after the initial decrease in effusion rate. A longer set of degassing data and a higher frequency of effusion rate values could help decipher such a relationship more precisely. The detailed channel-based effusion rate and degassing data may indicate a correlation on an even shorter timescale, and similar to that found at Stromboli by Ripepe et al. (2002). Figure 2.9a shows a surge in effusion rate between ~17:30 and 19:00 on May 30 that was coincident with an increase in puff frequency. Also, a decline in

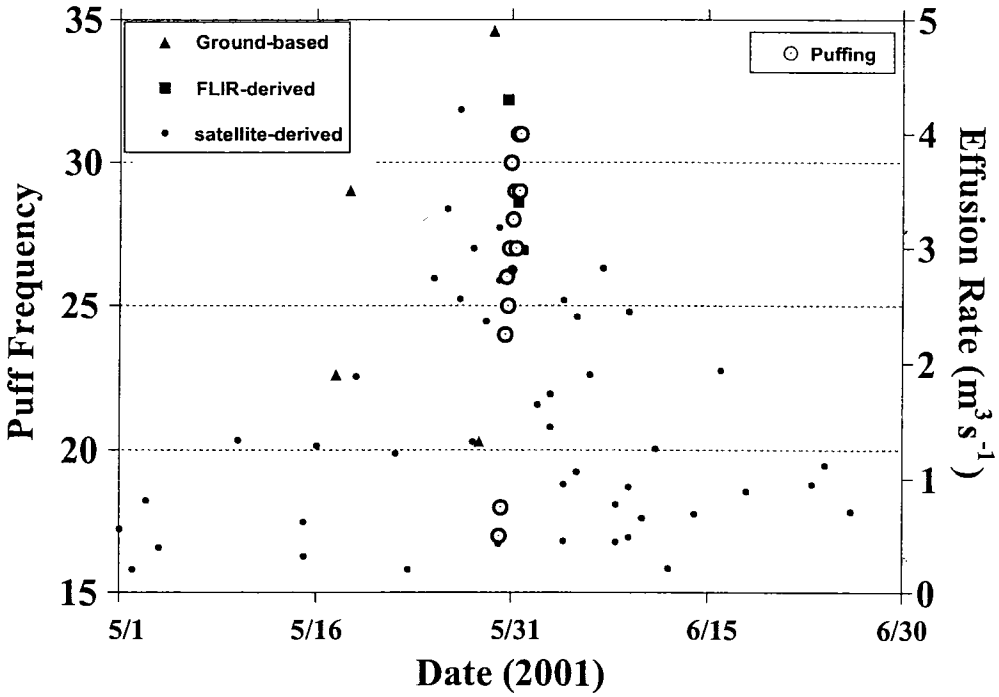

Figure 2.8 Plot of puff frequency data for May 29 to 31 and effusion rate data for May and June 2001. Puffing is plotted as puffs per minute data time-averaged over 3 hours at the mid-point time. FLIR-derived effusion rate squares represent the average effusion rate value for May 30 and May 31 plotted at the mid-point time for each day.

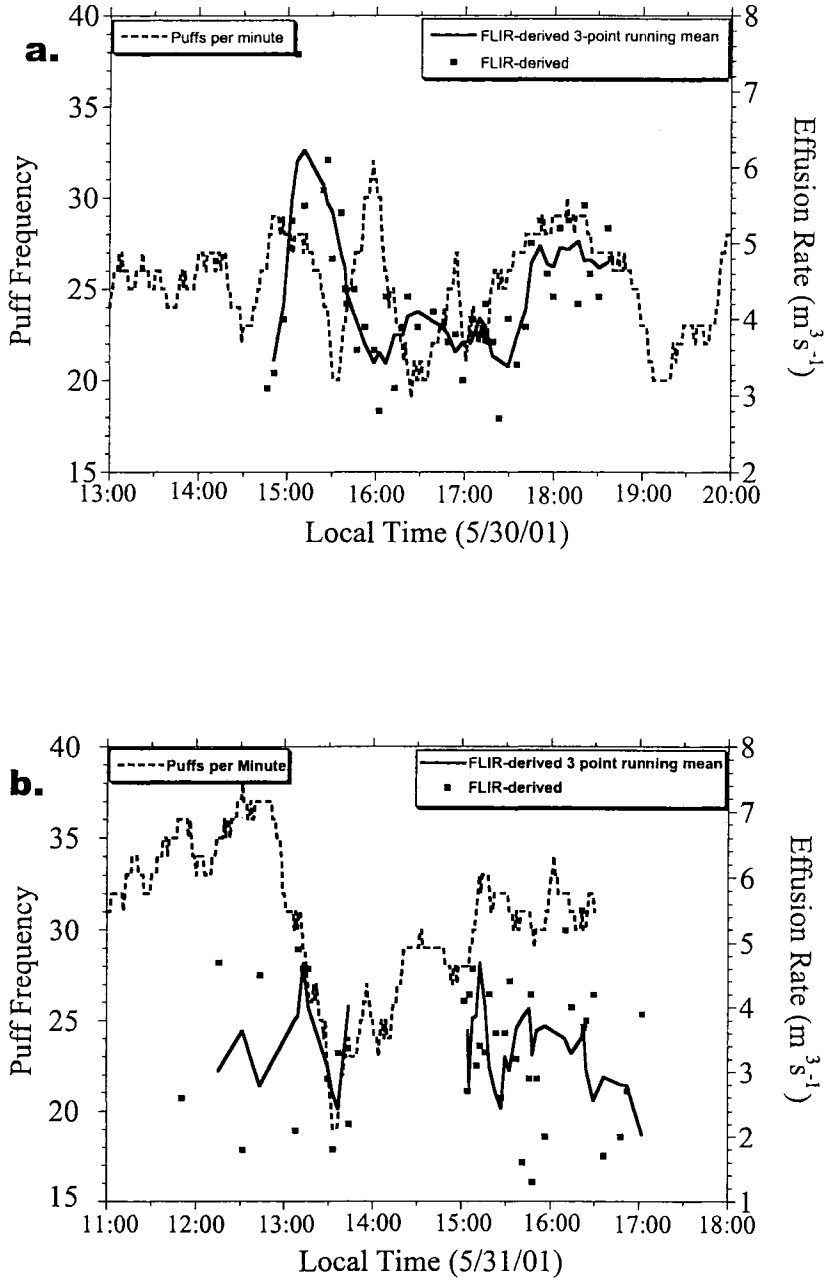

Figure 2.9 Plot of puff frequency and FLIR-derived effusion rate data for (a) May 30 (13:00 - 20:00) and (b) May 31 (11:00 - 18:00), 2001. Puff frequency data is plotted as puffs per minute time-averaged over 12 minutes at the mid-point time.

puff frequency commencing at ~14:50 on May 30 was followed ~30 minutes later by a decline in effusion rate (Figure 2.9a). However, the puff frequency peak that occurred at ~16:00 on May 30 is not reflected in the effusion rate data, and there is no clear link between puff frequency and effusion rate on May 31 (Figure 2.9). Again, a longer time series of data is needed to demonstrate whether or not there is any correlation.

Our working hypothesis is that oscillations in degassing and effusion rate would be related to changes in the supply rate of magma to Etna's shallow (near-vent) conduit system, such that an increase in supply of gas-rich magma would lead to both an amplification in puff frequency and heightened effusion (though not necessarily simultaneously). In an effort to constrain the time-scale of potential variations in this supply rate, we grouped the puffing data into five periods (Figure 2.6, Table 2.2) that are either bounded by major decreases in puff frequency (i.e. Period 3), or are characterized by a unique puff frequency (i.e. Period 1). The main periods identified range from 3 to 14 hours. Also, 26 oscillations of 19 to 126 minutes (mean = 82 minutes, standard deviation = 43 minutes) can be identified within our dataset. These minutes-long oscillations may be related to a third time scale of degassing and possibly supply processes.

2.5 Conclusions

This study identifies variation in effusion rate at Etna from January through August 2001 on timescales that span minutes to months, and variations in degassing that occur over minutes to hours. Furthermore, the timescale of this variation incorporated hours-, days- and weeks-long oscillations that were overprinted on a consistent ~8 month increase through the 2001 flank eruption.

An important and interesting question to consider is: what processes could have driven variation on the multiple timescales we have identified. In a very general sense, two possibilities

Table 2.2 Puffing Cycles Summary

Cycle No.	Onset Time (2001)	End Time (2001)	Duration (minutes)	Peak Time	Peak Frequency (puffs min^{-1})	Mean Frequency (puffs min^{-1})	σ Frequency (puffs min^{-1})
1	29 May 21:00	30 May 5:54	524	30 May 5:48	31	18	4.3
2	30 May 11:24	30 May 19:28	484	30 May 17:12	44	25	7
3	30 May 19:29	31 May 8:00	751	30 May 22:33	44	29	6
4	31 May 8:01	31 May 13:44	343	31 May 11:48	50	30	7
5	31 May 13:45	31 May 16:40	175	31 May 16:31	49	29	8

are: i) fluctuation in supply rate from the source region, or ii) conduit processes that interfere with a relatively stable rate of supply rate from the source region. Given a constant source supply rate, it is possible that some at-vent variation results from slowed ascent of magma in contact with irregular conduit walls during transport. Another effective process may be convective overturn in shallow portions of the system. In this case, effusion rate surges could be driven by the buoyancy of a relatively gas-rich bleb of magma gathering beneath a relatively degassed cap. If vesiculation continues, the gas-rich body of magma would be expected to push aside (or out) the degassed cap and erupt. If the degassed cap is ejected prior to the gas-rich body, we would expect some lag time between a peak in effusion rate and a peak in puff frequency, such as we observe during Pulse 3.

Following Ripepe et al. (2002), we can also consider a direct link between changing magma supply and changing volatile flux, which should drive consistent variation in the gas puffing frequency and effusion rate. Our data indicate that this may be true, though not conclusively. Longer datasets of these types are needed to identify the presence or absence of a correlation between degassing and mass discharge.

Finally, rank order analysis of our satellite-derived effusion rate data may reveal a maximum effusion rate threshold in the range of 3-5 m^3s^{-1} for Etna's typical persistent activity, and 25-30 m^3s^{-1} for the 2001 flank eruption. With data from more flank eruptions, the latter result could be expanded to attempt to classify a similar threshold for Etna during episodic flank eruptions. If more data supports our findings, it will provoke further investigation into what processes can cause such thresholds to exist.

Contributions. Andrew Harris, with Maurizio Ripepe, Sonia Calvari, Jon Dehn, and Scott Rowland designed, set up and ran the field experiment at Etna during May 2001. Harris and Ripepe installed and targeted the thermal infrared thermometers. Dehn and Rowland targeted the thermal imager (FLIR) and provided field notes, respectively. Calvari provided additional field measurements of effusion rate and activity reports for the January to August period. Ripepe and Harold Garbeil processed much of the infrared thermometer data, and Garbeil wrote software to extract the gas puff statistics. Kate Evans-Jones carried out pre-preprocessing of the AVHRR data. Harris provided spreadsheet-based algorithms that allowed extraction of hot spot area, thermal flux, and conversion to effusion rates in the AVHRR data. Matthew Patrick generated Figure 4 using a Matlab script written for the thermal infrared thermometer data set collected. John Bailey carried out manual processing, conversions, and generation of the field-based effusion rates. Note that Bailey, Harris, Dehn, Calvari, and Rowland published a companion to this study in *Bulletin of Volcanology* (Bailey et al., 2006).

Acknowledgements. Nicole Lautze thanks the National Weather Service for funding during this study, and the Italian Fulbright Commission for generous backing in Italy in 2000-2001. David Rothery, Dave Pyle and Bruce Houghton provided perceptive and insightful reviews that greatly contributed to the quality of this work. This study was supported by NSF grant EAR-0207734, and is HIGP publication number 1263 and SOEST publication number 6095.

CHAPTER 3. Physical mingling of magma and complex eruption dynamics in the shallow conduit at Stromboli volcano, Italy

Abstract. Strombolian eruptions are caused by the bursting of large gas bubbles through essentially stagnant melt that resides in the uppermost part of the conduit. We investigate the physical properties of this shallow melt via a detailed analysis of vesicularity textures in lapilli ejected during a period of moderate-intensity activity at Stromboli volcano (Italy) in 2002. The lapilli show clear evidence that the erupted material is the product of a late-stage, dynamic mingling of melts that are distinct in terms of density and rheology. Vesicle-volume distributions (VVDs) for two end-member melts indicate contrasting degrees of outgassing that can be linked to different residence times in the shallow conduit. We propose a model in which actively vesiculating melt rises with the gas phase and mingles with more mature, stagnant melt en route to the magma's free surface. We suggest that the complex rheology of this mingled melt feeds back to strongly influence eruption dynamics.

3.1 Introduction

Stromboli volcano (Aeolian Islands, Italy) is considered the archetype location for long-lived, mildly explosive Strombolian eruptions (Figure 3.1). Typical activity consists of continuous degassing that is punctuated by a discrete explosion every 5–20 min. Each explosion ejects crystal-rich basaltic scoria, generally to heights of 100–200 m. Rosi et al. (2000) determined that this eruption style has persisted without long breaks or changes for at least 1400 years. Melt generally resides at a high level in the conduit (20–200 m below the crater terrace; Ripepe et al., 2001b).

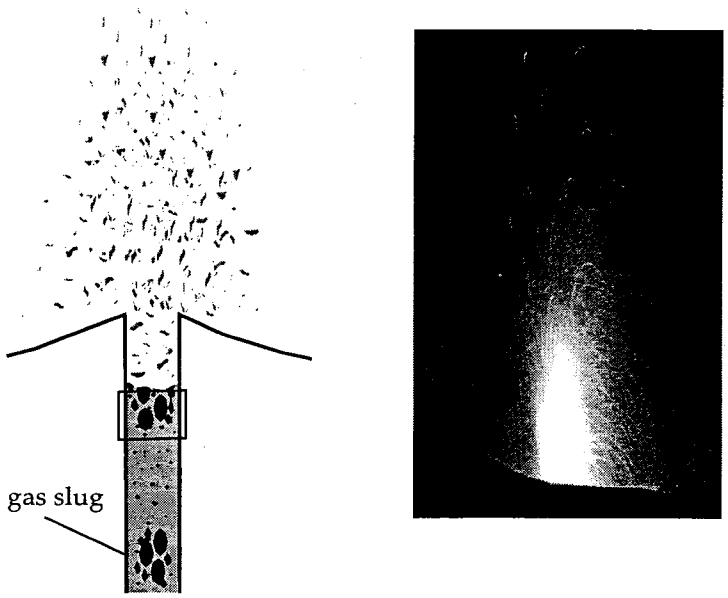

Figure 3.1 Schematic representation of a gas slug driving a Strombolian eruption (left), and photo of a SW crater explosion (right; taken by Jonathan Dehn on May 21, 2002). Short edge of photo ~60 m.

Strombolian eruptions are well understood to be driven by the intermittent rise and bursting of slugs of closely spaced, large (decimeter- to meter-sized) gas bubbles that have separated (decoupled) from the melt phase (Figure 3.1). A slug rises rapidly and breaks through the magma's free surface as a Strombolian explosion. At Stromboli, seismic data indicate that slugs undergo a rapid pressure change and acceleration at two locations 220 m and 260 m below the crater terrace (Chouet et al., 2003). We call the zone between these depths and the magma's free surface the "shallow conduit," and we infer this region to lie above the level of convective overturn of gas-rich magma, proposed by Allard (1994) and Stevenson and Blake (1998).

A major shortcoming in all current models is that, by default, they treat the physical properties of magma in the shallow conduit as constant. We envisage that this melt must continually evolve because of (1) ongoing vesicle evolution (growth, coalescence, and bubble loss), (2) cooling and crystallization, (3) mingling with newly arrived melt, and (4) removal and recycling by successive explosions. Such processes would cause changes in magma rheology and thereby influence eruption dynamics. This study aims to expand existing models by investigating the properties of ejecta from Stromboli's typical activity.

One major problem associated with categorizing melt from observed Strombolian eruptions has been the difficulty of collecting associated ejecta. High eruption temperatures, relatively coarse grain size, and very limited dispersal have generally made the collection of fresh lapilli too hazardous to attempt. A fortuitous combination of moderate eruption intensity and high wind velocities at Stromboli in 2002 permitted the collection of lapilli populations ~150–200 m from source. Our most striking discovery is the presence of two texturally distinct melt types that are mingled on a fine scale. We suggest that magma in the shallow conduit is constantly evolving

through mingling of these melts, and data given below indicate that the textural diversity arises through variable residence time.

3.2 Textural Diversity and the ejecta

This paper presents data from 200 lapilli that landed in a ~30 × ~60 cm bin placed ~150 m south-southeast of Stromboli's southwest crater between ~14:00 on 30 September and ~15:15 on 1 October 2002. These ejecta accumulated principally during moderate to strong explosions projecting clasts upward as far as 400 m. Visual observations yield an average of 15 events per hour occurring at the southwest crater during the collection. It is therefore likely that between 300 and 400 events occurred at the southwest crater during the collection, although direct observations suggest that between 60 and 80 explosions would have deposited lapilli within our bin.

The lapilli are uniformly metallic gray to black with ragged to elongate, weakly fusiform morphology. A high phenocryst content gives an irregular surface texture to the matrix that contains abundant millimeter-size, spherical to subspherical vesicles. Measurements of the bulk density of the lapilli (following Houghton and Wilson, 1989) yield a unimodal distribution with a notable tail of dense clasts (Figure 3.2). The mean density of 900 ± 160 $kg \cdot m^{-3}$ equates to ~70 vol% vesicles (calculated by using a dense-rock-equivalent [DRE] value of 2750 $kg \cdot m^{-3}$ from Barberi et al. [1993]), which is compatible with dry fragmentation of actively vesiculating melt (Mangan et al., 1993). The dense tail ranges from 1300 to 1600 $kg \cdot m^{-3}$ (~40–50 vol% vesicles) and represents clasts that are crystal rich and have atypically fluidal textures. On the basis of this distribution, we chose eight lapilli for petrographic analysis (represented by asterisks in Figure 3.2) from which we selected a high-, a medium-, and a low-density clast as representatives (gray asterisks)

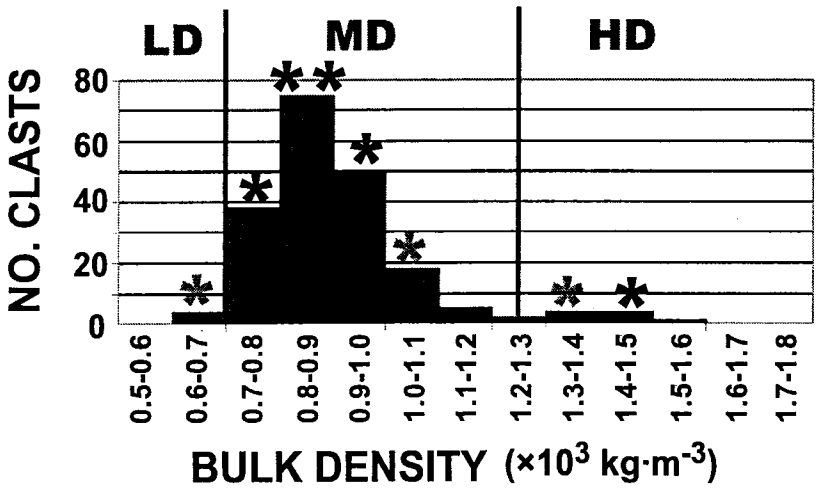

Figure 3.2 Plot of bulk densities of the 200 lapilli that comprise our sample. Asterisks indicate bins from which the largest 1 (or 2) clasts were chosen for petrographical analysis. Gray asterisks indicate those clasts from which quantitative vesicle size data were obtained. LD, MD, HD = low, medium, and high density, respectively.

for measurements of vesicle size. These have bulk densities (and vesicularities) of 1330 (52%), 1050 (62%), and 680 $kg \cdot m^{-3}$ (76%), respectively, and will be referred to as HD, MD, and LD in the following text.

All thin sections contain abundant phenocrysts, lack microlites, and have a relatively coarse vesicle population (Figure 3.3). We note two distinct vesicle populations: (1) spherical to subspherical vesicles 0.1–3 mm in diameter that vary in number density among thin sections and (2) complex amoeboid-like vesicles with diameters of 3 to >10 mm that are distributed uniformly among the sections.

On a microscopic scale, the most outstanding feature we observe is the occurrence of fine-scale physical mingling in the five lapilli within the medium density range (Figures 3.2, 3.3). HD and LD lapilli are homogeneous and exhibit strikingly different textures. The HD clast has a dark glass matrix, a higher abundance of phenocrysts, and a vesicularity that is dominated by a small number of large, amoeboid-like vesicles. The LD clast has a clear to transparent brown matrix, fewer phenocrysts, a higher number density of small- to medium-sized vesicles, and a distinct population of large vesicles. There is no preferred alignment of vesicles in either end member section.

In contrast, MD clasts show a heterogeneous texture caused by millimeter- to centimeter-scale mingling of the two end members (Figure 3.3). Zones with vesicle populations and glass transparency that are essentially visually identical to those of the HD and LD clasts can be identified in the MD clasts. The measured bulk densities of the five MD lapilli accurately reflect the relative proportions of the two end members in the given section. The MD clast shown in Figures 3.2 and 3.3 was specifically chosen as representative of this range because it has approximately equal proportions of HD and LD melt. Among the five MD lapilli, the mingled

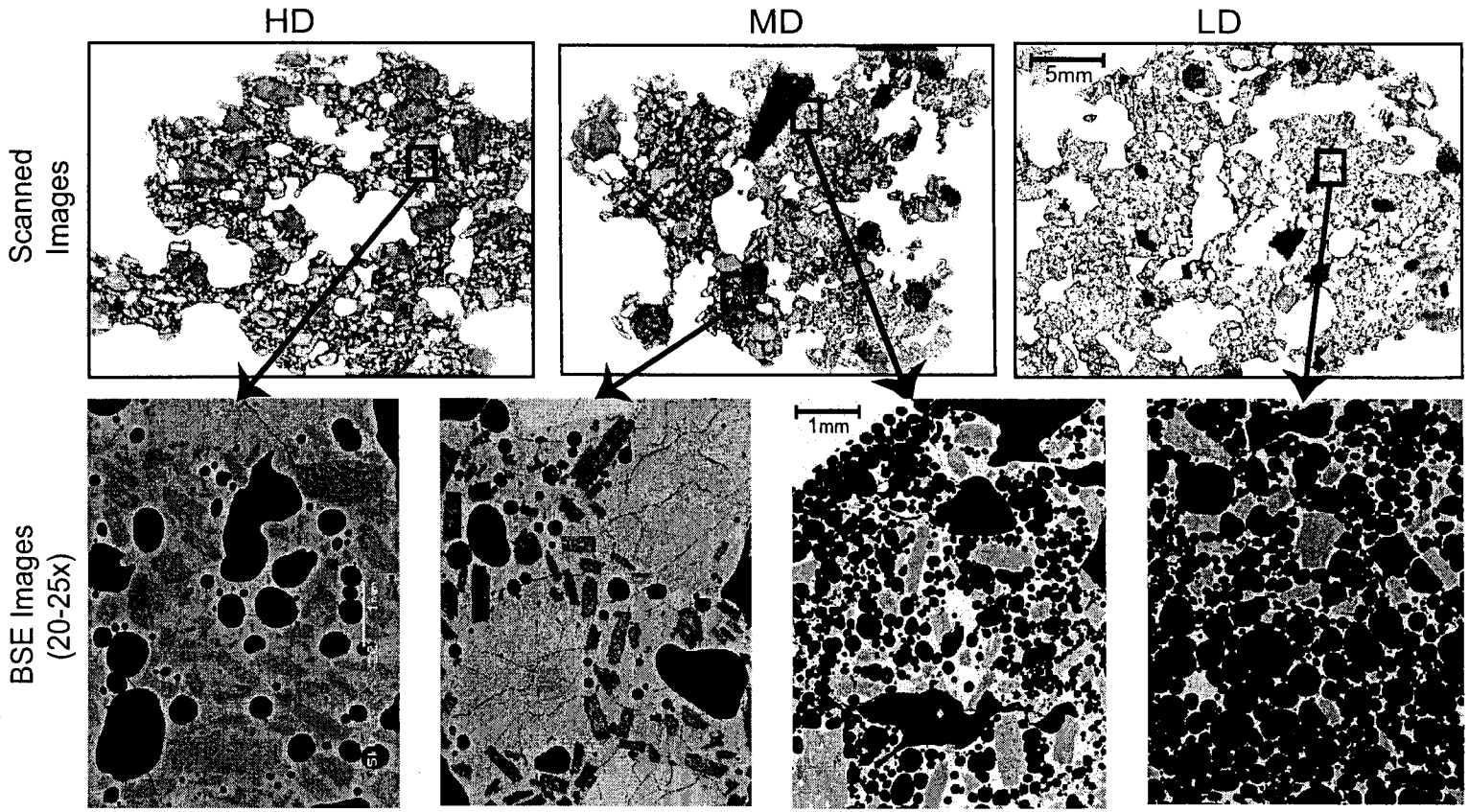

Figure 3.3 Scanned (top) and 20-25x magnification backscatter electron (BSE) (bottom) images of HD, MD, and LD scoria. Boxes on scans highlight areas representing the respective BSE images.

zones are similar in form; the interfaces are generally sinuous, sharp, and commonly marked by large vesicles or phenocrysts.

3.3 Comparing and explaining textures

The concept of magma mingling is not unknown at Stromboli, but has only been identified previously on rare occasions when the arrival of a chemically distinct melt batch triggered a major explosion or paroxysm (Metrich et al., 2001; Landi et al., 2004). In these cases, a batch of volatile-rich magma rapidly ascends from deep in the plumbing system and erupts as golden pumice, in part mingling on a coarser scale with Stromboli's typical black scoria. The idea that smaller quantities of melt mingle (in a more cryptic manner) over longer time scales is new. In this section, we present and interpret data that yield greater insight into how and why this fine-scale textural diversity occurs during periods of typical activity at Stromboli.

Major element data for HD and LD clasts (procedure detailed in Thordarson et al., 1996) show that their matrix glasses are chemically identical (Table 3.1). This finding indicates that the textural diversity is a purely physical phenomenon and is consistent with the well-documented notion of a continuous, chemically constant supply of magma (Rosi et al., 2000; Metrich et al., 2001).

Quantitative data regarding the number, shape, and size distribution of vesicles in scoria reveal information about the vesiculation history of the magma from which the clasts were derived. Vesiculation theory shows that a bubble will develop according to the stages of nucleation, growth, coalescence, and collapse (or bubble loss; Cashman and Mangan, 1994), and *vesicle-size distributions* and *vesicle-volume distributions* (VSDs and VVDs) yield insight into which of these processes dominate at the instant of magma fragmentation (Cashman and Mangan,

TABLE 3.1 CHEMICAL ANALYSIS OF GLASS MATRIX

	Label	SiO_2	TiO_2	Al_2O_3	FeO	MnO	MgO	CaO	Na_2O	K_2O	P_2O_5	Total
HD	Avg.	52.22	1.65	15.61	10.13	0.17	3.43	7.34	3.32	4.19	0.98	99.06
N = 10	Std. dev.	0.36	0.02	0.06	0.11	0.01	0.03	0.08	0.05	0.04	0.03	0.42
LD	Avg.	52.51	1.68	15.64	10.08	0.17	3.45	7.44	3.38	4.19	1.01	99.54
N = 27	Std. dev.	0.29	0.03	0.09	0.17	0.02	0.04	0.10	0.07	0.05	0.03	0.38

Note: Analysis conducted with defocused electron-microprobe beam to prevent Na loss.
N = number of analyses; HD = high density; LD = low density.

1994). *Vesicle number density* is generally linked to magma-ascent rate, such that a high number density is associated with a high rate of decompression and a low number density is linked to a slow, or staged ascent (Cashman and Mangan, 1994), but, in melt fragmented late in its vesiculation history, low number densities can also reflect the onset of coalescence and collapse.

Quantitative vesicle-size data for the HD, MD, and LD clasts were obtained via images of each thin section at multiple magnifications (procedure in Gurioli et al., 2004). For each clast we used a single image scanned at 1200 dpi and multiple backscattered-electron (BSE) images at 20–25× and 100× magnification. All images were transformed from grayscale to binary (vesicles and groundmass). Quantitative data for each vesicle area were obtained by using Scion Image; the values are converted to volumes and binned through the use of a 10^{-1} geometric scale following Sahagian and Proussevitch (1998).

Because the MD clast exhibits mingled textures, we did not average vesicle-size data across the entire thin section. Instead, the small- to medium-sized vesicle populations in homogeneous high-density (vesicle-poor) and low-density (vesicle-rich) zones within the MD thin section were imaged and analyzed separately at BSE magnifications (Figure 3.3). Large vesicles lie preferentially along the mingling boundaries, therefore those with an equivalent diameter of >0.7 mm were intentionally omitted from this analysis. The quantitative data attained from these images confirm visual observations that the size distributions of small- to medium-sized vesicles within the respective zones of the MD thin section mirror those of the HD and LD thin sections. For this reason, we are confident that the MD clast is a mingled composite of the two end members.

Complete size distributions including the large vesicles were measured for the HD and LD thin sections. Figure 3.4 shows that the LD clast has a bimodal size distribution reflected in a

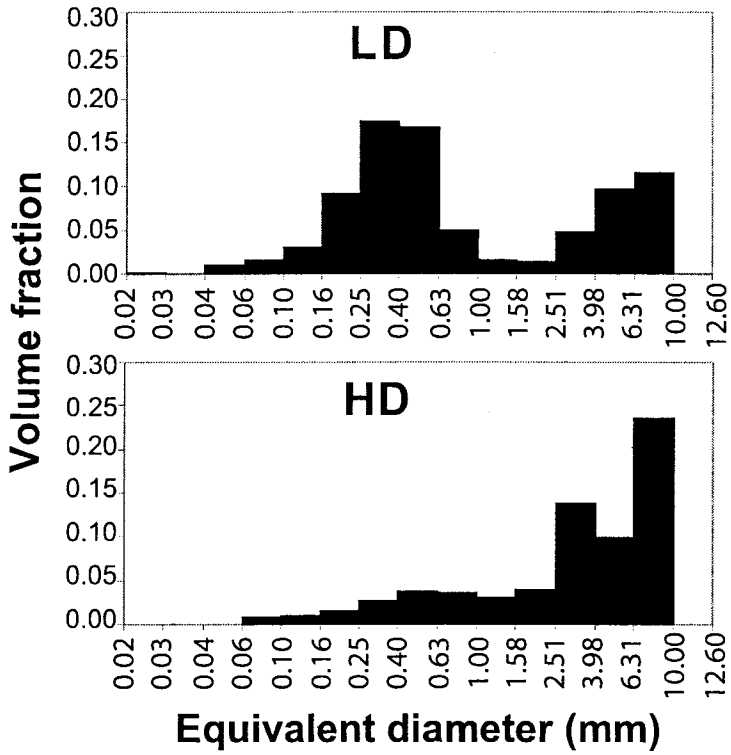

Figure 3.4 Histograms showing distribution of vesicle sizes in low-density (LD) and high-density (HD) clasts. Note contrasting bimodal vs. unimodal trends in LD and HD, respectively, and the complete absence of <25-micron-diameter vesicles. Bin values are calculated according to a geometric scale of 10 following Sahagian and Proussevitch (1998).

significant population of ~300–500 micron vesicles and a second population in the 5–10 mm size range. The spherical shape of the smaller vesicles suggests that they were growing at the time of fragmentation, whereas the complex amoeboid-like shape of large vesicles (in the scanned images, Figure 3.3) indicates that they are the coalesced products of two or more smaller vesicles. We therefore conclude that the dominant vesiculation processes occurring in the LD melt were growth and coalescence. In contrast, the vesicle population in the HD thin section is unimodal, with a volume-dominant population of coalesced vesicles in the 3–10 mm size range. The HD clast also has low bulk vesicularity with respect to the LD clast (52 vs. 76 vol% vesicles) and a lower number density (9×10^4 vs. 4×10^5 vesicles per cubic centimeter). This information leads us to conclude that outgassing was the dominant processes in HD melt at the time of fragmentation.

In comparing our quantitative vesicle data with those existing for other basaltic eruption styles, we first note that the minimum vesicle diameter in the Stromboli clasts (~25 microns) is similar to that found in scoria from Hawaiian fire fountain activity and in ash from the more explosive Keanakako'i eruption of Kilauea volcano (Mangan and Cashman, 1996; Mastin et al., 2004). Together, these data may indicate an approximate minimum stable size of bubbles in basaltic melt, which would suggest that both LD and HD melt underwent protracted bubble nucleation until close to the time of fragmentation.

Comparing data on vesicle number density, we find that the values for the HD and LD lapilli are higher than reported values for slow-rising magma that feeds Hawaiian lava flows (~10^3 cm^{-3}; Mangan et al., 1993), within and lower than the range for the fast-rising magma that produced the Keanakako'i deposit (9×10^4 to 1×10^7 cm^{-3}; Mastin et al., 2004), and similar to the range observed in scoria from magma that ascends at an intermediate rate and feeds sustained Hawaiian fire fountains (2×10^4 to 2×10^5 cm^{-3}; Mangan and Cashman, 1996). The data on vesicle

number density therefore suggest the early ascent rate of magma (e.g. below the shallow conduit) in our sample was closest to that of magma that feeds Hawaiian-style explosions.

What is the underlying cause of the 4.5 factor difference in vesicle number density between the HD and LD lapilli? Although a simple explanation would be that the HD melt ascended slowly relative to LD melt, the HD value remains significantly above that of flow-feeding magma (Mangan et al., 1993), and the HD clast has a reduced vesicularity (52% vs. 76%) dominated by millimeter-size vesicles. The combined information suggests that the reduction of vesicle number density in HD melt is brought about instead by coalescence and bubble loss. We conclude that both HD and LD melt types had similar rates of early ascent and bubble nucleation, producing number densities on the order of ~10^5 cm^{-3}, but that an extended residence time for HD melt close to the magma's free surface allowed prolonged coalescence and outgassing prior to fragmentation. This concept has a significant impact on our model for eruption dynamics.

3.4 Dynamic Model

In this section we address the questions of where the diverse vesicle textures formed and what process enabled the fine-scale mingling. Is it possible that the textural diversity formed simultaneously? We reason that even the most extreme disequilibrium conditions are unlikely to simultaneously produce the diverse textures. Could either HD or LD melt represent the film of melt that encloses and accompanies rapidly ascending gas slugs? HD melt is an unlikely candidate, as it exhibits evidence of prolonged shallow residence. However, LD melt is likely to represent this film, on the basis of its relatively high number density and more youthful vesicle texture.

What was the timing of the mingling process? We envision a scenario in which the HD end member represents long-resident shallow melt and the LD end member represents slug-enclosing material. As depicted in Figure 3.5, gas slugs transport LD melt closer to the free surface and also catalyze the physical interaction (likely both mixing and mingling) of the two melts. Mingling is likely to occur on time scales of minutes or less, and to be greatest along the slug margins (Figure 3.5) and possibly where there is turbulence in the slug wake. A given explosion ejects diverse melt types both as individual ejecta and as composite, mingled scoria. Some amount of LD melt must be left behind as each gas slug rises, making mingling a method of shallow melt replenishment. The replenished melt would begin to evolve toward HD-type melt, which leads us to conclude that there is an ongoing evolution of, and interactions among, small quantities of melt at various stages of degassing.

The continually shifting physical composition of melt in the shallow conduit at Stromboli must influence variations in eruption intensity and style. Frequent arrival of gas slugs will lead to a relatively fluid mingled melt that is rich in the LD phase. Conversely, a low frequency of gas slugs will allow melt close to the free surface to outgas and become increasingly viscous. Rheological stiffening of this shallow melt will feed back to slow slug ascent rates and therefore change the vigor of Strombolian explosions. We conclude that the shallow conduit at Stromboli is a dynamic environment and suggest that continual changes in shallow melt rheology have a strong influence on the observed pattern of Strombolian activity.

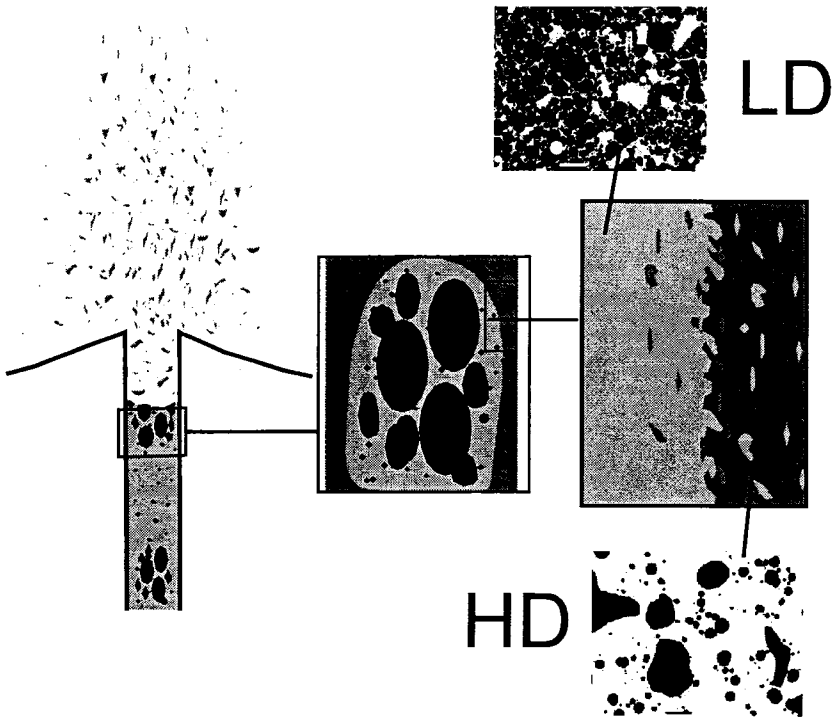

Figure 3.5 Schematic illustration of concepts presented in our dynamic model. Low-density (LD)-type melt rises with gas slugs, mingling with high-density (HD)-type melt at slug borders and near magma's free surface. Small boxes are binary backscattered-electron (BSE) images of LD and HD vesicle populations (vesicles are shown as black and bar at bottom of images is 1 mm). Diameter of gas slug shown here is approximately meters.

Acknowledgements. We thank Nancy Adams, Mike Burton, Julia Hammer, Andy Harris, Matt Patrick, Maurizio Ripepe, Julia Sable, Don Swanson, and Lionel Wilson and an unknown reviewer for insightful comments on earlier versions of this paper. The work was supported by National Science Foundation grant EAR-0207734 and an NSF Graduate Research Fellowship (to Lautze).

CHAPTER 4. Linking variable explosion style and magma textures during 2002 at Stromboli volcano

Abstract. Microtextural characteristics of fresh ejecta from Stromboli volcano were examined from three periods of differing eruption style and intensity in 2002. Activity shifted from relatively weak and infrequent ash-charged explosions during January through May into two broad cycles of waxing activity in June through late September, and late September through December, followed by the onset on 28 December of the 2002/2003 effusive eruption. Analyzed sets of lapilli from May, September/October, and 28 December show contrasts in the physical properties of magma resident in the shallow conduit during this range of activity. Three distinct textures are observed among the analyzed pyroclasts: low density (LD) with an abundance of subspherical bubbles, the presence of large, irregularly shaped bubbles, and a light-to-transparent glass matrix; transitional texture (TT) with an intermediate number of subspherical bubbles, a high frequency of large, irregularly-shaped bubbles, and a honey colored glass matrix; and high density (HD) with sparse relatively small bubbles, conspicuous large irregular bubbles, and a dark glass matrix. Observational and quantitative data (density, vesicle size) indicate that these textures are linked through variable residence time in Stromboli's shallow conduit, with an ongoing evolution from LD to HD magma. Calculations suggest that residual LD magma will evolve to HD texture in a period of hours to days.

Contrasting amounts of the LD, TT, and HD magmas are present in each sample, with the most TT in May, the most LD in September/October, and the most HD in December. Differences in calculated viscosity between LD and HD magmas (in the range of 2000 to 2600 and 3000 to 5000 Pa s, respectively) must have implications for rates of bubble slug ascent and processes of fragmentation. This study suggests that an increasing maturity of magma in Stromboli's shallow

conduit feeds back to reduce the intensity of explosions, whereas a steady flux of LD magma favors more powerful explosions.

4.1 Introduction

Stromboli volcano, Italy (Figure 4.1), is well-known for intermittent and mild explosive eruptive activity. The first reports of activity at Stromboli date to the 4th century B.C., and the current pattern of eruption has persisted without long breaks or changes since at least 600 A.D. (Rosi et al., 2000). Typical activity at Stromboli consists of continuous non-explosive degassing that is punctuated by mild explosions of crystal-rich basaltic scoria and/or ash ejected to heights of 100-200 m. Explosions generally occur at a frequency ranging from three to twelve times per hour, and occur from a small number of long-lived vents (Washington, 1917) within three active craters (Northeast, Central, Southwest; Figure 4.1). Several decades of intense research have created a convincing general model to explain this style of eruption (Blackburn et al., 1976; Wilson, 1980; Vergniolle and Jaupart, 1986; Jaupart and Vergniolle, 1988; Jaupart and Vergniolle, 1989; Parfitt and Wilson, 1995; Parfitt, 2004), that is consistent with evidence from seismic (Chouet et al., 1999; Chouet et al., 2003; Marchetti and Ripepe, 2005), infrasound (Ripepe and Marchetti, 2002), and thermal (Harris and Stevenson, 1997; Ripepe et al., 2005a) studies at Stromboli. On a longer time scale (i.e. decades to centuries) at Stromboli, typical behavior of this type alternates with powerful paroxysms (e.g. 5 April 2003) and episodes of lava effusion (e.g. December 2002 to July 2003; Barberi et al., 1993; Calvari et al., 2005; Ripepe et al., 2005a; Calvari et al., 2006).

There was clear variation in the pattern of typical mild explosions at Stromboli in 2002. Small scale fluctuations were manifested as shifts in clast ejection height, predominant clast size, and

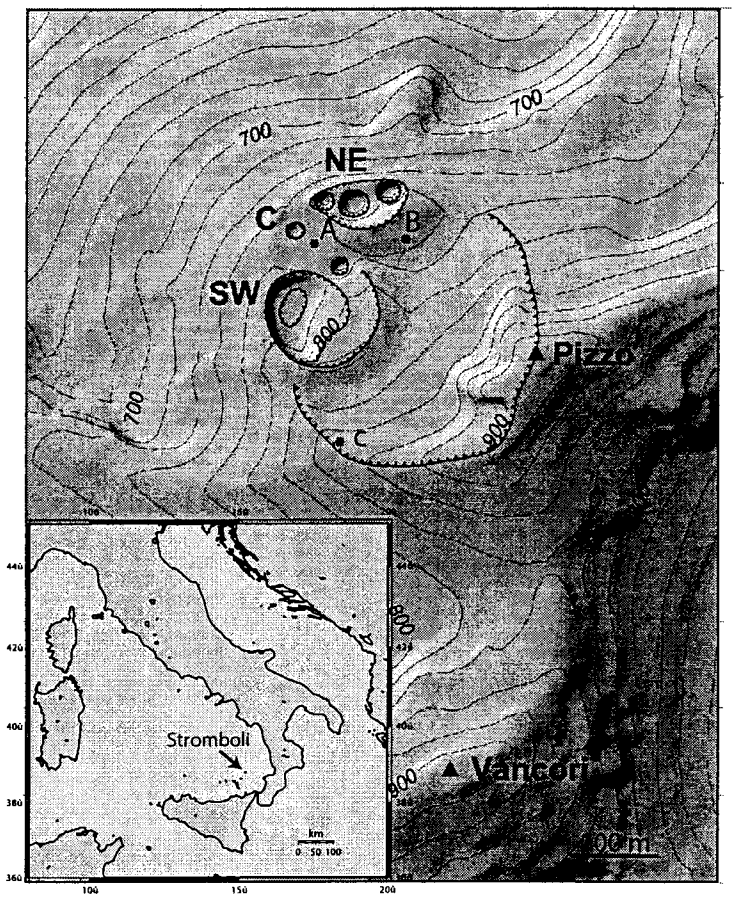

Figure 4.1 Map of Stromboli's vents and craters (NE = Northeast, C = Central, SW = Southwest). A and B are locations of sample collection in May 2002. C is location of sample collections in September/October and December. Pizzo is a point of observation. Vancori is the highest point on Stromboli island. Inset is a location map of Italy showing location of Stromboli. DEM is courtesy of Anthony Finizola.

the frequency of explosions. This variation is common at Stromboli and has been documented to occur on time scales ranging from minutes through months (e.g. Ripepe et al., 2002; Patrick et al., in press). Despite intensive study at Stromboli in recent years, the cause of such fine scale variability in eruptive pattern is not well understood. This paper is one of a series focusing on those influences that fine-tune this pattern of typical Strombolian eruptions (Lautze and Houghton, 2005; Patrick et al., in press) and investigates a probable link between the rheological properties of magma resident in the shallow conduit (inferred from textures of the ejecta) and the pattern of explosions at Stromboli during three intervals of typical behavior recorded in 2002. Contrasts are identified among the ejecta from a period of weak, ash-rich, and infrequent explosions (May 2002), a phase of powerful, frequent, spatter-rich explosions (September/October 2002), and a time of powerful explosions just preceding a months-long effusive phase (December 2002).

4.2 Background

4.2.1 Variability in intensity and style of 'typical' explosions at Stromboli

Strombolian explosions are modeled as the rapid, decoupled ascent and bursting of one or more large bubbles or slugs of bubbles (dm- to m-scale) at a static free-surface of fluid melt in the shallow conduit (Blackburn et al., 1976; Jaupart and Vergniolle, 1989; Parfitt and Wilson. 1995; Parfitt, 2004). At Stromboli, seismic data indicate that rapid bubble/slug expansion (James et al., 2004) begins ~250 m below the active crater terrace (Chouet et al., 2003; Ripepe et al., 2005a).

Variability in this explosive behavior takes two forms: style and intensity. Chouet et al. (1999) defined two styles at Stromboli, linked to the grain size of the ejecta: type 1 spatter/scoria - dominant explosions, and type 2 ash-dominant explosions (see also Patrick et al., in press) and

these have been related to contrasting forms of geophysical signal (Ripepe et al., 1993, Ripepe and Gordeev, 1999). Variations in the intensity of explosions, as reflected in contrasts in ejected mass and column height, are only weakly coupled to changes of style, i.e., the strongest explosions are generally spatter-rich, though Patrick et al. (in press) show that there is a considerable overlap in intensity between the two styles.

4.2.2 Textural studies

Quantitative data regarding the number, shape, and size distribution of bubbles in pyroclasts yield insight into the degassing history of magma prior to eruption (Klug et al., 2002; Polacci et al., 2003; Klug and Cashman, 1994). A single bubble may mature via a four stage process: (i) nucleation, (ii) free growth (through diffusion and decompressional expansion), (iii) bubble-bubble interaction and coalescence and (iv) collapse or escape of the bubble from the melt phase (Cashman and Mangan, 1994). In many eruptions, each stage is likely to be protracted so that early-formed bubbles grow and coalesce as new bubbles nucleate (Blower et al., 2002). Each process imparts a distinctive signature on the distribution of vesicle sizes, with the final form of a vesicle size distribution (VSD) reflecting both the duration and rate of each of these processes (Blower et al., 2001). In general, a high bubble number density is associated with a high rate of magma decompression (e.g. rapid nucleation), while a low number density is linked to slower or staged ascent (Cashman and Mangan, 1994). In mature and/or low viscosity melts, low number densities can also result from advanced coalescence and outgassing. The rheology of the melt phase changes significantly during the period of vesiculation and degassing.

Scoria ejected from Stromboli volcano over ~28 hours in September/October 2002 exhibit two distinct textures that reflect contrasting degassing histories, and late-stage, dynamic mingling of

these magmas (Lautze and Houghton, 2005). This paper examines the nature and the complex rheology of Stromboli magma over a longer time period, and considers the potential for the changed rheology to influence eruption dynamics.

4.2.3 Activity at Stromboli in 2002-2003

Activity was unusual in that it included a major paroxysm, an effusive phase, and intervals of typical explosive activity (Calvari et al., 2005a; Calvari et al., 2006; Ripepe et al., 2005a). We focus only on the last. From January through June 2002, relatively low intensity activity at Stromboli was characterized by infrequent and relatively weak, often ash-rich explosions (INGV-Catania). An increase in the frequency and intensity of events began in June, with a second increase occurring in late September (Figure 4.2; Alean et al., 2005). Activity reports (INGV-Catania) indicate that September to December was a period of high activity manifested as alternating weak and powerful scoria-rich explosions at the NE and SW craters. The magma's free surface was at a very high level during at least the later part of this time, and a lava overflow from the rim of the Central crater occurred in November (Bonaccorso et al., 2003; Calvari et al., 2005). Explosions then increased in both frequency and intensity in early December (Calvari et al., 2005). On 28 December, the wide fan-like shape of explosions at the NE crater suggested magma at depths very close to the crater rim, and at ~18:30 local time (= GMT + 1) explosions ceased, a ~300 m long fissure opened at the northern base of the NE crater, and an ~8 month long effusive phase commenced (lasting through July 2003; Bonaccorso et al., 2003; Ripepe et al., 2005a; Calvari et al., 2005). The effusive phase was interrupted by a powerful paroxysm on 5 April 2003 (Ripepe et al., 2005a; Calvari et al., 2006).

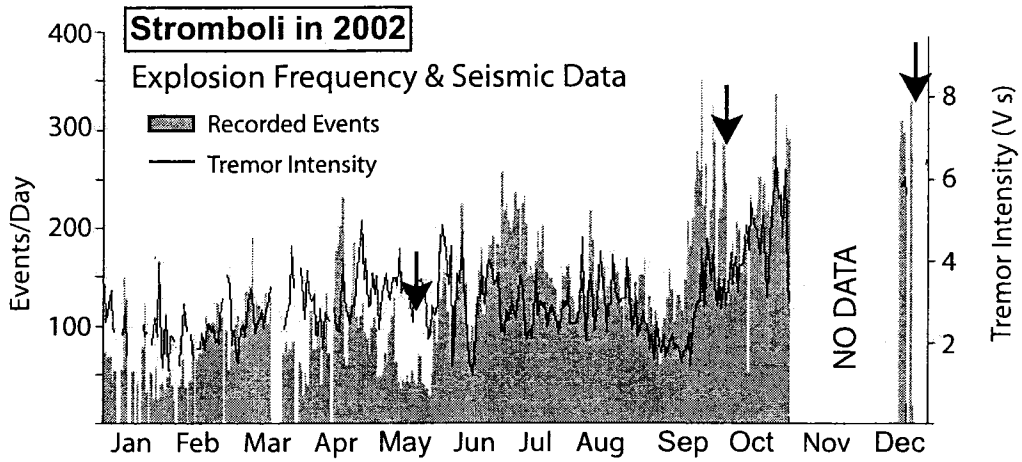

Figure 4.2 Plot of explosion frequency and tremor intensity at Stromboli in 2002. Arrows represent three sample collection times. Note the low event frequency January through May, followed by two cycles of waxing activity beginning in June and September. Graph modified from Alean et al. (2005).

4.3 Methods and Data

4.3.1 Sampling, Activity and the Ejecta

Our samples were collected at locations shown in Figure 4.1. In May, explosions at both the NE and SW craters were infrequent and ash-dominant. Our sample from May consists of five lapilli that were ejected during 18 and 22 May and fell into one of two 30 x 60 cm aluminum bins placed within 20 m of the NE crater rim (at locations A and B, Figure 4.1). During intermittent logging of the activity over these 4 days, an average of 4 ash-rich explosions per hour were observed at the NE crater, with a combined total of 1 to 15 explosions per hour at the NE and SW craters (J. Bailey, pers. commun., 2002).

Conversely, frequent and scoria-rich explosions during September/October allowed collection of large numbers of lapilli. This study focuses on a sample of 200 lapilli from multiple explosions that occurred between ~14:00 30 September and ~15:15 1 October (Lautze and Houghton, 2005), and which collected in a bin placed at location C (Figure 4.1). Eruptive activity was logged for 3.5 hours during the collection period on 30 September, and for 4.25 hours (following the collection period) on 1 October (A.J.L. Harris pers. commun., 2002). On both afternoons, moderate to powerful scoria-rich explosions dominated at the SW crater, while weaker and ash-rich explosions occurred at the NE crater. NE crater ash pulses were 10-100 m high, with fallout of larger tephra restricted to the crater terrace (i.e. within 20-30 m of source). Ejecta from the SW crater repeatedly reached elevations > 300 m and occasionally 400 m above the crater rim. Lapilli fell frequently on "Pizzo" Sopra la Fossa (~300 m from source), and we observed lapilli fall on Vancori (~150 m above and >1 km W of source; Figure 4.1) from the largest explosions. On the afternoon of 30 September, 13 events per hour occurred at the SW crater (c. 2 and 6 events per hour were observed over the same time interval at the Central and

NE craters, respectively). An increase in explosive intensity was observed between the afternoons of 30 September and 1 October, so it is likely more of the sample is from 1 October. Direct observations of the distribution of lapilli fall in the vicinity of the collection bin suggest that each large explosion contributed 1 to 3 lapilli to the total sample.

The December 2002 sample consists of 100 lapilli deposited at location C. The lapilli were collected by Marco Piermattei and Maurizio Ripepe (Università di Firenze) in the first week of January 2003, and are inferred to be from explosions that occurred on December 28th (as no further explosive activity occurred between 28 December 2002 and March 2003; Calvari et al., 2005). The very recent nature of the lapilli was determined from their position on the surface above a layer of fresh ash and external features such as sheen and preservation of delicate texture (M. Piermattei, pers. commun., 2005).

Scoria from the three time periods appear relatively uniform in hand specimen. These ejecta are metallic gray (September/October) to black (May, December), have an irregular, blocky morphology, and a delicate, web-like to ragged microtexture.

4.3.2 Bulk Density/Vesicularity

The bulk density of each lapillus was measured using methods described by Houghton and Wilson (1989). The vesicularity of each clast was calculated from the bulk density using a dense rock equivalent (DRE) value of 2750 kg/m^3 for Stromboli magma (Barberi et al., 1993). The density data for the September/October and December samples show comparable distributions in the form of a unimodal peak with a tail of denser clasts, but with a shift to a higher density range in December (Figure 4.3). Narrow density distributions with well-defined peaks are thought to indicate that the magma fragmented over a narrow vesicularity range, whereas

May 2002

clast	density	vesic
a1	0.91	67.0
a2	0.97	64.8
a3	1.07	61.2
a4	1.22	55.6
a5	1.35	50.8

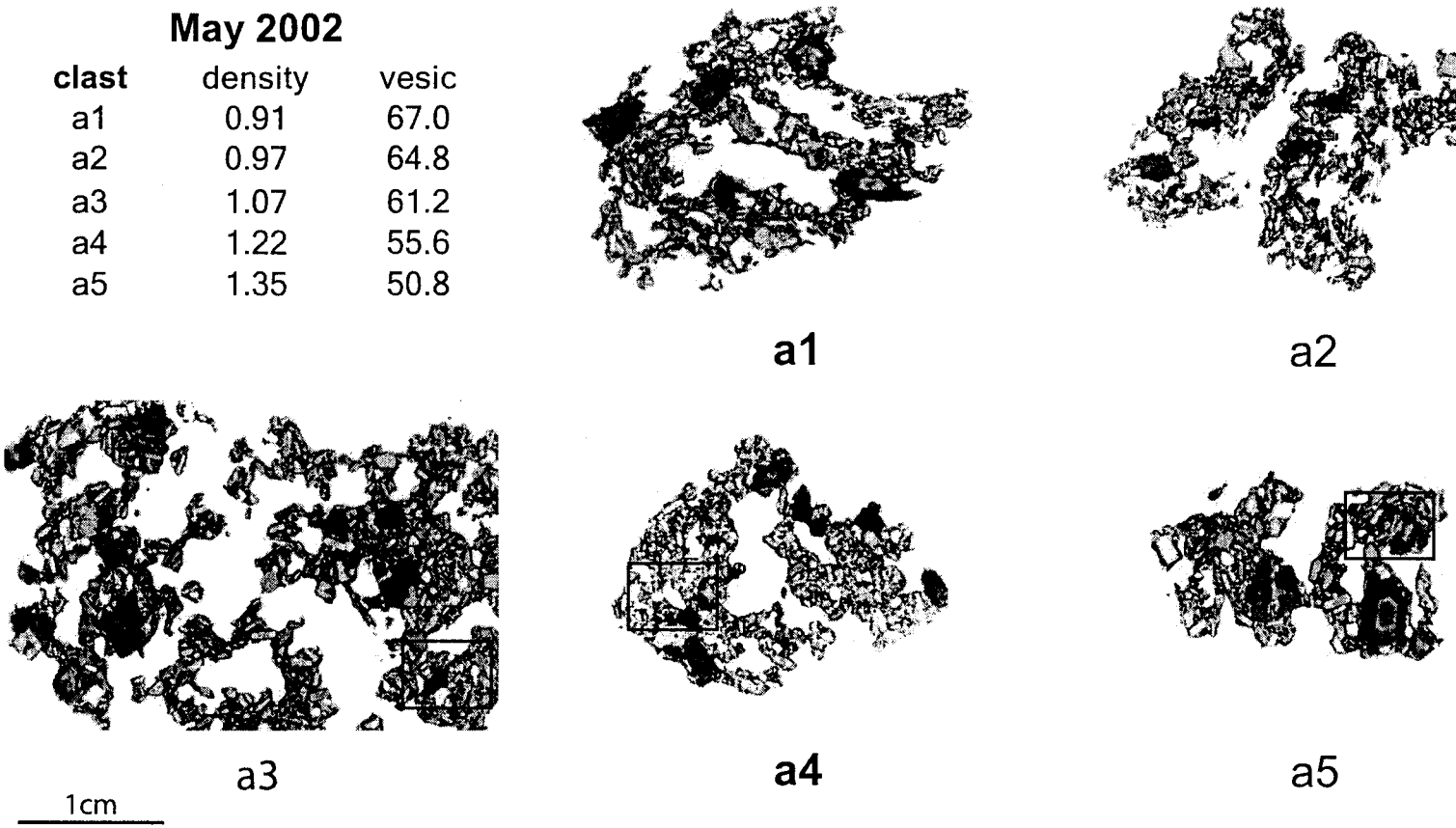

Figure 4.3 Density data for each lapillus and scanned images of selected lapilli for each sample. (a) May: table of density and scanned image for each lapillus in sample. (b) and (c) show plots of density data and scanned images of select clasts in September/October and December samples, respectively. All images are shown at same scale. Numbers on density plot refer to numbers below each scanned image. Boxes on certain scanned images are approximate locations of backscatter electron (BSE) images shown in Figure 4.4. Numbers in bold refer to clasts on which quantitative vesicle analysis were performed (Figure 4.5). Note the shift to higher density of ejecta from September/October to December.

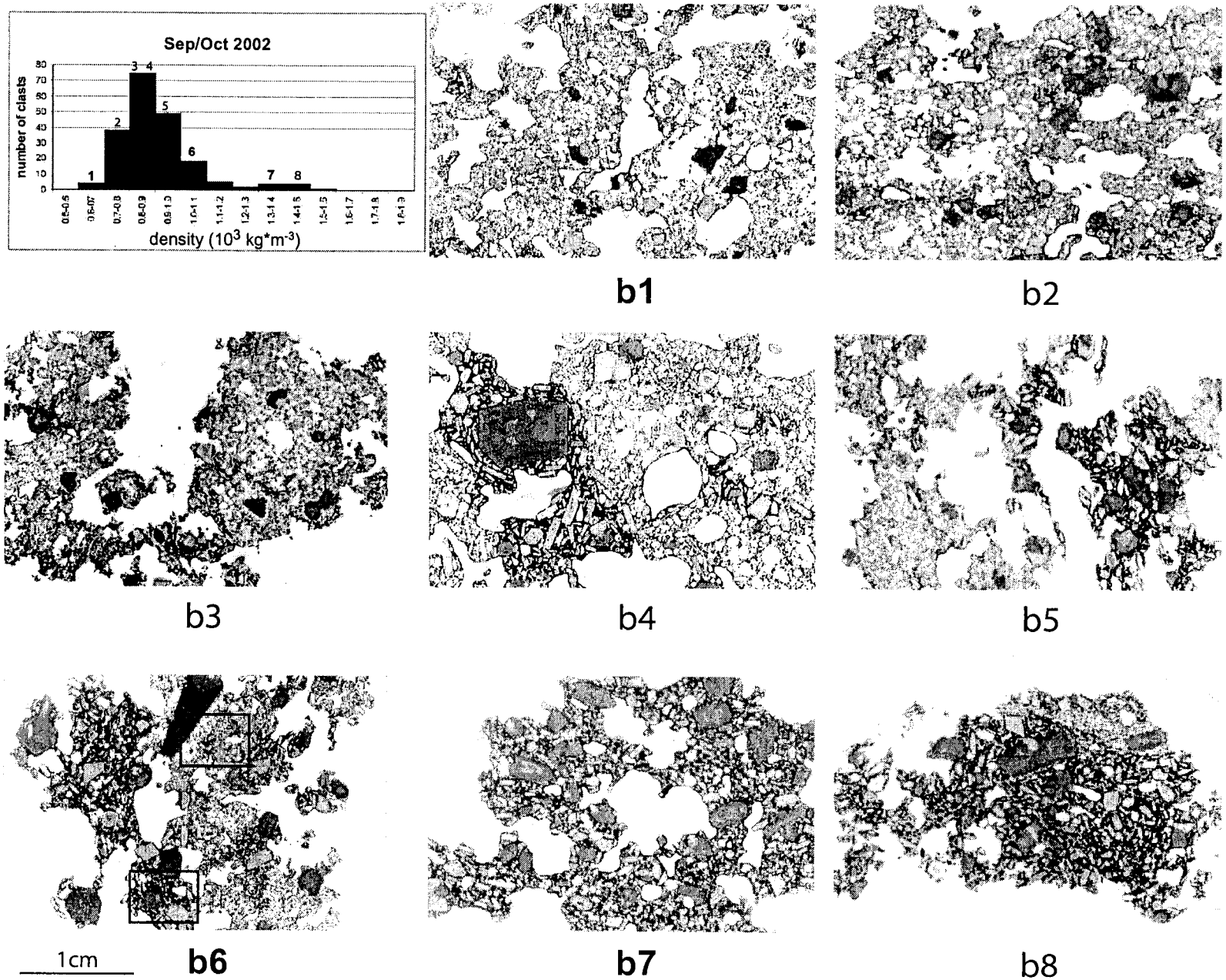

Figure 4.3(b)

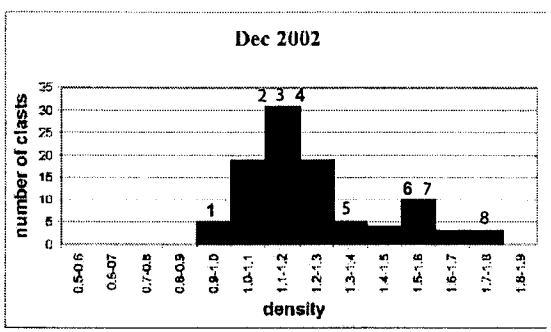

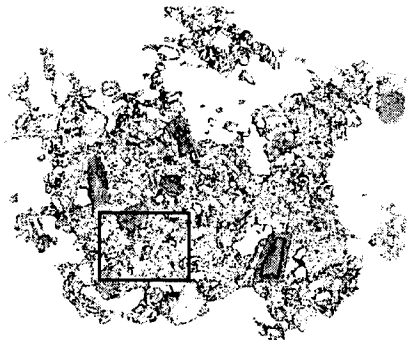

c1

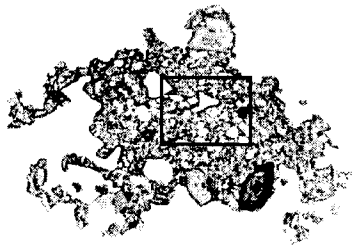

c2

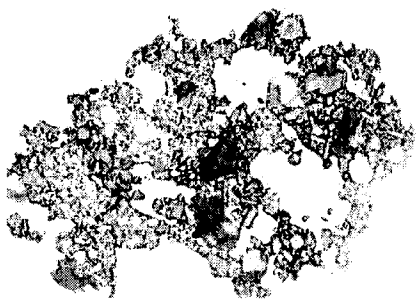

c3

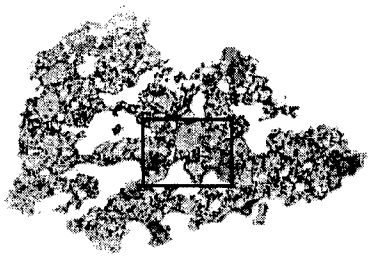

c4

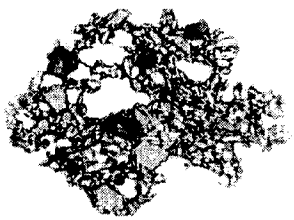

c5

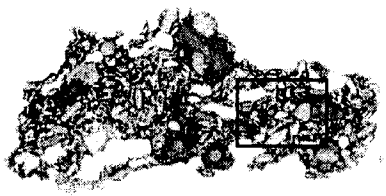

c6

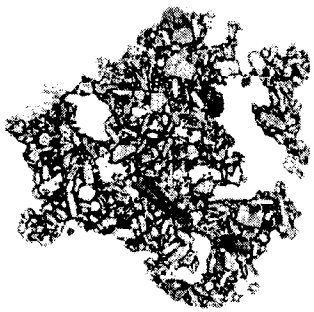

c7

c8

1cm

Figure 4.3(c)

broadly unimodal or polymodal distributions represent more complex vesiculation patterns commonly involving extended and contrasting patterns of magma ascent and fragmentation (Mangan et al., 1993; Houghton et al., 2004; Adams et al., in press). The form of the distribution for the September/October and December samples would suggest a relatively uniform vesiculation history for the majority of the ejected magma, however further observations show that several clasts are composites of two magmas with different degassing histories. The tail of denser clasts represents the presence of a small amount of crystal-rich and outgassed magma. The distribution of density values for the May sample (five lapilli) is not representative and hence not reliable, though the values are useful for comparison. The mean bulk density and corresponding vesicularity from the May, September/October and December samples, respectively, are 1091 kg/m^3 ± 183 and 60 % ± 7; 896 kg/m^3 ± 155 and 67 % ± 6; 1231 kg/m^3 ± 217 and 55 % ± 8. Note that the average bulk density increases from September/October to May to December.

4.3.3 Petrography

The density data given in Figure 4.3 served as a filter to select clasts for petrographical analysis. 1200 dpi scans of the selected lapilli are shown in Figure 4.3. Clasts are numbered in order of increasing density, with the numbers below each image corresponding to the numbers on the respective density distribution. Note that clasts a1-a5 were ejected in May, b1-b8 in September/October, and c1-c8 in December. All images are shown at the same scale; scans with large rock areas (e.g. a4, b1) have been cropped.

The Stromboli 2002 lapilli are highly porphyritic (10-40 vol %) and highly vesicular (40-80 vol %). On a vesicle-free basis, phenocrysts comprise 25 to 50 % of the rock, with the order of

abundance plagioclase > clinopyroxene > olivine. Abundant plagioclase crystals are euhedral to subhedral and vary gradationally in size from ~5 mm to sub-mm. Clinopyroxene crystals are 5-10 mm and generally subhedral. Olivine crystals are 1-5 mm, and subhedral to anhedral. The vesicles are dominantly spherical to sub-spherical, 0.1-3 mm in diameter, with a sparser population of sub-spherical to irregularly-shaped bubbles that are ~1 mm to >1 cm. The phenocrysts do not appear to serve as a nucleation point for vesicles; however bubbles are in some cases clustered between or bent around crystals (Figure 4.4).

4.3.4 Microtextures

4.3.4.1 Observed Textural Variation and Physical Mingling

Lautze and Houghton (2005) discussed the presence of fine-scale mingling between two physically distinct magmas in the September/October sample. This study focused on b1, b6, and b7 as representative of low density (LD), mingled (MD), and high density (HD) clasts, respectively. The May and December samples include, in addition, pyroclasts with a transitional texture (TT), of which a4 and c4 demonstrate the clearest examples (Figure 4.3). The higher magnification images in Figure 4.4 enable a closer comparison of these textures.

The LD and HD textures are visually distinctive. LD texture consists of clear-to-transparent pale brown glass, with the highest number density of small- to medium- sized spherical bubbles and larger, irregularly shaped bubbles. HD texture has a dark brown glass matrix, relatively few small spherical bubbles, and also large, irregular bubbles. The transitional (TT) clasts characteristically have a honey-colored glass matrix, an intermediate number of subspherical bubbles, and the continued presence of large bubbles (Figure 4.3). Lautze and Houghton (2005)

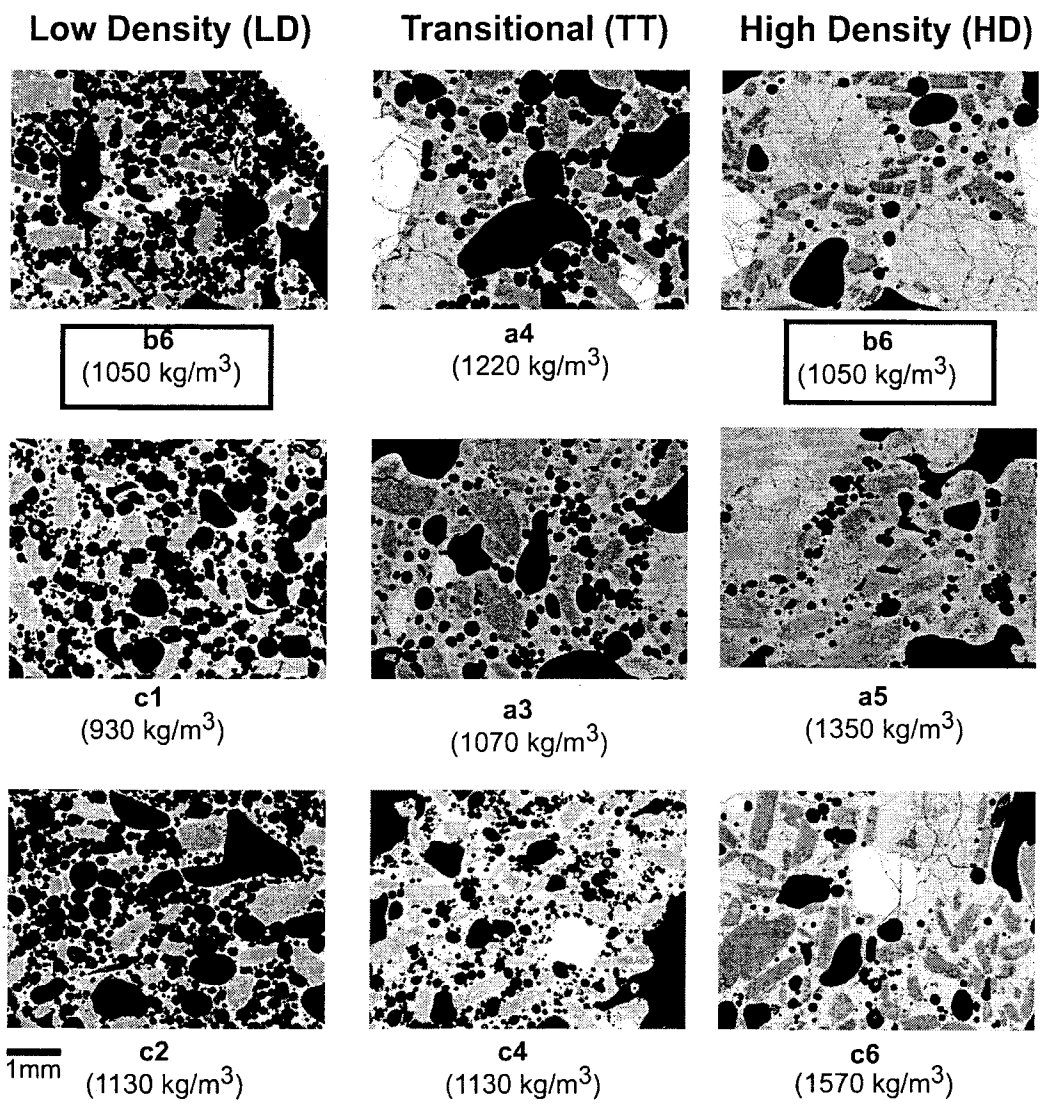

Figure 4.4 Backscatter electon (BSE) images at 25x magnification chosen to highlight the diversity among the low density (LD), transitional (TT) and high density (HD) textures. The bold notation below each image refers to the lapillus shown as a scanned image in Fig. 4.3, and the number in parenthesis is the bulk density of each lapillus pictured. Boxes identify lapilli from Lautze and Houghton (2005).

show that the glass chemistry is identical among scoria with HD and LD textures, and we assume all scoria in this study have the same melt chemistry.

Note that while mingling between HD and LD textures in a single clast is common (i.e. b2-b6, c1-c3), there does not appear to be any mingling associated with the transitional magma. The only clast dominated by LD magma (b1) has a density < 700 kg/m^3 and clasts of HD magma have densities >1300 kg/m^3 (e.g. a5, b7-8, c5-8). The density range between 700 and 1300 kg/m^3 includes both, a) clasts of TT texture (e.g. a1-a4, c4) and b) mingled HD-LD clasts (e.g. b2-b6, c1-c3).

4.3.4.2 *Quantitative Analysis of Mingling Forms*

In order to evaluate the dynamics of the mingling process among HD and LD, a procedure to analyze the size and shape of the mingled domains was devised. This analysis included clasts b1-b6 and c1-c3. Individual domains tend to be irregularly shaped, vary in size, and are delineated either by sharp borders with the contrasting texture or by large (> 2 mm) bubbles. To measure the size of individual domains, Adobe Photoshop was used to outline each region of either HD or LD on the scanned images of clasts b1-b6 and c1-c3 (Figure 4.3). Scion Image software was used to obtain the area of each domain. Groundmass, crystals, and bubbles < 2 mm were included in this analysis. Large bubbles and crystals not readily attributed to a given domain were excluded.

Between 9 and 20 total (HD + LD) independent domains on each image were identified. Combining all data, the minimum domain area is 0.10 mm^2, the maximum is 417 mm^2, and the average is ~32 mm^2 (Table 4.1). The average size of LD domains is greater than that of HD (56 versus 18 mm^2), although their size ranges are comparable. Data for each sample show that the

Table 4.1 Dimensions of mingled regions in mm^2

TOTAL					
ave(all)	32	ave(HD)	18	ave(LD)	56
min (all)	0.10	min(HD)	0.10	min(LD)	0.26
max(all)	417	max(HD)	379	max(LD)	417
SEPT/OCT					
ave(all)	38	ave(HD)	21	ave(LD)	65
min (all)	0.10	min(HD)	0.10	min(LD)	0.35
max(all)	417	max(HD)	379	max(LD)	417
DEC					
ave(all)	18	ave(HD)	11	ave(LD)	29
min (all)	0.16	min(HD)	0.16	min(LD)	0.26
max(all)	188	max(HD)	92	max(LD)	188

Notes: Sept/Oct includes data from clasts b1-b6.
December includes data from clasts c1-c3.
Total includes data from both time periods.
Separate data is also given for the HD and LD zones.

average and maximum domain size in December is significantly smaller than in September/October (Table 4.1). This is likely influenced by the fact that sizes of the December lapilli are smaller.

4.3.4.3 Proportion of Each Texture Erupted

To evaluate the relative amounts of HD, LD and TT ejected during each sample period (i.e. May, September/October, December) Adobe Photoshop and Scion Image software were again used to record the total area of each magma type in each image shown in Figure 4.3. As before, this analysis excluded those large bubbles and phenocrysts that could not be attributed to a specific domain in mingled clasts. The total (bulk) fraction of each melt type erupted (Table 4.2) was obtained by multiplying the fraction of HD, LD, and TT measured on each thin section by the number of clasts in the equivalent density bin, and then summing these fractions over the entire sample. An approximate erupted dense rock equivalent (DRE) proportion was obtained by correcting for the measured vesicularities of b1 for LD magma, c4 for TT magma, and c8 for HD magma.

This analysis shows that the most LD texture is erupted in September/October; the most TT texture in May; and the most HD texture in December (Table 4.2). Note that no LD magma is observed in the May ejecta, and no TT magma is observed in September/October. Specifically, in the May sample, clasts a1-a4 are composed entirely of TT, and a5 is composed entirely of HD. The September/October clast b1 is the only clast composed dominantly of LD magma (85%), clasts b2-b6 are mingled composites of the magma types in varying proportions, and b7-b8 are entirely (or nearly entirely) HD magma. In December, clasts c1-c3 are mingled composites of HD and LD, c4 is dominantly TT, and c5-c8 are composed of HD magma.

Table 4.2 Proportion of each magma type erupted

	Fraction HD	Fraction LD	Fraction TT	
May	0.37	0.00	0.63	BULK
Sept/Oct	0.50	0.50	0.00	
Dec	0.56	0.32	0.12	
May	0.48	0.00	0.52	DRE
Sept/Oct	0.67	0.33	0.00	
Dec	0.70	0.20	0.09	

4.3.5 Quantifying vesicle populations for LD, TT, and HD textures

4.3.5.1 Vesicle Volume Distributions

To assess typical vesicle volume distributions (VVDs) associated with each texture, we used clasts b1 and c1 to represent LD texture, clasts a1 and c4 to represent TT texture, and clasts b7 and c6 to represent HD texture. Data for mingled clasts were excluded because the size distribution in these cases is a composite of HD and LD textures. A total of 11 to 16 images per clast were obtained at multiple magnifications in order to account for the range of vesicle sizes. These images included the 1200 dpi scan shown in Figure 4.3, and multiple backscatter electron (BSE) images at 25 (or 20)x, and 100x magnifications (attained using the UH Manoa JEOL-5900LV Scanning Electron Microprobe (SEM) operating at 20 kV accelerating voltage and 1 nA beam current). Given the limited rock area per thin section, it was not always possible to account for the largest bubble population (c. > 7 mm) in a statistically viable manner. For clasts b1 and b7 it was possible to expand the surface area using two further scans of additional cut faces through the clast on which only bubbles with equivalent diameters 2-10 mm were measured.

The scanned and SEM images were manually processed following techniques described by Adams et al. (in press). Incompletely coalesced or interconnected bubbles were separated by adding a line of minimum thickness (2-pixels), phenocrysts were highlighted, and any thin section impurities were erased. Two binary files for each image were obtained: 1) bubbles and white background, and b) phenocrysts and white background. The area of every vesicle and phenocryst in each image was measured from these binary files in Scion Image.

Following Adams et al. (in press), the image reference area (A_i) was then calculated by subtracting the area of phenocrysts and the area of incomplete (or edge) vesicles from each

image area. The diameter of an equivalent circle was calculated using the area of each complete vesicle (invoking a circular/spherical approximation for bubble shape). A total reference area per magnification (A_t) was calculated by summing the reference area of all images of a given magnification, and the vesicle equivalent diameters for each magnification were grouped and binned using a geometric scale of 10^{-1} following Sahagian and Proussevitch (1998). The areal number density (N_A) was then calculated for each bin, i.e. number of bubbles of a given cross-sectional diameter per reference area (A_t), and cumulative areal number densities (N_{Atot}) for each clast (Table 4.3). The N_A values for each bin were converted to volumetric number densities (N_V) using stereology equations described in Sahagian and Proussevitch (1998). These steps account for the probability that a vesicle will be intersected at less than its maximum diameter. Vesicle volume distributions (VVDs; Figure 4.5) for the analyzed clasts were plotted using the N_V values for each bin.

The VVDs for the three textures are bimodal, with a small vesicle population from 0.02 to 1 mm and a large vesicle range from 3 to 10 mm (Figure 4.5). In general, the small vesicles are spherical to sub-spherical, while the large bubbles exhibit irregular forms (Figures 4.3, 4.4). The large vesicles make up 35-85 % of the total vesicularity and also align preferentially along the boundaries between HD and LD regions in mingled clasts (e.g. b4, b6, c3; Figure 4.3). In a later section we use these vesicularity data in viscosity calculations to speculate on the extent to which bubbles of this dimension are coupled or decoupled from the adjacent melt.

A change from LD to HD via TT is recorded in the relative proportions of the two dominant vesicle size populations. The larger bubble population is present in all clasts, but strongly dominates the volume fraction of vesicles in clasts with HD texture. The smaller vesicle population progressively declines from LD to HD. These data are used to infer contrasting

Table 4.3 Quantitive Vesicle Data

clast	type	sample	N_{Atot} (mm^{-2})	N_{Vtot} (mm^{-3})	N^m_{Vtot} (mm^{-3})	n (mm^{-4})
b1	LD	S/O	2.9×10^1	4.2×10^2	1.7×10^3	4.5×10^4
c1	LD	Dec	6.7×10^1	1.2×10^3	3.4×10^3	1.3×10^5
a1	TT	May	3.0×10^1	3.3×10^2	9.9×10^2	1.9×10^4
c4	TT	Dec	6.9×10^1	1.3×10^3	3.2×10^3	1.4×10^5
b7	HD	S/O	7.1	9.3×10^1	1.9×10^2	8.7×10^3
c6	HD	Dec	2.3×10^1	4.2×10^2	7.4×10^2	4.5×10^4

Notes: N_a, N_v, n values are sum of bins from 0.02 to 10 mm

N^m_v is calculated using the vesicularity calculated from measured bulk density.

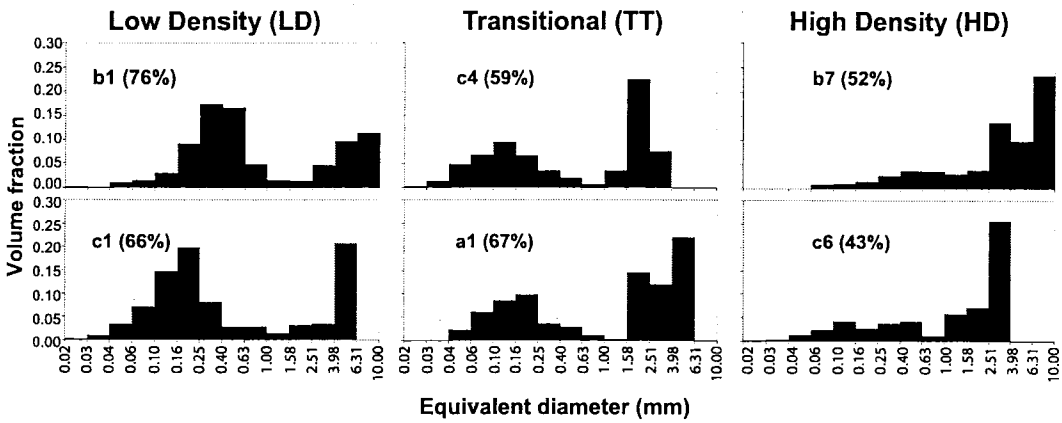

Figure 4.5 Vesicle volume distributions (VVDs) for clasts b1 and c1 to represent the low density (LD) texture, c4 and a1 to represent the transitional (TT) texture, and c6 and b7, to represent the high density (HD) texture. The numbers in parenthesis are the bulk vesicularity of each clast. Note the shift from LD to HD via TT with respect to the volume fraction of rock composed of bubbles within the small (0.03-1 mm) population.

residence times for the various magma types. The minimum vesicle size is ~25 microns (e.g. clasts b1, c1, c4, c6), and bubbles smaller than 50 microns make a negligible contribution to the total vesicularity of all clasts (Figure 4.5). This is consistent with the possibility that ~25 microns approximates to the minimum stable size of bubbles in basaltic melt (Sparks, 1978; Lautze and Houghton, 2005).

4.3.5.2 *Vesicle Number Density*

A summation of the N_V values for each bin yields a clast's cumulative volumetric number density, i.e. number of vesicles per unit volume, or N_{Vtot} (Cashman and Mangan, 1994). The N_{Vtot} values refer to the number of vesicles per unit volume of clast matrix (i.e. clast volume minus phenocrysts). Subtracting the volume of vesicles (measured from bulk density) from the matrix volume yields a melt-referenced cumulative volume number density (N^m_{Vtot}), which corrects for the misleading effects of the vesicle population on number density (Klug et al., 2002). The vesicle population ***n*** (in Table 4.3) refers to the number of vesicles in each size increment per unit volume (mm^{-4}).

The volumetric number densities (N_{Vtot}) and melt-corrected number density (N^m_{Vtot}) values for all clasts cluster in the range of 10^2 to 10^3 mm^{-3} (Table 4.3). Clast c1 (LD) has the highest N^m_{Vtot}, and values generally decrease through the clasts with TT (a1, c4) and HD (b7, c6) textures. For all textures, N_{Vtot} and N^m_{Vtot} values are significantly larger in the December ejecta. This can be explained by the absence of the larger vesicle population in these selected clasts.

4.4 Summary

4.4.1 Similarities among HD, TT, LD textures

4.4.1.1 Bubble populations and form of mingling

The uniform spherical shape of bubbles in the smaller size population (< 1-2 mm) is distinctive, and indicates simple radial growth. The lack of a stretched fabric within this size population implies conditions of low shear and negligible acceleration of magma prior to fragmentation (Bagdassarov and Pinkerton, 2004). It also suggests a lack of post-fragmentation deformation, as molten clasts would be subject to high levels of shear during aerial flight and on impact. This, together with the ragged form of the lapilli, indicates nearly instantaneous quenching of these lapilli at or just after fragmentation, which distinguishes these Strombolian ejecta from achneliths, a common product of Hawaiian fire fountaining (Wentworth and MacDonald, 1953). Bubbles > 2 mm tend to have more irregular forms in all 2002 clasts, indicating that they are the products of coalescence. As the small bubble population declines in significance from LD through to HD, these coalesced bubbles make up an increasing proportion of the total vesicularity.

The mingling forms we observe are rather uniform. The sinuous form of the border between zones and the generally nebulous form of the zones themselves suggests that the mingling process is dynamic. The sharpness of the border between HD and LD magmas is evidence for the absence of the onset of a homogenization, or mixing process. The pattern of large bubbles aligned along the boundary between zones of HD and LD texture, such as in clasts b4-b6 and c3 (Figure 4.3), suggests that these bubbles may be partially decoupled from the melt phase.

4.4.1.2 *Sparse microlites*

The 2002 Stromboli ejecta have a glassy groundmass with few microlites. The absence of a microlite-rich groundmass in Stromboli's black scoria implies that those processes which cause microlite crystallization--cooling (i.e. a temperature decrease), and effective undercooling (i.e. a reduction in the liquidus temperature through volatile exsolution; Cashman and Blundy, 2000)--must be muted at Stromboli. While undercooling has been cited as less pronounced in basalts relative to more evolved compositions (Spera, 2000), it is surprising that microlite crystallization via cooling does not occur in the longer-resident shallow conduit magma. This, in itself, may be a limiting factor in determining maximum shallow residence time. It is worth noting that we have observed microlites in samples of both golden pumice from the 5 April 2003 paroxysm, and the December 2002 lava flow at Stromboli. Perhaps relatively high rates of ascent, as postulated for the 5 April 2003 magma (Bertagnini et al., 2003; Aiuppa and Frederico, 2004), are required to promote significant undercooling of Stromboli melt, whereas surface flowage is required to cool the melt sufficiently to enable microlite crystallization. We infer the lack of microlites in the 2002 scoria to indicate a uniform slow ascent of magma from depth under near-isothermal conditions, and the maintenance of high temperatures up until the time of fragmentation. Such maintenance of high temperatures is likely facilitated by upward thermal mixing associated with passage of the gas slugs.

4.4.2 Distinction between HD, TT and LD textures

Vesicularity data provide genetic links between the HD, TT, and LD textures. The reduction in bulk vesicularity from LD (~70-75%) to HD (~45-50%) is accommodated by a decreasing proportion of small bubbles. Of the total vesicularity, the percentage comprised of bubbles ≤

1.00 mm in diameter decreases from ~70% in LD through ~40-50% in TT to ~20-30% in HD (Figure 4.5). This shift of bubbles into the larger population from LD through to HD is explained by a slowing of bubble nucleation in parallel with continued free growth and coalescence. The lower bulk vesicularity of HD clasts is explained by extended outgassing (via escape of large bubbles) from HD magma.

The existence of small spherical bubbles (< 100 μm) in all clasts indicates that free growth of this subpopulation is occurring in the melts of all textures, but to varying extents. The dominance of small bubbles in LD clasts suggests that free growth is the dominant vesiculation process in this magma, whereas the lower bulk vesicularity and depletion in small bubbles in HD clasts indicates that outgassing was the dominant process in HD magma. These data therefore demonstrate that HD had a longer residence time in the shallow conduit relative to LD magma. VVD plots (Figure 4.5) indicate that the TT texture is a transitional state for magma in an evolution from LD and HD.

The single order of magnitude variation in number density among the HD, TT, and LD magmas is small compared with that documented within samples from Plinian basaltic eruptions, which commonly exhibit a range of three orders of magnitude (e.g. ~10^4-10^6 mm^{-3}; Sable et al., in press). This suggests that the magma of all three textures at Stromboli had relatively similar rates of early nucleation and ascent. The N_{Vtot} values for Stromboli are also larger than those published values for Hawaiian lava flows (~1 mm^{-3}; Mangan et al., 1993), and for Hawaiian reticulite (~1-10 mm^{-3}; Mangan and Cashman, 1996). This latter effect is due to extended vesicle growth and coalescence in the fountain in reticulite (Mangan and Cashman, 1996). Our data are within the lower range for the fast-rising magma that produced a subplinian phase of the Keanakako'i deposit of Kilauea volcano (~10^2 to 10^4 mm^{-3}; Mastin et al., 2004), and

slightly larger than the range observed in scoria from sustained Hawaiian fire fountains (10 to 10^2 mm^{-3}; Mangan and Cashman, 1996; Mastin et al., 2004). Thus we suggest that the early ascent rate of Stromboli's magma was between that of magma feeding the Keanakako'i eruption and magma that feeds Hawaiian-style explosions (Lautze and Houghton, 2005). We consider the textural diversity among HD, TT, and LD to be a late stage feature that is superimposed upon the similar initial ascent and degassing conditions of Stromboli magma (Lautze and Houghton, 2005). The slight decrease in N_{vtot} from HD through TT to LD (Table 4.3) can be explained by extended coalescence and outgassing of TT and HD magmas within Stromboli's shallow conduit. This is supported by VVDs for the three magma types (Figure 4.5), which indicate increasing maturity of the vesicle population from LD through TT to HD. We therefore conclude that the three magma types experienced similar conditions of early ascent and bubble nucleation, producing N_{vtot} (and $N^{m}{}_{vtot}$) on the order of ~10^3 mm^{-3}, but that a longer shallow residence for TT and especially HD magma allowed extended evolution (coalescence and outgassing) of these vesicle populations prior to fragmentation.

4.5 Conduit and Explosion Dynamics

4.5.1 Origin of Textures and Model for Mingling

Erupted magma at Stromboli is typically rich in both bubbles and phenocrysts, with the proportion of crystals and bubbles among the HD and LD magmas varying significantly (Figure 4.3). The physical changes in magma in Stromboli's shallow conduit occur as a result of two processes: 1) on-going vesiculation (bubble growth, coalescence, escape) in the intervals between the passage of bubble slugs (which transforms LD via TT to HD), and 2) mingling and mixing of LD and HD during the passage and in the wake of bubble slugs (Seyfried and Freundt,

2000). We have proposed that gas slugs are the dominant agent of mingling for Stromboli's shallow conduit, such that each gas slug brings a small volume of fresh (LD) magma into the shallow conduit as a film, or envelope, around the slug (Lautze and Houghton, 2005). During the dynamic processes of slug ascent and magma fragmentation, some LD magma is mingled with the longer resident HD and TT magmas that are passively residing in the shallow conduit (Figure 4.6), and a combination of magma types is ejected. LD magma not erupted with its parent gas slug serves to continuously replenish the shallow conduit. The bubble population in this remaining LD magma will then seek to evolve through TT toward the HD texture via free growth, coalescence, and outgassing of bubbles.

The processes of mingling and vesicle evolution compete to influence the physical properties of magma in Stromboli's shallow conduit. Mingling is likely to predominate during episodes of powerful explosions and especially high explosion frequency (parameters often correlated), when we infer that the flux of LD magma into the shallow conduit is high. During such high activity periods, relatively high mass eruption rates decrease the average residence time of magma in Stromboli's shallow conduit (considering a static level of the magma's free surface). This is thus reflected in a relatively high proportion of fresh LD magma and the appearance of abundant mingling in the ejecta. Conversely, vesicle evolution and restricted amounts of mingling can be linked with a low flux of gas-rich magma into the shallow conduit (i.e. low levels of activity). The low mass eruption rate during episodes of low activity means that the bulk average residence time of magma in the shallow conduit is long, which feeds back to enable evolution of magma towards the HD end member prior to ejection.

The sharp border between LD/HD domains indicates that this evolution process occurs at a faster rate than the mingled magmas are able to homogenize. Textural homogenization would

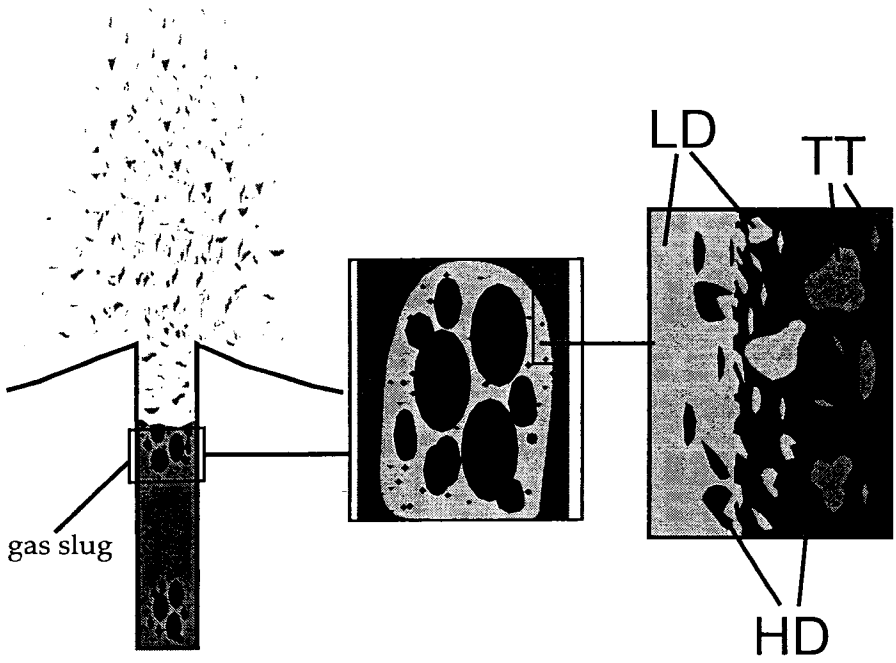

Figure 4.6 Cartoon of dynamic model adapted from Lautze and Houghton (2005). Low density (LD) magma rises as an envelope with the gas slug, and mingles with high density (HD) magma during the slug's ascent to the magma's free surface. The LD magma not erupted with its parent gas slug evolves toward transitional (TT) and high density (HD) textures within the shallow conduit.

occur due to the migration of mm- to sub-mm- size bubbles from LD to HD. Incomplete diffusion would appear as a gradational border between magma types. Given that cm-size bubbles tend to occur along the border between magma types (Figure 4.3), it is probable that HD and LD magmas independently reside adjacent to one another for amounts of time that would enable cm- but not mm- sized bubbles to migrate to the border.

4.5.2 Bulk Magma Viscosity

The viscosities of the HD and LD magmas were calculated as follows: 1) following Shaw (1972) to establish the melt (glass) viscosity (η_1) as a function of composition and temperature, 2) to account for the crystal content (η_2), applying the equation: $\eta_2/\eta_1 = (1 - \sigma)^{-1}$, where σ is the bubble corrected crystal fraction (M. Manga, pers. commun., 2005), and 3) to account for the vesicle population (η_3), applying $\eta_{3min}/\eta_2 = (1 - \alpha)^{-1}$ and $\eta_{3max}/\eta_2 = (1 + 9\alpha)$, where α is the crystal-corrected vesicle fraction (Llewellin and Manga, 2005). The compositional data for HD and LD magma are published in Lautze and Houghton (2005), and a temperature of 1100 ºC was used (Metrich et al., 2001). Table 4.4 shows the values, source, and solutions to the other parameters. This method yields an approximate viscosity range of 2000 to 2600 Pa s for LD, and 3000 to 5000 Pa s for HD magma.

These viscosity estimates for shallow conduit magma at Stromboli enable an assessment of the rise rate of small bubbles in LD and HD magmas using Stokes Law:

$$\text{bubble ascent velocity} = (2/9)(\rho_l - \rho_b)gR^2(1/\eta_m)$$

where ρ_b is the density of the bubble (~ 0), ρ_l is the liquid (melt) density [2650 kg/m^3, as calculated for the composition of b1 glass (in Lautze and Houghton, 2005) following Bottinga and Weill (1970)], g is the acceleration due to gravity, R is the bubble radius, and η_m is the bulk magma

Table 4.4 Parameters used in viscosity calculation

	Value HD	Value LD	Data source
α	0.75	0.5	image processing data (this paper)
σ	0.82	0.86	bulk vescularity data (this paper)
η_1	150 Pa s	150 Pa s	Shaw (1972)
η_2	600 Pa s	300 Pa s	M. Manga (pers. comm.)
η_{3min}	3000 Pa s	2000 Pa s	Llewellin and Manga (2005)
η_{3max}	5000 Pa s	2600 Pa s	Llewellin and Manga (2005)

viscosity (η_3). Stokes Law is valid for laminar, low Reynolds number ($Re << 1$), steady-state flow of bubbles through stationary magma, which is a suitable approximation for bubbles of diameter 1 cm or smaller. The ascent velocities for bubbles from 1 cm to 1 micron were thus calculated using the above viscosity values (Table 4.5).

4.5.3 Small Bubble Dynamics and Magma Residence Times

Given that the dominant difference between the LD and HD magma types is the number of sub-cm sized bubbles (Figure 4.4), the amount of time it would take such bubbles to travel through a domain of LD can be used to estimate the maximum residence time of LD magma in Stromboli's shallow conduit. This logic relies on the assumption that migration of sub-cm bubbles would lead to an apparent 'homogenization' or mixing of the two magma types. The values in Table 4.5 and data on average domain sizes (Table 4.1) can be used to calculate this time. Approximating a circular geometry to the average LD domain area of 56 mm^2 (Table 4.1) gives an approximate radius of ~4 mm. For the rise rates shown in Table 4.5, a 1 mm bubble will therefore rise through an average LD domain in a period of hours (90 to 120 minutes for a 4 mm radius of LD), a 0.1 mm bubble will reside within an LD domain for ~1 week, and a .01 mm bubble for nearly 2 years. Given the predominance of bubbles in the 0.1-0.5 mm diameter size range in LD (Figure 4.5), we estimate a maximum residence time of days for LD magma, compared to a minimum of seconds (when erupted with the parent gas slug). The flux of rising bubbles through the shallow conduit precludes any estimate of the maximum residence time for HD magma but it seems plausible that HD can reside within the shallow conduit from days to months.

Table 4.5 Bubble Ascent Rate (mm/min)

bubble diam. (mm)	Viscosity (Pa s) 2000	2600	3000	5000
10	4.3	3.3	2.9	1.7
1	0.043	0.033	0.029	0.017
0.1	4.3×10^{-4}	3.3×10^{-4}	2.9×10^{-4}	1.7×10^{-4}
0.01	4.3×10^{-6}	3.3×10^{-6}	2.9×10^{-6}	1.7×10^{-6}

We have previously noted that a sharp boundary exists between the HD and LD magma types, and that cm-sized bubbles often align along this boundary. The alignment of cm-sized bubbles along mingled boundaries suggests that these bubbles migrate through LD magma and slow when they reach a boundary with HD magma. Table 4.5 shows that the relative velocity difference of cm-sized bubbles in HD versus LD magma is, at most, 2.5 mm/minute. It therefore seems plausible that a mingled boundary will serve as a collection point for cm-size bubbles, before their procession into and through HD magma. Coalesced, cm-sized bubbles will rise through HD magma at a rate of 2-3 mm/min (Table 4.5). Ignoring bubble expansion and considering the time it will take a 1 cm bubble to rise through HD magma over the full depth of the shallow conduit (~150 to 250 m depending on the level of the magma's free surface; Ripepe et al., 2001a; Chouet et al., 2003) yields 34 days (at a rise rate of 3 mm/min and 150 m conduit fill) to 87 days (at a rise rate of 2 mm/min through 250 m of HD magma). This decoupling of cm-sized bubbles may provide an explanation for the continuous, passive degassing, which is documented at Stromboli (Allard et al., 1994).

In reality, the discussion in this section simplifies processes that are complex and highly dynamic. For example, the nature of LD magma at 250 m depth, versus near the magma's free surface will vary significantly (due to decompressional expansion of bubbles). A simple calculation suggests a factor of 40 times volumetric expansion of bubbles (corresponding to a factor of 3.4 increase in diameter or 12 in buoyant rise speed) will occur from 250 m depth to atmospheric pressure. The detailed modeling effort that would account for such complexities is beyond the scope of this paper. The discussion above remains useful in that it provides a context from which to consider bubble movement and magma residence times.

4.5.4 Linking magma rheology and eruption style in 2002

The relative abundances of the LD, TT, and HD magma types residing in Stromboli's shallow conduit vary with time (Table 4.2), and we expect that the resulting rheological changes (Table 4.4) influence the style of eruption. In this section we attempt to link the observed pattern of explosions in May, September/October and December with our viscosity and proportionality data.

Predicting how viscosity changes will influence eruption is not straightforward because the effect of a given viscosity change will act to influence both slug ascent rate and bubble overpressure in ways that have competing influences on explosion intensity. A lower magma viscosity (i.e. a high proportion of LD magma) will lead to an increase in slug ascent rate (Seyfried and Freundt, 2000). This can be expected to increase explosion intensity because a fast moving slug will have more (kinetic) energy available to fragment and propel ejecta out of the vent. Also, a faster moving slug might be expected to arrive at the magma's free surface with a higher bubble overpressure because it would have had less time to equilibrate during ascent. However, a relatively low viscosity conduit fill would also facilitate decompressional expansion of the gas slug during ascent (Seyfried and Freundt, 2000), therein leading to lower bubble overpressure as the slug reaches the magma's free surface and acting to decrease eruption intensity. Quantification of such parameters is again beyond the scope of this study. We consider what can be evidenced from data presented in this paper, which indicate that slug ascent velocity is a more influential parameter. This is consistent with models of bubble growth presented in Seyfriend and Freundt (2000), which suggest that significant bubble overpressures only develop in magmas with viscosities at least two orders of magnitude higher than approximated here (A. Freundt, pers. comun., 2006).

An association between relatively high viscosity conduit fill and weak explosions seems to hold during May 2002, while a link between low viscosity magma and high explosion intensity is convincing in September/October. In May, a relatively low frequency of dominantly weak, ash-charged explosions occurred, and there is an absence of LD magma in the ejecta (Figure 4.2, Table 4.2). From this it can be inferred that there was only a small supply rate of new magma into the shallow conduit in May, which would have facilitated evolution of the existing shallow magma toward the more viscous HD and TT types. In this case, relatively high viscosity conduit fill was linked with ash-rich and weak explosions, suggesting that the material properties of the relatively viscous magma influenced the fragmentation process (Figure 4.7).

September/October was a time of frequent and powerful, spatter-rich explosions, with the highest abundance of LD magma and prevalence of mingling in the ejecta. The abundance of ejected LD magma is likely to indicate a relatively large flux of new magma into the shallow conduit, which would have equated to relatively low viscosity conduit fill. The high levels of activity are also expected to correlate with high discharge rates, which would have restricted the opportunity for shallow magma to evolve toward the more viscous types. In the case of September/October, the energetic explosions and high degree of mingling are consistent with high slug ascent velocities (Figure 4.7).

December is somewhat more perplexing. Reports indicate that December was a time of powerful explosions, and the onset of the effusive eruption (on December 28) has been linked with a large flux of new magma into the shallow conduit (Ripepe et al., 2005a; Calvari et al., 2005), yet the highest proportion of mature HD magma appears in the December sample. While this at first seems counterintuitive, note that more than 30% of the analyzed December sample does consist of LD magma, and that magma was very high in the conduit just preceding the

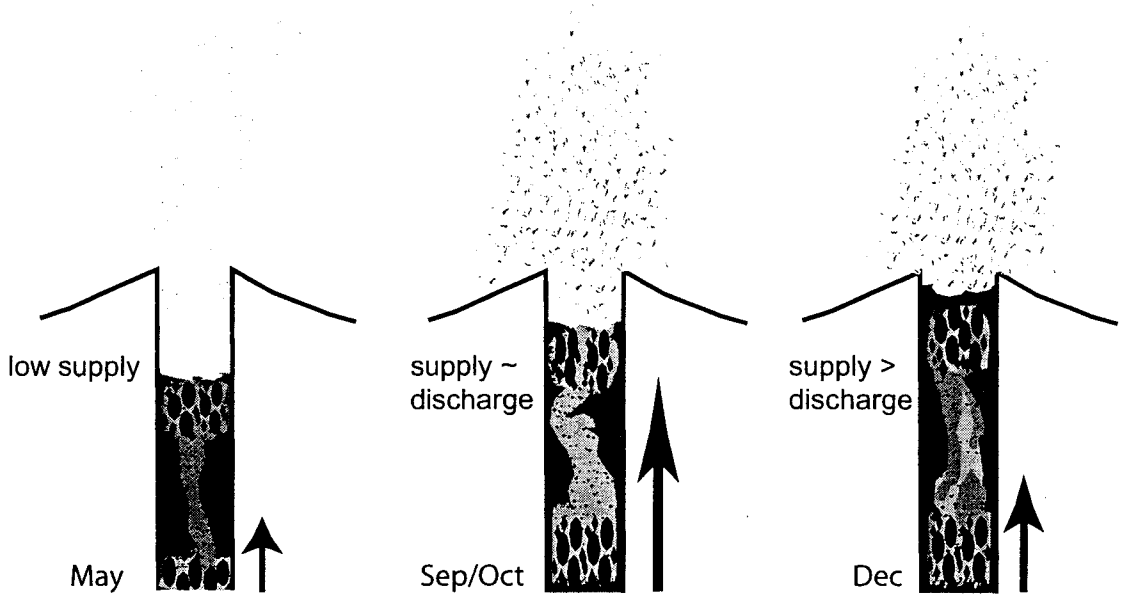

Figure 4.7 Schematic illustrating the possible variable proportions of magma types in Stromboli's shallow conduit during May, September/October, and December 2002 sample collection periods. Light gray = LD magma, dark gray = HD magma, intermediate gray = TT magma. Arrows represent gas slug velocity.

effusive phase (Bonaccorso et al., 2003; Calvari et al., 2005). If the magma's free surface was rising up to the onset of the effusive eruption, then the magma supply rate must have exceeded the discharge rate. This would allow a relatively large proportion of magma within the shallow conduit to evolve toward the HD end member, while still incorporating a significant flux of new magma into the system. If the new magma formed an annulus in the center of the conduit, for example, slugs could maintain the ability to ascend at high rates to feed energetic explosions (Figure 4.7). At the same time, a high proportion of HD magma in the shallow conduit would facilitate a 'pressurization' of the shallow conduit leading into the effusive eruption, as proposed by Calveri et al. (2005) and Ripepe et al. (2005a), given that the effusion commenced from fissure along the NE flank of the NE crater (Calveri et al., 2005; Ripepe et al., 2005a).

4.6 Conclusions

This study proposes that evolving material properties of shallow magma are a factor that can contribute to variable explosive intensity at volcanoes characterized by Strombolian eruptions. Three texturally diverse magmas at Stromboli result from a combination of on-going vesicle evolution and a mingling process that is driven by ascent of gas slugs and new melt. The vesicularity textures in samples collected over narrow time windows indicate that magma in Stromboli's shallow conduit just before any explosion has a range of residence times, likely spanning seconds to hours for LD magma, and hours to months for HD magma. The changing proportion of each magma type erupted during three phases of variable eruptive activity in 2002 suggests a link between the viscosity of shallow magma (which may vary between ~2000 and 5000 Pa s) and eruption intensity. These viscosities imply cm-size bubbles will migrate through

the shallow conduit on timescales of 1 to 3 months, and thus are potentially a major contributor to passive degassing at Stromboli.

We propose that mingling predominates during intervals of frequent, intense explosions, and vesicle evolution predominates during periods of weak, infrequent explosions. Two scenarios exist, in which, a) an increased flux of gas-rich magma permits continuing high or waxing intensity of eruption and vigorous mingling of magma types (September/October 2002), while b) a decreased supply of new magma causes waning eruption intensity and inhibits mingling (May 2002). This study of the 2002 ejecta shows that the continually shifting physical state of magma filling Stromboli's shallow conduit influenced variations in eruption intensity and style during Stromboli's spectrum of typical activity. Similar processes are likely to occur at other volcanoes characterized by Strombolian volcanism.

Acknowledgements. The authors thank Armin Freundt, Jacopo Taddeucci, and Lionel Wilson for reviews that strengthened the quality of the submitted manuscript. Sarah Fagents, Michael Garcia, and Andrew Harris also provided highly valuable reviews of a draft manuscript. John Allen, Andrew Harris, and especially Michael Manga imparted indispensable assistance with the viscosity calculations. We thank Anthony Finizola for assistance with the May lapilli collection, and Marco Piermattei and Maurizio Ripepe for collecting and sending the December sample. John Bailey, Andy Harris and Glynn Williams-Jones are gratefully acknowledged for the 2002 eruption logs, as is hospitality of Maurizio Ripepe during the field campaigns. This work was sponsored by National Science Foundation grant EAR-0207734 and an NSF Graduate Research Fellowship (to Lautze). May 2002 sample collection was funded by a Hawaii Institute of Geophysics and Planetology internal grant.

CHAPTER 5. Single explosions at Stromboli in 2002: use of lapilli microtextures to map a Strombolian fragmentation zone

Abstract. A combination of fortuitous eruptive and wind conditions at Stromboli volcano in September 2002 enabled the collection of samples of multiple lapilli from individual observed explosions. These ejecta present an opportunity to analyze the vesicularity of material ejected in a single Strombolian explosive event at Stromboli. Samples of between 40 and 92 lapilli were collected from each of six sequential explosions on 30 September 2002, and 28 lapilli were obtained from a single explosion ~24 hours later (1 October). Density measurements and microtextural observations showed that considerable heterogeneity existed within each of the seven samples. Centimeter to millimeter size bubble-rich and bubble-poor zones are present and are, in places, mingled together. These data indicate that the shallow conduit at Stromboli is a texturally diverse environment at the instant of a single explosion, and that a similar range of heterogeneity can persist through closely-spaced sequences of explosions on a timescale of hours. The 1 October sample contains a greater abundance of bubble-rich magma, which may reflect increase in the frequency and power of explosions.

5.1 Introduction

The textures of juvenile pyroclasts in fall deposits preserve a record of the physical state of the magma at or close to fragmentation (Mangan and Cashman, 1993; Cashman and Mangan, 1994). Such textures have been used as a sensitive record of the ascent and decompression histories of magma through the shallow conduit, and/or changes in these processes with time (e.g., Hammer et al., 1999; 2000; Houghton et al., 2004; Gurioli et al., 2005; Polacci et al., 2003, 2006). A major constraint on the precision of such data is the sampling interval, as this defines the window of

time over which the material was erupted. Of necessity, samples are generally collected after an eruption ceases, and across some finite thickness of deposit-- either an entire bed or some part thereof. In that single Strombolian explosions have eruption durations of seconds, they present an opportunity to sample material fragmented and ejected over a very narrow time window. In comparison, the shortest known sampling interval for a comparable clast population collected in real time (for a Hawaiian eruption) is several minutes (W. Rose, unpublished data, 1985).

Suitable conditions for single-event collections of lapilli from Strombolian explosions are rare, as the ejecta are not generally accessible at safe distances from the source vents. All previous studies (e.g. McGetchin and Chouet, 1974; Andronico et al. 2004a, 2004b, 2005; Polacci et al., 2006; Lautze and Houghton 2005, in press) analyzed mixed suites of pyroclasts from multiple Strombolian explosions. Thus, it has not been possible to constrain the characteristics of ejecta from a single explosion, nor to constrain changes in the eruption assemblage on short time scales (minutes to hours).

A combination of strong southerly winds and episodic powerful lapilli-rich explosions enabled the collection of seven suites of lapilli from single explosions at Stromboli during 30 September and 1 October 2002. Samples were collected directly following each explosion at 13:55, 14:24, 14:39, 15:03, 15:32 and 15:40 on 30 September and at 13:56 on 1 October. These samples represent a rare opportunity to view dynamics occurring within the fragmentation zone at the instant of a single explosion, and from explosion to explosion.

We have previously analyzed an overnight sample of 200 lapilli that collected over a ~28-hour-long interval (multiple explosions) which included the individual explosions discussed here (Lautze and Houghton, 2005, in press). The present study: a) evaluates whether progressive or systematic changes in the shallow magma occurred over the ~2 hour explosion sequence on 30

September, b) compares the six samples of lapilli collected on 30 September to the sample collected on 1 October, and c) compares these single explosion data to that of the September/October 28-hour sample (hereafter referred to as 'overnight sample'; Lautze and Houghton 2005, in press). The value of this study is twofold. Firstly, a) and b) assess changing eruptive dynamics on finer time scales than previously possible at Stromboli and elsewhere. Secondly, c) establishes the extent to which an overnight sample reflects instantaneous fragmentation conditions.

5.2 Background

5.2.1 Strombolian explosions

The mechanism of Strombolian explosions is understood to be the decoupled rise and bursting of slugs of large (dm- to m-scale) decoupled bubbles through a relatively static, free surface of fluid melt (Blackburn et al., 1976; Wilson 1980; Wilson 1980; Parfitt and Wilson 1995; Jaupart 1996; Parfitt 2004). The gas slugs develop as a consequence of the growth and coalescence of bubbles within the conduit (Jaupart and Vergniolle 1989; Parfitt and Wilson 1995; Parfitt, 2004). At Stromboli, seismic data indicate that slugs either form, or undergo a rapid pressure change and acceleration, in a region approximately 250 m below the active crater terrace (Chouet et al., 1999; Chouet et al., 2003; Marchetti and Ripepe, 2005). The slugs ascend in the shallow conduit and burst at the magma's free-surface (Ripepe et al., 2001b; Ripepe and Marchetti, 2002).

Classic studies considering Strombolian eruptions emphasized the role of gas slugs in the explosion process (e.g. Walker, 1973; Fisher and Schminke, 1984; Cas and Wright, 1987). Recent studies have begun to consider that evolving properties of the magma phase influence the nature of explosions. Andronico et al. (2004a; 2004b; 2005) and Lautze and Houghton (in press) for

example, identify a link between changing properties of the shallow magma and the style of explosion at Stromboli volcano during 2002 to 2004.

5.2.2 Stromboli volcano

Stromboli is the most active and northernmost volcano of the Aeolian arc in the southern Tyrrhenian Sea, Italy (Figure 5.1). Stromboli's persistence of mild discrete explosive eruption in historical times (Rosi et al., 2000) led to global usage of the term Strombolian to describe this style of activity (Walker 1973; Pyle 1989), and has given Stromboli its reputation as a relatively steady-state volcano (e.g. Giberti et al., 1992; Ripepe et al., 1993). Stromboli has been the focus of recent attention due to anomalous eruptive activity in 2002 and 2003, which included extended passive lava emission (28 Dec 2002 to 20 July 2003; Calvari et al., 2005; Ripepe et al., 2005a), a volcanogenic tsunami (30 Dec 2002; Bonaccorso et al., 2003; Tinti et al., 2003), and a major paroxysm (5 April 2003; Calvari et al., 2006; Rosi et al., 2006). This chapter focuses on a period of more typical explosive activity that preceded these atypical events.

Stromboli's typical activity occurs as discrete, mild explosions of crystal- and bubble- rich basaltic bombs, lapilli, and/or ash (Francalanci et al., 2005; Lautze and Houghton, in press; Patrick et al., in press). Explosions generally have a duration of seconds, occur at a typical frequency of nine per hour, and emit ejecta to heights of 50 to 300 m (Ripepe et al., 2005a). Such variations in explosion duration, column height, and dominant particle size can occur on time scales of minutes to months, and have been discussed in Chouet et al. (1999), Ripepe et al. (2002, 2005b), Lautze and Houghton (in press) and Patrick et al. (in press). The explosions occur at one of three active craters [Northeast (NE), Central (C), and Southwest (SW)] located on a terrace ~800 m above sea level (a.s.l.; Figure 5.1; Harris et al., 1996). The crater terrace lies within a sector

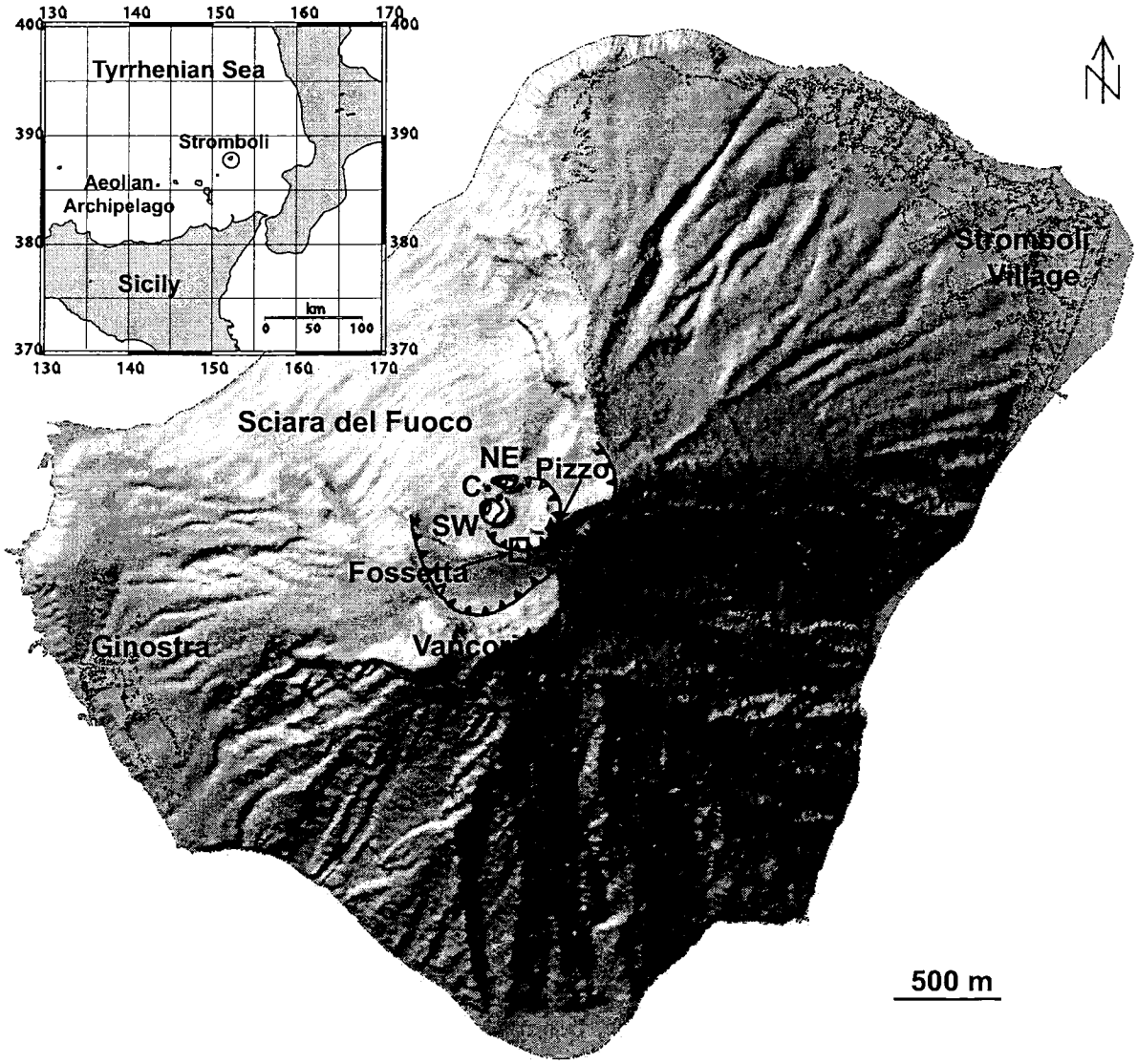

Figure 5.1 Digital elevation map (DEM) of Stromboli island, showing geography of summit area and location of Stromboli and Ginostra villages. Vancori lies at 924 m, Pizzo at 918 m, and the active craters (SW = southwest, C = central, NE = northeast) at ~800 m. Fossetta rim (hatched line) descends from the Pizzo to elevations approximately equal to crater terrace. Small box along the Fossetta rim is location of photo in Figure 5.2. Insert is location map, with the island of Stromboli circled. *DEM courtesy of Anthony Finizola.*

collapse feature called the Fossetta (Pasquare et al., 1993; Tibaldi, 2001). The Pizzo Sopra la Fossa (or Pizzo) marks the highest point (918 m a.s.l.) of the Fossetta. Pyroclasts generally fall within the Fossetta rim, or tumble down a collapse scar called the Sciara del Fuoco and into the sea (Figure 5.1).

5.3 Eruptive Activity and Sampling in September/October 2002

5.3.1 Activity and sampling opportunities

The samples discussed in this paper were collected during a four-day-long period on Stromboli between 29 September and 2 October 2002. Here, we summarize our field observations at the time of the explosions, and data from an eruption log (unpublished) that was taken for between 2 to 4 hours each afternoon or evening by Andrew Harris and Glyn Williams-Jones. Over these four days, eruptive activity was strongest at SW crater, with approximately twice the number of explosions that occurred at the NE crater, and rare, sometimes pulse-like degassing occurring at the Central crater. Explosions from the SW crater were bomb- and lapilli- dominated with little-to- no ash, while ejecta from the NE crater consisted predominantly of reddish-brown ash. The NE crater explosions tended to be of longer duration (roughly 10-20 seconds versus 5-10 seconds for the SW crater), but of lower column height. Lapilli fall on the Fossetta rim was common from SW crater explosions, and fresh small lapilli also fell as far as Vancori (~200 m above and ~1.2 km W of the crater terrace; Figure 5.1). This activity at the NE and SW craters may be a short-term and atypical reversal of the normal contrast between the two craters. Longer lasting, ash-rich explosions at the SW crater and shorter, lapilli- and bomb- rich events at the NE crater are reported as occurring in May 2001 (Ripepe and Marchetti, 2002) and in May and September 2002 (Marchetti and Ripepe, 2005). Also, geophysical signals associated with the SW crater are

typically more complex and of longer duration. Such signals are noted in infrasonic (Ripepe and Marchetti, 2002), seismic (Ripepe et al., 1993; Marchetti and Ripepe, 2005) and thermal (Ripepe et al., 2005b) data.

Our ability to collect lapilli-sized clasts was largely wind dependant. On 29 September, fresh lapilli was deposited on the Pizzo and Fossetta rim, however relatively low winds during our time at the summit (from 12:00 to 18:00) meant that we were only able to sample ash-sized material on this day. We noted moderate intensity explosions at both the SW and NE craters, and loud gas-rich detonations from the Central crater. Explosion frequency was every few minutes, and explosions projected ash and some incandescent ejecta to a few hundred meters above the vents. Fourteen and seven events per hour at the SW and NE craters, respectively, occurred between 15:24 and 18:44 (Harris and Williams-Jones, pers. comun., 2002).

High winds on the afternoon of 30 September enabled the collection of lapilli from a sequence of six individual explosions. We observed an event recurrence of 4 to 12 minutes and SW crater eruption heights of ~300 m. Thirteen and 6 events per hour at the SW and NE craters, respectively, occurred between 16:53 and 20:18 (Harris and Williams-Jones, pers. comun., 2002).

On 1 October, intermediate winds carried ash and lapilli to the Pizzo and Fossetta rim. A 1-3 cm thick bed of lapilli deposited over the previous ~24 hours made distinguishing lapilli from a given explosion difficult. There was a scaling up in activity with respect to the previous day. SW crater eruption heights were up to ~350 m, and an average of 16 and 8 explosions per hour at the SW and NE craters, respectively, occurred between 15:20 and 20:34 (Harris and Williams-Jones, pers. comun., 2002).

Low to intermediate winds on 2 October carried only ash-sized material to the Fossetta rim, though activity levels remained high. Ejecta from SW crater reached heights up to ~300 m with

an average of 16 and 5 explosions per hour at the SW and NE craters, respectively between 14:17 and 16:37 (Harris and Williams-Jones, pers. comun., 2002). Harris and Williams-Jones (pers. comun., 2002) report a peak in explosion frequency and ejecta height on 1 October.

5.3.2 Field Techniques

The lapilli populations were collected along the southern Fossetta rim (Figures 5.1, 5.2). Strong winds efficiently partitioned the ejecta such that 1-4 cm lapilli were transported along steeply inclined trajectories over the SW crater rim to the Fossetta, whereas bombs to coarse lapilli followed steep and symmetrical trajectories and generally fell within 20 to 30 m of source. Depending on wind direction, the dispersal axis of lapilli varied by ~100 m along the Fossetta rim (Figure 5.3).

We collected freshly fallen lapilli from a given explosion across a newly-cleared area of several square meters. The density of lapilli on the ground was only approximately 2 to 10 clasts per m^2 per explosion, such that this process was highly effective (i.e. it was easy to find and collect all newly fallen lapilli in the collection area). We collected between 28 and 92 unambiguous freshly fallen lapilli in a period of 1 to 3 minutes following each explosion. New clasts were recognized on the basis of direct observations—they displayed a distinctive gray translucence and an elevated temperature for some minutes. Not every explosion could be sampled, as fluctuations in explosion intensity as well as wind speed and direction affected the dispersal of clasts. However, a consistency of explosion intensity and wind speed/direction on the afternoon of 30 September enabled collection from six explosions over a ~2 hour interval (Samples 11 to 16). One explosion was sampled in the same manner on 1 October (Sample 21; Figure 5.3).

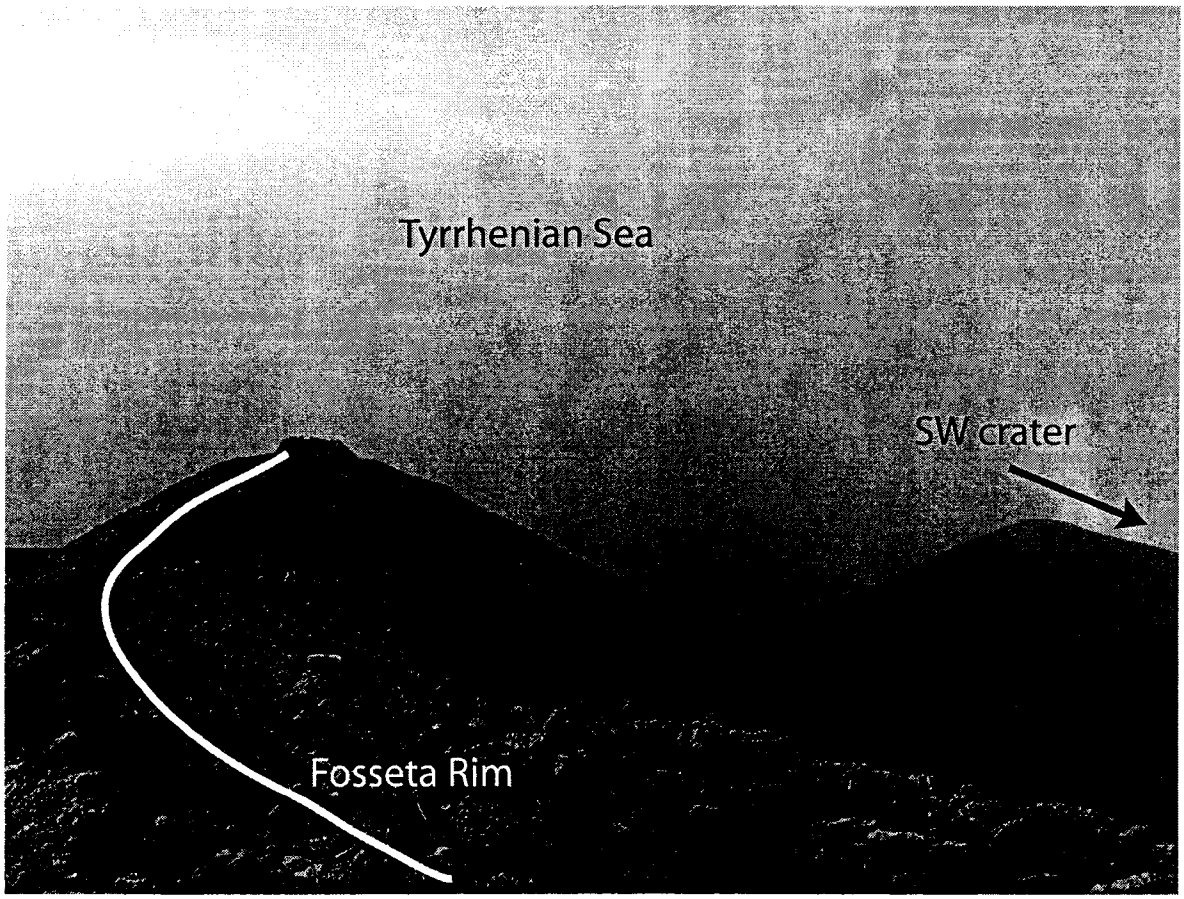

Figure 5.2 Photo of Fossetta rim (white line) along which samples were collected. The southern rim of the SW crater is in right of photo. Width of the Fossetta rim (foreground of picture) is ~4 m. Distance along length of the Fossetta rim in image is ~150 m; distance from location of photo to rim of SW crater is ~150 m. Samples were collected in region within ~50 m of bottom edge of photo.

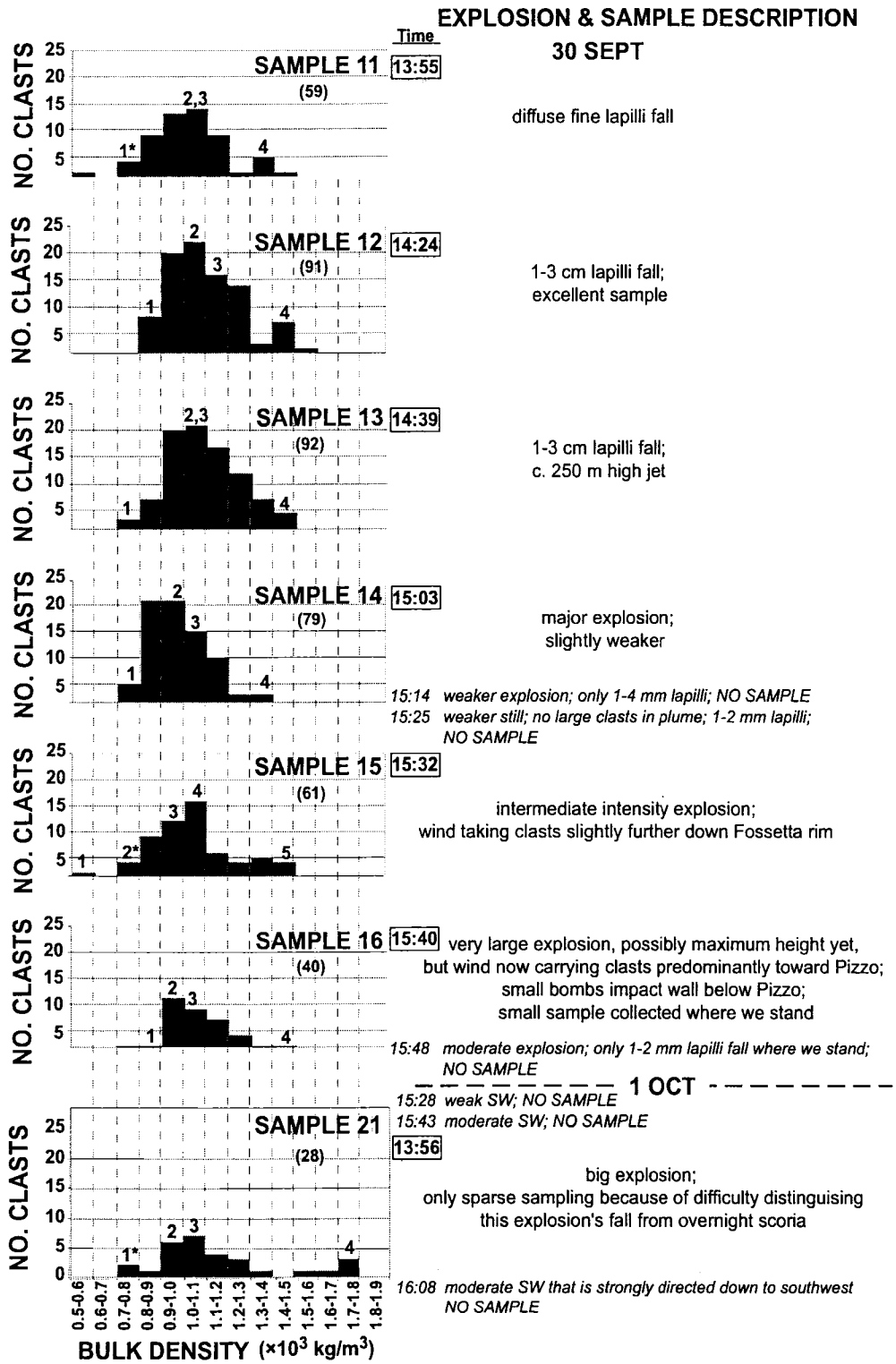

Figure 5.3 Bulk density data for each sample, with time and brief description of linked SW crater explosion. Numbers in parenthesis are the number of lapilli in each sample. Numbers above bins represent thin sections, as shown in figure 5.4; those with asterisk indicate lapilli with corresponding vesicle volume distributions shown in Figure 5.6. Recorded events between sampled explosions are written in italics.

5.4 Data

5.4.1 Qualitative Observations

The lapilli from each single explosion appear relatively similar in hand specimen. They are metallic gray in color, both crystal- and vesicle-rich, generally sub-rounded to elongate, complex in form, and highly delicate. Sub-mm sized bubbles are spherical in shape, whereas larger bubbles are complex and irregular. The population of mm- to cm- sized phenocrysts is euhedral to subhedral. Within each sample, a range in density is qualitatively apparent, reflecting contrasting vesicularity among the clasts. Some clasts appear foam-like and/or have abundant mm- to cm- sized bubbles; others are more compact, lack larger bubbles and/or have populations of more widely dispersed small bubbles. Stretched vesicles are apparent in a subset of the lapilli.

Thin section analysis reveals that low density (LD) and high density (HD) textures (Lautze and Houghton 2005) are apparent within each sample (Figures 5.4, 5.5). Millimeter- to cm- sized larger bubbles are present to varying degrees within both textures, and mingling of domains of LD and HD textures is common in lapilli of the low to intermediate density range (e.g. lapilli 12-1, 14-2; Figures 5.4, 5.5).

5.4.2 Density

The density of each lapillus was measured following Houghton and Wilson (1989). Thin sections were made from the largest 1 or 2 lapilli from bins representing the extremes and mean densities of each sample (plus any outliers, Figure 5.3). Sections were cut to maximize rock area and to enable assessment of the textural diversity within each sample. A scan of each thin section is shown in Figure 5.4.

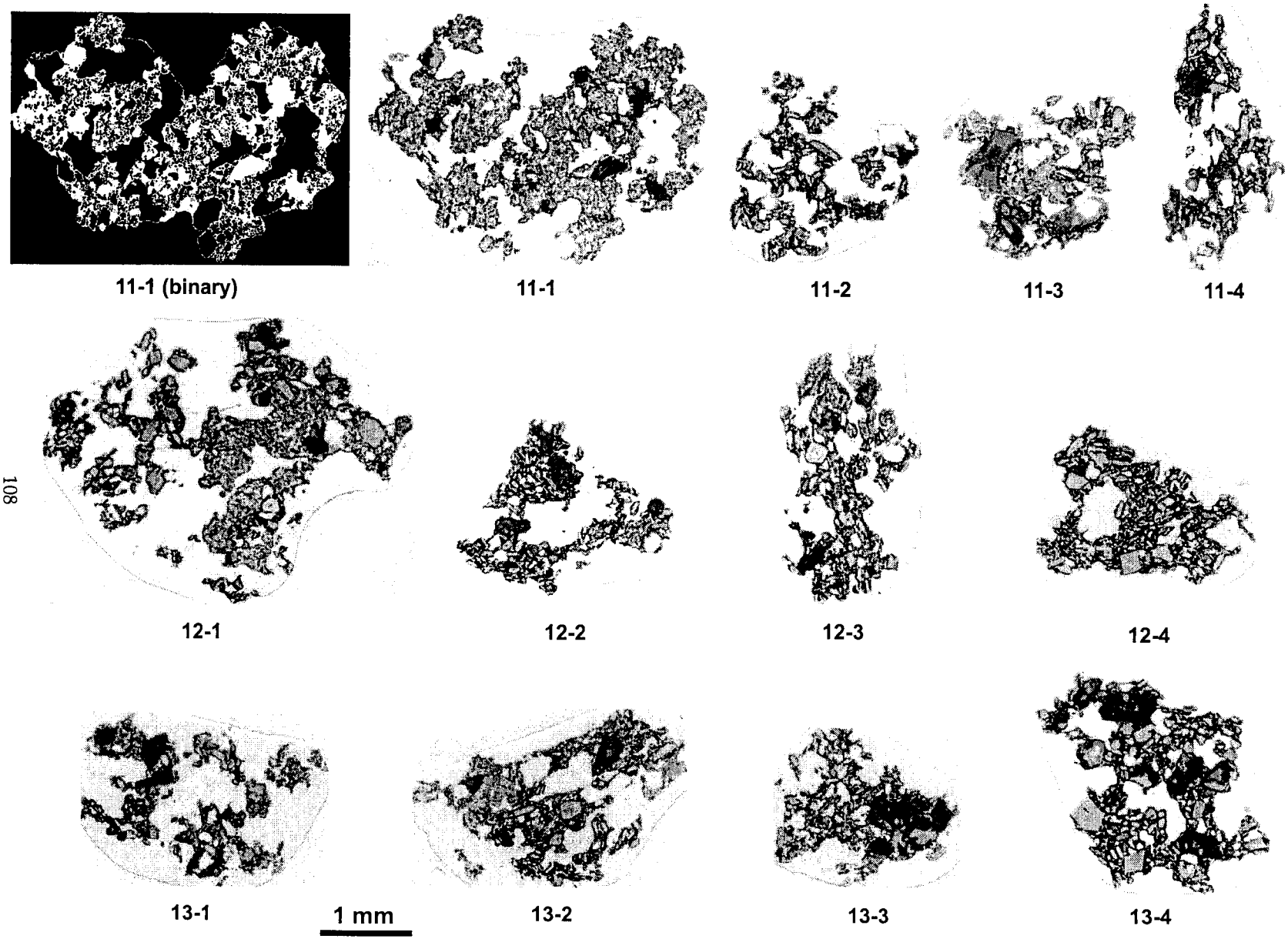

Figure 5.4 (a)

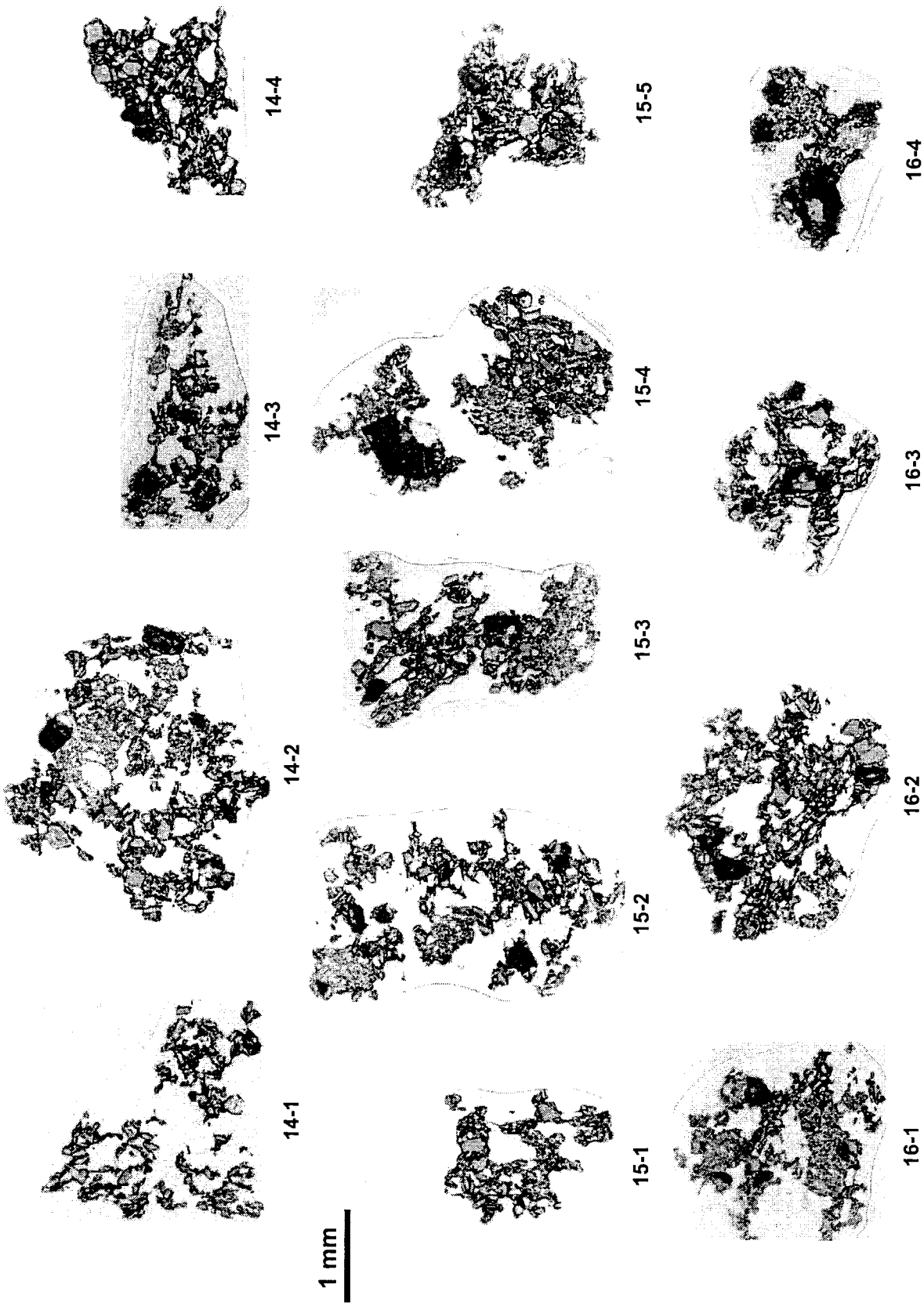

Figure 5.4 (b)

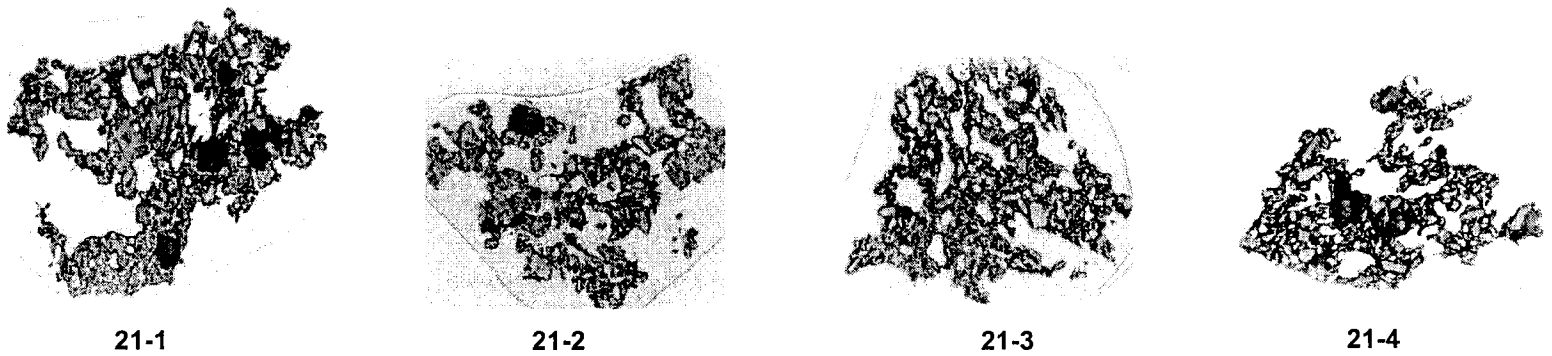

Figure 5.4 (c) Scanned images of thin sections of select lapilli. For each scan, the first number refers to the sample number; the second number corresponds to the density bin (Figure 5.3). All images are shown at the same magnification, and show the total rock area on each section. A binary image of clast 11-1 is shown in Figure 5.4 (a), in which bubbles are black, and phenocrysts and matrix glass are white.

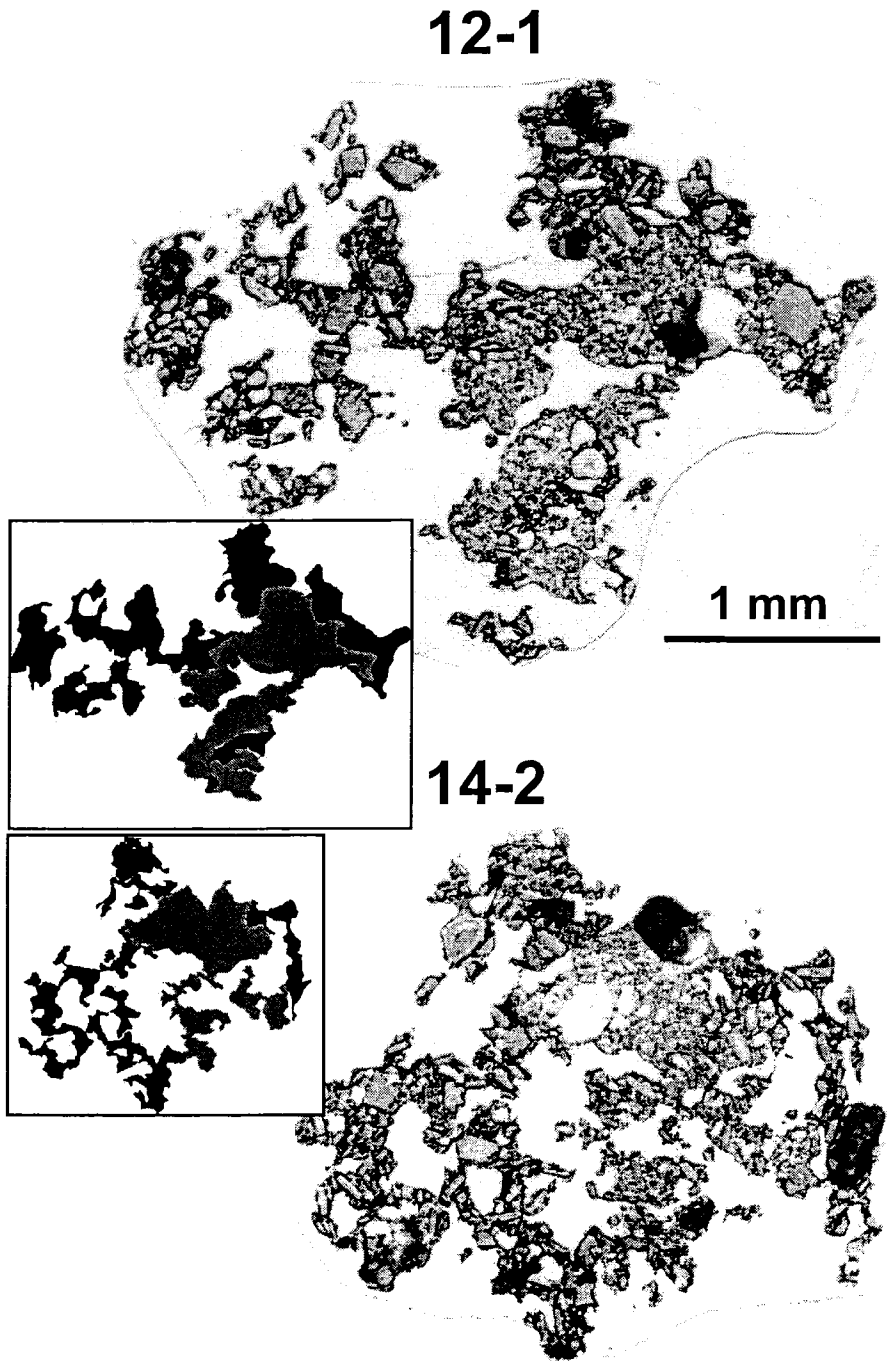

Figure 5.5 Larger images of clasts 12-1 and 14-2; with small images to left highlighting the area of high density (in black) and low density (in gray).

The density data show comparable distributions for all samples, though Sample 21 has an extended tail of denser clasts (Figure 5.3). For all samples, the density values cluster in a range of 900 to 1200 kg m^{-3}, which corresponds to a bulk vesicularity of 57 to 67% (applying a dense-rock-equivalent value of 2750 kg m^{-3}; Barberi et al., 1993). The majority of clasts in this range are mingled composites of the HD and LD textures (e.g. 12-1, 14-2; Figure 5.5). The end member low density lapilli, with values of 500 to 900 kg m^{-3} (68-80% bubbles) generally have a foam-like appearance due to a high abundance of LD material (e.g. clasts 11-1, 12-1, 21-1; Figures 5.3, 5.4). The end member HD lapilli have values >1300 kg m^{-3} (< 53% bubbles) and lack significant regions of LD texture (e.g. clasts 13-4, 15-5, 21-4; Figures 5.3, 5.4). Variability in the large (>1 mm) bubble population explains an observed bulk density range of up to 800 kg m^{-3} (from 1000 kg m^{-3} in clasts 13-4, 14-4, 15-5 to 1800 kg m^{-3} for clast 21-4) in lapilli composed entirely of HD magma (Figures 5.3, 5.4).

5.4.3 Proportion of LD and HD per sample

The procedure described in Lautze and Houghton (in press) was used to assess the relative proportions of LD and HD magma present within each sample (Figure 5.5). This involved obtaining the area fraction of LD and HD on each thin section (Figure 5.3), multiplying these values by the number of clasts in the section's respective density bin, and summing these products across the density range for each sample. The proportion of the two magma types is relatively consistent throughout the six samples collected on 30 September (samples 11-16), varying from 37- 45 % bulk percent LD magma (Figure 5.6). Sample 21 (collected the subsequent day) contains more LD magma at 50 bulk percent. The overnight sample that spans this period is the same as sample 21 (Figure 5.6).

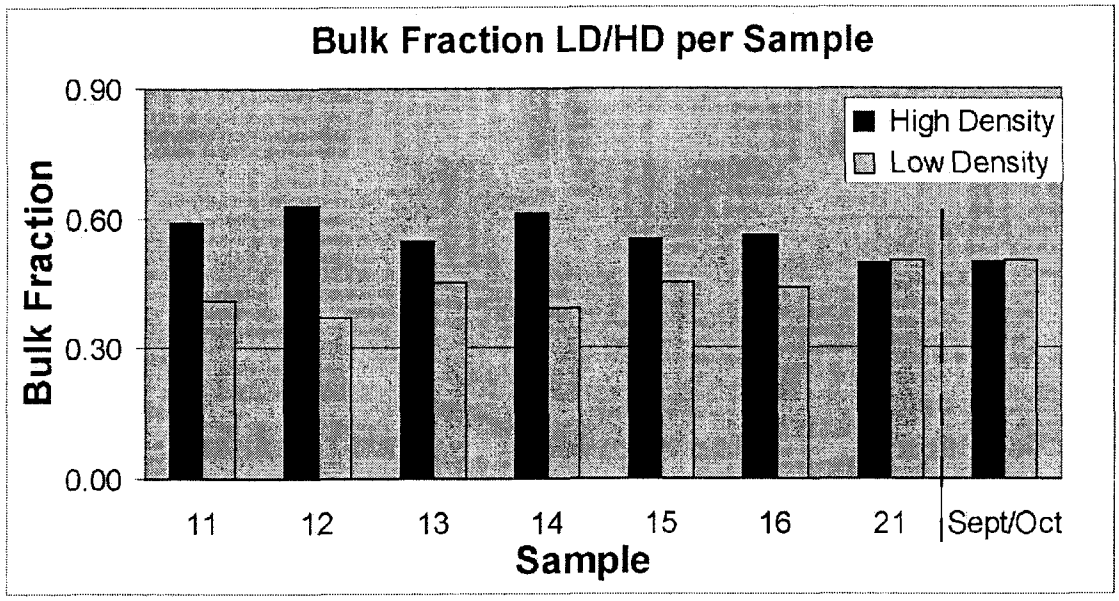

Figure 5.6 Plot showing the bulk fraction of low density (LD) and high density (HD) magma in each of the seven single explosion samples. Data to the right of the dashed line are from Lautze and Houghton (in press) and refer to the Sept/Oct overnight sample. Samples 11 through 16 were collected 30 September and sample 21 was collected on 1 October.

5.4.4 Quantitative Vesicularity Data

Bubble number densities and vesicle volume distributions (VVDs) for end-member, low density lapilli were measured following Adams et al. (2006) and Lautze and Houghton (in press). The low density texture has the least amount of modification of the original bubble population by coalescence and outgassing (Lautze and Houghton, in press). Clasts 11-1, 15-1, 21-1 were selected for this analysis in order to represent the duration of the sampling interval, and on the basis of thin section quality (Figures 5.3, 5.4).

The vesicle number density (N_{Vtot}) for these three clasts cluster at ~10^3 mm^{-3} (Table 5.1). The vesicle volume distributions show similar bimodal distributions, with independent small and large bubble populations having diameters in the range of 0.04-1.00 mm, and 1.58-6.31 mm, respectively (Figure 5.7). The three lapilli analyzed each have a bulk vesicularity of 72%; the large bubble population comprises a roughly equal percentage of this total (26, 32 and 27% in clasts 11-1, 15-1, and 21-1, respectively).

5.5 Discussion

5.5.1 Diversity within single samples

Given that typical explosions at Stromboli have a duration of approximately 5 to 15 seconds (Ripepe et al., 1993; Hort et al., 2003; Patrick et al., in press), the seven single explosion samples are each a snap shot of Stromboli's fragmentation zone on this time-scale. Assuming an ejecta volume of ~2 to 5 m^3 per explosion [calculated using an ejecta mass of 2000 to 5000 kg (Ripepe et al., 1993; M. Patrick, unpublished data), an average bulk density of 1000 kg/m^3 (this paper)], and a conduit radius of 10 m, this yields a fragmentation zone thickness of a few centimeters at most. As such, the single event samples indicate that, at the instant of fragmentation, this thin zone

Table 5.1 Quantitive Vesicle Data

clast	N_{Atot} (mm^{-2})	N_{Vtot} (mm^{-3})	N^m_{Vtot} (mm^{-3})	n (mm^{-4})
11-1	6.1×10^1	1.0×10^3	3.6×10^3	1.2×10^5
15-1	5.8×10^1	1.1×10^3	4.0×10^3	1.7×10^5
21-1	5.6×10^1	9.1×10^2	3.3×10^3	1.1×10^5

Notes: N_a, N_v, n values are sum of bins from 0.02 to 10 mm

N_{Atot} is the number of vesicles per unit area

N_{Vtot} is the number of vesicles per unit volume

N^m_v is the melt-corrected number of bubbles per unit volume, and calculated using the vesicularity calculated from measured bulk density

n is the number of vesicles per each size increment per unit volume

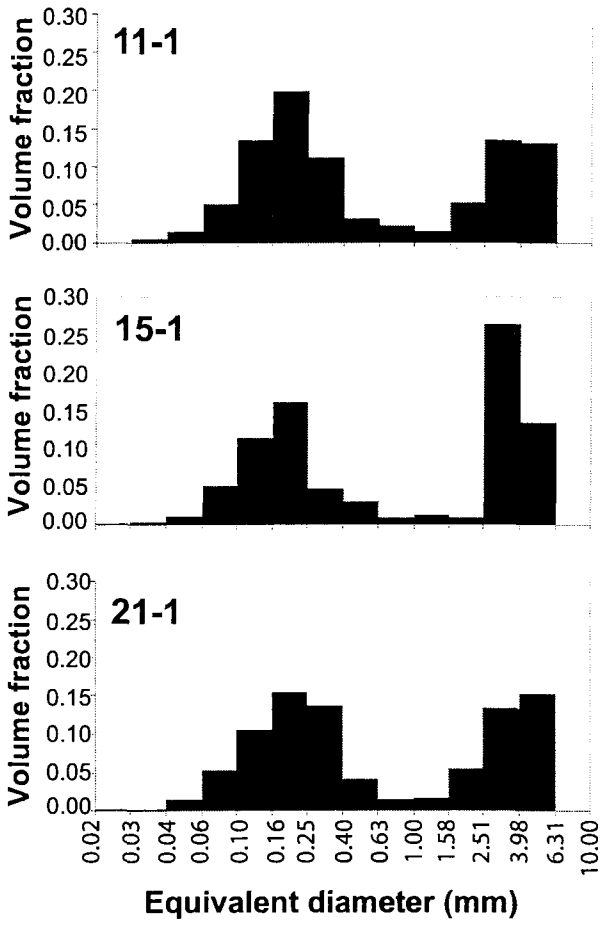

Figure 5.7 Vesicle volume distributions (VVDs) for clasts 11-1, 15-1, 21-1, show similar bimodal distribution of bubbles of 0.03 to 1 mm and 1 to ~6.31 mm. The three clasts each have a bulk vesicularity of 72 %.

shows fine-scale physically heterogeneity. This is an important refinement of the conclusion reached by Lautze and Houghton (2005), which showed that such heterogeneity existed in a sample collected from multiple explosions over ~24 hours.

5.5.2 Comparison of single event samples

Density and microtextural observations for samples 11 to 16 and 21 show only small variation (Figures 5.3, 5.4, 5.6; Table 5.1). This demonstrates that a similar range of magma textures can be preserved in Stromboli's shallow conduit on time scales of 2 to 24 hours. These data highlight the preservation of a similar range of textural heterogeneity through sequences of explosions. Note that this preservation occurs despite indications of dynamic shallow conduit conditions (Lautze and Houghton 2005, in press).

Sample 21 shows a similar textural diversity but a higher proportion of LD magma as compared to the six samples (11 to 16) collected ~24 hours earlier (Figure 5.6). The slight increase in the abundance of LD in sample 21 is likely explained by the increase in explosion frequency and vigor that was observed from 30 September to 1 October (discussed in section 5.3.1). Over months-long time periods, Lautze and Houghton (in press) also identified a positive correlation between an increasing abundance of LD and the power of explosion. This study indicates a coupling between the proportion of HD and LD magmas and explosion intensity on a finer scale than was detected previously.

5.5.3 Comparison with overnight sample

Petrological observations and quantitative vesicle size data show that identical HD and LD magmas are present in the September/October single-event and overnight samples. This

confirms that the extent of textural diversity observed in the overnight sample was present within each explosion, rather than accumulated from ejecta emitted over the ~28 hour sequence of explosions. The overnight sample shows no wider range of textures than observed within each of the single explosions.

One important finding is a similarity among the density and proportionality data for sample 21 and the overnight sample. This is perhaps not surprising, considering evidence that more frequent and powerful explosions occurred on 1 October, and given that more powerful explosions eject large masses to greater distances, i.e. the similar data are likely because more of the overnight sample is composed of ejecta from 1 October. However, these results are significant because they suggest that any form of bulk sampling, even over ~24 periods, is biased toward more powerful explosive events.

5.6 Conclusions

Unusual eruptive and weather conditions enabled the collection of seven samples each from individual explosions at Stromboli during 30 September to 1 October 2002. Within each sample, cm- to mm-sized mingled zones of bubble-rich and bubble-poor magma indicate the existence of considerable but consistent diversity within the fragmentation zone at the point of a single explosion.

Lautze and Houghton (in press) present evidence for a link between contrasting melt properties in the shallow conduit and differing eruption styles at Stromboli on a time scale of months. Here, we extend that comparison to consider changes on time scales of a day (e.g. September 30 versus 1 October) and of hours (e.g. between samples 11 through 16). The existence of only small textural contrasts among the individual samples indicates that a similar range of

heterogeneity persists through numerous explosions, and over the 24 hour sample period. Density and proportionality data for the two hour sequence of six explosions show that it is possible to maintain very similar degrees of physical spatial diversity through hours-long sequences of explosions. A comparison of density and proportionality data among the six samples collected on 30 September and sample 21 shows that the proportions of melt type can shift on time scales as short as a day, presumably during conditions of both waxing and waning explosive intensity. This implies a sensitive coupling between magma properties and explosion vigor.

Acknowledgments. We offer a gracious thank you to Andrew Harris and Glyn Williams-Jones for sharing their eruption log. Thanks also to Matt Patrick for sharing unpublished ejecta mass data and being helpful in myriad other ways. Sarah Fagents, Andrew Harris, and Mike Garcia added detailed commentary to improve the quality of this chapter. The work was supported by National Science Foundation grant EAR-0207734 and an NSF Graduate Research Fellowship (to Lautze).

CHAPTER 6: Conclusions

6.1 Summary

This dissertation employed a variety of methods to highlight and explain changes in the pattern of observed eruption at Etna and Stromboli volcanoes during eruption episodes in 2001 and 2002, respectively. The Etna study (chapter 2) quantified variations in the rates of lava effusion and degassing in 2001. A long-term data set (January to August) included both satellite- and ground-based time series of effusion rates; short-term data included field-based effusion rate and degassing data collected May 29 to 31. The long-term data showed four pulses between January and July that occurred along an increasing average trend (from 1.1 to 8.8 m^3s^{-1}) and led into a major flank eruption (17 July to 9 August; effusion rate averaged 22.2 m^3s^{-1}). The short-term data highlighted a general increase in at-vent puff frequency from May 29 to 31, with hour-long and sometimes positively correlated variations in both degassing and lava flow velocity (with minutes-long oscillations). Combined, the short and long term data implied that a clear months-long increase in supply of magma to Etna's near-vent system was overprinted by an hours-to-weeks timescale of oscillation.

The Stromboli studies (chapters 3 through 5) were the first to examine and explain the microtextural characteristics of ejecta from Strombolian explosions. Chapter 3 provided detailed analysis of ejecta from a sample of 200 lapilli collected over 24 hours. This study was the foundation for chapters 4 and 5. Chapter 4 contrasted the characteristics of lapilli samples from multiple explosions (i.e. overnight samples) collected during 3 intervals of variable eruptive pattern in 2002. Chapter 5 looked at seven lapilli suites that were each collected from a single observed explosion over a ~24 hour period in 2002.

In chapter 3, the occurrence at Stromboli of a fine scale mingling between two magmas with distinctive bubble textures (low density, LD, and high density, HD) was documented. LD was defined as having an abundance of subspherical bubbles, the presence of large, irregularly shaped bubbles, and a light-to-transparent glass matrix. HD was defined as having sparse relatively small bubbles, conspicuous large irregular bubbles, and a dark glass matrix. Chapter 4 compared vesicularity textures in lapilli from May (weak, infrequent, ash-rich explosions), September (powerful, frequent, scoria-rich explosions), and late December (powerful, less frequent explosions just before effusive phase) of 2002. In addition to the LD and HD textures, clasts showing a transitional texture (TT) were identified among these ejecta. TT was defined as having an intermediate number of subspherical bubbles, a high frequency of large, irregularly-shaped bubbles, and a honey colored glass matrix. Vesicularity data indicated that the textures are linked via an ongoing, time-dependant evolution of increasing degrees of vesicle coalescence and outgassing from LD to TT to HD magma. Given the previously established model for Strombolian explosions, these studies ascribed an origin for the variable textures in which the LD magma rises with a rapidly ascending gas slug, mingling with more mature, stagnant HD melt while en route to the magma's free surface. LD magma not erupted with its parent gas slug begins an evolution towards the HD end member.

In chapter 4, a link between the effect of changing vesicularity on the rheology of shallow magma and eruption style was explored. Variable amounts of the LD, TT, and HD magmas were present in each sample, with the most TT in May, the most LD in September, and the most HD in December. Methods to calculate the viscosity of a bubble- and crystal- rich system were investigated as part of this study. This was predicated on the basis that viscosity influences the rate of bubble slug ascent and the process of fragmentation. Calculations gave a viscosity

difference in the range of 2000 to 2600 Pa s for LD and 3000 to 5000 Pa s for HD. These results suggested that increasing maturity (i.e. increasing residence time) of magma in Stromboli's shallow conduit (with resultant increase in viscosity) feeds back to reduce the intensity of explosions, whereas a steady flux of LD magma favors more powerful explosions.

In chapter 5, views of the fragmentation zone during single Strombolian explosions were presented. Density and microtextural data show that considerable heterogeneity exists within each of the seven samples, and that this diversity is maintained from explosion to explosion. This chapter concluded that the shallow conduit at Stromboli is a texturally diverse environment at the point of a single explosion, and that a similar range of heterogeneity persisted through the sequence of sampled explosions. An increase in the proportion of LD magma among samples spaced ~24 hours apart correlates with an apparent increase in explosion vigor.

6.2 Limitations on current research and methodologies

6.2.1 Coarse bubble population

A recurring issue in the Stromboli studies involved the inability to statistically constrain the centimeter size bubble population in lapilli size particles. Repeatedly, one or two centimeter-sized bubbles comprised ~50% of a clast's vesicularity. In a few instances, a seemingly-arbitrary lack of big bubbles caused an LD clast to have an anomalously high bulk density.

Two potential ways to get around this problem would be to: 1) collect and analyze bigger clasts, or 2) exclude bubbles ≥ 1cm from the analyses. A clear obstacle to the former regards hazard associated with collecting large particles from observed explosions. This perhaps indicates a need to explore robotic/engineering possibilities. The latter solution is justifiable in part because data suggest that the large bubbles are decoupled from the magma and are released

through passive degassing. For this reason, the ability to statistically represent the large bubble population is not expected to enhance the understanding of explosion dynamics. Where possible, much of the vesicularity analysis did exclude (or at least permit exclusion) of the large bubble population (e.g. proportionality and mingling form analyses excluded large bubbles, and $N^{m}{}_{V_{tot}}$ values exclude all bubbles; chapters 3 through 5). However the presence of the large bubbles, in even a transient fashion, is a major factor in constraining the density of the melt in the shallow conduit.

6.2.2 Lack of applicable viscosity equations

At present there is no existing method to quantitatively assess the viscosity of a three-phase system with high particle density. Current literature considers only two- phase systems of melt and crystals (March, 1981; Pinkerton and Stevenson, 1992; Lejeune and Richet, 1995), or melt and bubbles (Lejeune et al., 1999; Manga and Lowenberg, 2001; Llewellin et al., 2002(a, b); Pal 2003), and generally at particle concentrations under 50%. Current fluid mechanical theory which does consider three phases (e.g. Phan-Thien and Pham, 1997) makes approximations which, for Stromboli (and presumably many other volcanological systems), result in unrealistic solutions. Michael Manga derived an equation that accounts for the high crystallinity of the HD and LD magmas (chapter 4). However, this equation still considers only 2-phases simultaneously and is an approximation. Both theoretical and analogue approaches are likely to shed light on this issue

6.3 Ideas for future work

The research presented in this dissertation provides a foundation for several paths of continued work, which might be expected to contribute further understanding to the problems of understanding conduit and eruption processes during Strombolian explosions. Some directions which were precluded from this study due to time constraints are:

- detailed textural and chemical characterization of crystals in HD, TT and LD magma types *(microtextural zoning in crystals may show evolution in parallel with vesicularity).*
- testing for statistical variance within the bubble populations of non-mingled HD and LD clasts *(to assess how alike the textures are from clast to clast, and with time).*
- textural analysis of golden pumice erupted during Stromboli's paroxysmal eruptions *(to better constrain degassing processes that occur deeper in Stromboli's conduit system).*
- characterization of microtextures from subplinian eruptions *(to obtain insight into trigger for subplinian eruptions).*
- constraint of the rheology of three phase systems at high particle concentration *(to better understand fluid mechanical dynamics in shallow conduit).*
    - via analogue experiments.
    - via derivation of equations from first principles.
- investigation into occurrence of magma mingling in ejecta from Strombolian explosions at other volcanoes.

Appendix

This appendix serves as repository for data that was not included in the chapters, which are on the attached DVD. The text below explains the system of files and folders on the DVD.

1) The file "Stromboli Samples 2002.xls" shows the label and a brief description of each sample collected at Stromboli. There are three worksheets for the May, Sept, and Dec sampling times.

2) The folder "Density" contains three files each with the density data for the relevant samples from each time period (i.e. May.xls, Sept.xls, Dec.xls). Each sample from each time period has a separate worksheet, with the sample name referring to the label as shown in the file "Stromboli Samples 2002.xls". The right-hand-most column of each spreadsheet, labeled "no." uniquely identifies each clast within each sample (i.e. clast no. 2 within sample 19 is subsequently identified as 19-2). It is in this way that clasts were uniquely identified throughout my research, which defines how clasts are often labeled in this appendix. Samples and clasts were generally re-labeled when included in specific studies in order to simplify the presentation of the data for the reader. The table on the final page of this appendix associates the "sample-clast" labeling scheme (from the density files) with labeling schemes used in chapter 3 through 5. This table should be referred to when going through the following folders/files in the appendix.

3) The folder "Images_raw" contains all the raw images used in this dissertation. This folder contains three subfolders: May, Sept, Dec. The Sept subfolder further contains two folders: Overnight, and SingleSeries. The May, Dec, and Sept->Overnight folders all contain images

labeled consistent with data as presented in Chapter 4. The Sept-> SingleSeries images are labeled according to the "sample-clast" scheme. SEM images were obtained for select clasts from each sample to obtain quantitative vesicularity data. These SEM images are included as separate subfolders.

4) The folder "Images_layers" also contains three subfolders: May, Sept, Dec. The Sept folder again contains two folders: Overnight, and SingleSeries. Within each of these (four) folders are two folders: VVDs, and Proportion. Within each 'VVDs' folder are the binary images needed to obtain the quantitative vesicularity data for the select clasts. Within each 'Proportion' folder are the binary images needed to obtain the proportionality data for each time period.

5) The folder "Bubstat" contains an interactive Matlab program created by Todd Bianco and Eric Mittelstaedt with volcanological input by myself. This program inputs multiple raw data files on the area and size of vesicles per clast and outputs volumetric vesicularity data, as shown in chapters 3 through 5. Eleven subfolders within "Bubstat" contain the inputs and outputs for each of the eleven clasts analyzed quantitatively. The raw data files are multiple .txt files within each subfolder. The outputs from the program for each of the eleven clasts were manipulated from .txt files and are contained in an independent subfolder within bubstat entitled "global_out.xls".

6) The folder "Proportion" contains two files: proportion_overnights, and proportion_SingleSeries, with the proportionality data as given in chapters 4 and 5.

Collection Time	sample-clast	re-label	use of re-label
	05-08b	a1	ch4
	05-08c	a2	ch4
May	05-08a	a3	ch4
	05-07a	a4	ch4
	05-07b	a5	ch4
	19-11	LD(b1)	ch3(ch4)
	19-04	b2	ch4
	19-20	b3	ch4
September	19-14	b4	ch4
(overnight)	19-19	b5	ch4
	19-58	MD(b6)	ch3(ch4)
	19-52	HD(b7)	ch3(ch4)
	19-79	b8	ch4
	30-01	c1	ch4
	30-15	c2	ch4
	30-03	c3	ch4
December	30-10	c4	ch4
	30-14	c5	ch4
	30-21	c6	ch4
	30-08	c7	ch4
	30-18	c8	ch4
	11-03	11-1	ch5
	11-23	11-2	ch5
	11-27	11-3	ch5
	11-34	11-4	ch5
	12-01	12-1	ch5
	12-23	12-2	ch5
	12-14	12-3	ch5
	12-49	12-4	ch5
	13-03	13-1	ch5
	13-07	13-2	ch5
September	13-20	13-3	ch5
(Single Series)	13-15	13-4	ch5
	14-09	14-1	ch5
	14-01	14-2	ch5
	14-25	14-3	ch5
	14-72	14-4	ch5
	15-57	15-1	ch5
	15-02	15-2	ch5
	15-05	15-3	ch5
	15-10	15-4	ch5
	15-27	15-5	ch5
	16-05	16-1	ch5
	16-02	16-2	ch5
	16-13	16-3	ch5
	16-38	16-4	ch5
	21-01	21-1	ch5
	21-02	21-2	ch5
	21-13	21-3	ch5
	21-16	21-4	ch5

References

Adams NK, Houghton BF, Fagents SA, Hildreth W (2006) The transition from explosive to effusive eruptive regime: the example of the 1912 Novarupta eruption, Alaska. Geological Society of America Bulletin 118:620-634

Aiuppa A, Federico C (2004) Anomalous magmatic degassing prior to the 5th April 2003 paroxysm on Stromboli. Geophysical Research Letters 31 doi:10.1029/2004GL020458

Alean, J., Carniel R., Fulle M., Stromboli online - Volcanoes of the World on Swisseduc.ch, http://stromboli.net, 2005

Allard P, Carbonnelle J, Metrich N, Loyer H, Zettwog P (1994) Sulphur output and magma degassing budget of Stromboli volcano. Nature 368:326-330

Alparone S, Andronico D, Giammanco S, Lodato L (2004) A multidisciplinary approach to detect active pathways for magma migration and eruption at Mt. Etna (Sicily, Italy) before the 2001 and 2002-2003 eruptions. Journal of Volcanology and Geothermal Research 136(1-2):121-140

Andronico D, Caruso S, Corsaro R, Cristaldi A, Del Carlo P, Miraglia L, Pompilio M, Zanon V (2004a) Caratterizzazione delle ceneri emesse dallo Stromboli nel 2003, INGV Report No. UFVG2004/23

Andronico D, Caruso S, Cristaldi A, Del Carlo P (2004b) Caratterizzazione delle ceneri emesse dallo Stromboli nel periodo gennaio-giugno 2004. INGV Report No. UFVG2004/77

Andronico D, Caruso S, Corsaro R, Cristaldi A, Del Carlo P, Miraglia L (2005) Caratterizzazione dei prodotti esplosivi emessi dallo Stromboli nel periodo luglio-dicembre 2004. INGV Report No. UFVG2005/52

Andronico D, Calvari S, Lodato L (in prep) Eruptive activity at Etna volcano before the 2001 flank eruption

Bagdassarov N, Pinkerton H (2004) Transient phenomena in vesicular lava flows based on laboratory experiments with analogue materials. Journal of Volcanology and Geothermal Research 132:115-136

Bailey JE, Harris AJL, Dehn J, Calvari S, Rowland SK (2006) The changing morphology of an open lava channel on Mt. Etna. Bulletin of Volcanology 68:497-515

Barberi F, Rosi M, Sodi A (1993) Volcanic hazard assessment at Stromboli based on review of historical data. Acta Vulcanologica 3:173–187

Behncke B, Neri M (2003) The July–August 2001 eruption of Mt. Etna (Sicily). Bulletin of Volcanology 65:461-476

Bertagnini A, Landi P (1996) The Secche di Lazzaro pyroclastics of Stromboli Volcano: a phreatomagmatic eruption related to the Sciara del Fuoco sector collapse. Bulletin of Volcanology 58:239-245

Bertagnini A, Metrich N, Landi P, Rosi M (2003) Stromboli volcano (Aeolian Archipelago, Italy): An open window on the deep-feeding system of a steady state basaltic volcano. Journal of Geophysical Research 108 doi:10.1029/2002JB002146

Blackburn EA, Wilson L, Sparks RSJ (1976) Mechanisms and dynamics of strombolian activity. Journal of the Geological Society of London 132:429-440

Blower JD, Keating JP, Mader HM, Phillips JC (2001) Inferring volcanic degassing processes from vesicle size distributions. Geophysical Research Letters 28:347-350

Blower JD, Keating JP, Mader HM, Phillips JC (2002) The evolution of bubble size distributions in volcanic eruptions. Journal of Volcanology and Geothermal Research 120:1-23

Bonaccorso A, Calvari S, Garfi G, Lodato L, Patane D (2003) Dynamics of the December 2002 flank failure and tsunami at Stromboli volcano inferred by volcanological and geophysical observations. Geophysical Research Letters 30:1-4

Bottinga Y, Weill DF (1970) Densities of liquid silicate systems calculated from partial molar volumes of oxide components. American Journal of Science 269:169-182

Branca S, del Carlo P (2005) Types of eruptions of Etna volcano AD 1670-2003: implications for short-term eruptive behaviour. Bullentin of Volcanology 67:732-742

Calvari S, INGV - Sezione di Catania scientific staff (2001) Multidisciplinary approach yields insight into Mt. Etna eruption. Eos, Transactions, American Geophysical Union 82:653-656

Calvari S, Coltelli M, Neri M, Pompilio M, Scribano V (1994) The 1991-1993 Etna eruption: chronology and lava flow-field evolution. Acta Vulcanologica 4:1-14

Calvari S, Neri M, Pinkerton H (2003) Effusion rate estimations during the 1999 summit eruption on Mount Etna and growth of two distinct lava flow fields. Journal of Volcanology and Geothermal Research 119(1-4):107-123

Calvari S, Pinkerton H (2004) Birth, growth and morphologic evolution of the 'Laghetto' cinder cone during the 2001 Etna eruption. Journal of Volcanology and Geothermal Research 132: 225-239

Calvari S, Spampinato S, Lodato L, Harris AJL, Patrick MR, Dehn J, Burton MR, Andronico D (2005) Chronology and complex volcanic processes during the 2002-2003 flank eruption at Stromboli volcano (Italy) reconstructed from direct observations and surveys with a handheld thermal camera. Journal of Geophysical Research 110 doi:10.1029/2004JB003129

Calvari S, Spampinato L, Lodato L (2006) The 5 April 2003 vulcanian paroxysmal explosion at Stromboli (Italy) from field observations and thermal data. Journal of Volcanology and Geothermal Research 149(1-2):160-175

Carey SN, Sigurdsson H (1982) Influence of particle aggregation on deposition of distal tephra from the May 18, 1980 eruption of Mount St. Helens volcano. Journal of Geophysical Research 87(B8):7061-7072

Cas RAF, Wright JV (1987) Volcanic successions: Modern and ancient. Allen and Unwin, London:528 pp.

Cashman KV, Mangan MT (1994) Physical Aspects of Magmatic Degassing II. Constraints on vesiculation processes from textural studies of eruptive products. In: Carroll MR, Holloway JR (eds) Volatiles in Magmas:447-478

Cashman K, Blundy J (2000) Degassing and crystallization of ascending andesite and dacite. Philosophical Transactions Royal Society of London Series A-Mathematical Physical and Engineering Sciences 358:1487-1513

Chester DK, Duncan AM, Guest JE, Kilburn CRJ (1985) Mount Etna, The Anatomy of a Volcano. Chapman and Hall, London:404 pp.

Chouet B, Saccorotti G, Dawson P, Martini M, Scarpa R, Deluca G, Milana G, Cattaneo M (1999) Broadband measurements of the sources of explosions at Stromboli Volcano, Italy. Geophysical Research Letters 26:1937-1940

Chouet B, Dawson P, Ohminato T, Martini M, Saccarotti G, Giudicepietro F, de Luca G, Milana G, Scarpa R (2003) Source mechanisms of explosions at Stromboli Volcano, Italy, determined from moment-tensor inversions of very-long-period data. Journal of Geophysical Research 108:1-25

Coltelli M, Del Carlo P, Vezzoli L (1998) Discovery of a Plinian basaltic eruption of Roman age at Etna volcano, Italy. Geology 26:1095-1098

Coltelli M, Del Carlo P, Vezzoli L (2000) Stratigraphic constrains for explosive activity in the last 100 ka at Etna volcano, Italy. International Journal of Earth Sciences 89(3):665-677

Coltelli M (2006) Etna explosive eruptions and the INGV reponse to improve an ash-cloud monitoring system. COV4 Abstracts Volume:19

Dozier J, (1981) A method for satellite identification of surface temperature fields of subpixel resolution. Remote Sensing of Environment 11:221-229

Falsaperla S, Lanzafame G, Longo V, Spampinato S (1999) Regional stress field in the area of Stromboli (Italy): insights into structural data and crustal tectonic earthquakes. Journal of Volcanology and Geothermal Research 88(3):147-166

Fisher RV, Schmincke H-U (1984) Pyroclastic rocks. Springer-Verlag, Heidelberg, Germany, pp 472

Francalanci L, Taylor SR, McCulloch MT, Woodhead JD (1993) Geochemical and isotopic variations in the calc-alkaline rocks of Aeolian arc, Southern Tyrrhenian Sea, Italy - constraints on magma genesis. Contributions to Mineralogy and Petrology 113(3):300-313

Francalanci L, Davies GR, Lustenhouwer W, Tommasini S, Mason PRD, Conticelli S (2005) Intra-grain Sr isotope evidence for crystal recycling and multiple magma reservoirs in the recent activity of Stromboli volcano, southern Italy. Journal of Petrology 46(10):1997-2021

Giberti G, Jaupart C, Sartoris G (1992) Steady-state operation of Stromboli volcano, Italy: constraints on the feeding system. Bulletin of Volcanology 54(7):535-541

Gillot PY, Keller J (1993) Radiochronological dating of Stromboli. Acta Vulcanologica 3:69-78

Gillot PY, Kieffer G, Romano R (1994) The evolution of Mount Etna in the light of potassium-argon dating. Acta Vulcanologica 5:81-87

Guest JE, Murray JB (1979) An analysis of hazard from Mount Etna volcano. Journal of the Geological Society of London 166:347-354

Gurioli L, Houghton B, Cashman K, Cioni R (2004) Complex changes in eruption dynamics during the 79 AD eruption of Vesuvius. Bulletin of Volcanology 67:144-159

Harris AJL, Rothery DA, Carlton RW, Langaas S, Mannstein H (1995) Non-zero saturation of AVHRR thermal channels over high temperature targets: evidence from volcano data and a possible explanation. International Journal of Remote Sensing 16:189-196

Harris AJL, Stevens NF, Maciejewski AJH Roellin PJ (1996) Thermal evidence for linked vents at Stromboli. Acta Vulcanologica 8(1):57-61

Harris AJL, Blake S, Rothery DA, Stevens NF, (1997a) A chronology of the 1991 to 1993 Mount Etna eruption using advanced very high resolution radiometer data: Implications for real-time thermal volcano monitoring. Journal of Geophysical Research 102:7985-8003

Harris AJL, Butterworth AL, Carlton RW, Downey I, Miller P, Navarro P, Rothery DA (1997b) Low-cost volcano surveillance from space: case studies from Etna, Krafla, Cerro Negro, Fogo, Lascar and Erebus. Bulletin of Volcanology 59:49-64

Harris AJL, Stevenson DS (1997) Thermal observations of degassing open conduits and fumaroles at Stromboli and Vulcano using remotely sensed data. Journal of Volcanology and Geothermal Research 76(3-4):175-198

Harris AJL, Sherman SB, Flynn LP, Rothery DA, Oppenheimer C (1999) Mass flux measurements at active lava lakes: implications for magma recycling. Journal of Geophysical Reseach B: Solid Earth 104(4):7117– 7136

Harris AJL, Murray JB, Aries SE, Davies MA, Flynn LP, Wooster MJ, Wright R, Rothery DA (2000) Effusion rate trends at Etna and Krafla and their implications for eruptive mechanisms. Journal of Volcanology and Geothermal Research 102:237-270

Hornig-Kjarsgaard I, Keller J, Koberski U, Stadlbauer E, Francalanci L, Lenhart R (1993) Geology, stratigraphy and volcanological evolution of the island of Stromboli, Aeolian arc, Italy. Acta Vulcanologica 3:21-68

Hort M, Seyfriend R, Voge M (2003) Radar Doppler velocimetry of volcanic eruptions: theoretical considerations and quantitative documentation of changes in eruptive behavior at Stromboli volcano, Italy. Geophyiscal Journal International 154:515-532

Houghton BF, Wilson CJN (1989) A vesicularity index for pyroclastic deposits. Bulletin of Volcanology 51:451-462

Houghton BF, Wilson CJN, Del Carlo PO, Coltelli M, Sable JE, Carey R (2004) The influence of conduit processes on changes in style of basaltic plinian eruptions: Tarawera 1886 and Etna 122 BC. Journal of Volcanology and Geothermal Research 137:1-14

James MR, Lane SJ, Chouet B, Gilbert JS (2004) Pressure changes associated with the ascent and bursting of gas slugs in liquid-filled vertical and inclined conduits. Journal of Volcanology and Geothermal Research 129(1-3):61-82

Jaupart C, Vergniolle S (1988) Laboratory models of Hawaiian and Strombolian eruptions. Nature 331(6151):58-60

Jaupart C, Vergniolle S (1989) The generation and collapse of a foam layer at the roof of a basaltic magma chamber. Journal of Fluid Mechanics 203:347-380

Jaupart C (1996) Physical models of volcanic eruptions. Chemical Geology 128:217-227

Keller J, Hornig-Kjarsgaard I, Koberski U, Stadlbauer E, Lenhart R (1993) Geological Map of the

island of Stromboli - scale: 1:10.000. Acta Vulcanologica 3:Appendix

Klug C, Cashman KV (1994)Vesiculation of May 18, 1980, Mount St-Helens Magma. Geology 22(5):468-472

Klug C, Cashman KV, Bacon CR (2002) Structure and physical characteristics of pumice from the climactic eruption of Mount Mazama (Crater Lake), Oregon. Bulletin of Volcanology 64:486-501

Kokelaar P, Romagnoli C (1995) Sector collapse, sedimentation and clast population evolution at an active island-arc volcano: Stromboli, Italy. Bulletin of Volcanology 57:240-262

Landi P, Métrich N, Bertagnini A, Rosi M (2004) Dynamics of magma mixing and degassing recorded in plagioclase at Stromboli (Aeolian Archipelago, Italy). Contributions to Mineralogy and Petrology 147:213–227

Lautze NC, Harris AJL, Bailey JE, Ripepe M, Calvari S, Dehn J, Rowland SK, Evans-Jones K (2004) Pulsed lava effusion at Mount Etna during 2001. Journal of Volcanology & Geothermal Research 137:231-246

Lautze NC, Houghton BF (2005) Physical mingling of magma and complex eruption dynamics in the shallow conduit at Stromboli volcano, Italy. Geology 33(5):425-428

Lautze NC, Houghton BF (in press) Linking explosion intensity and magma rheology during 2002 at Stromboli volcano. Bulletin of Volcanology

Lejeune AM, Richet P (1995) Rheology of crystal-bearing silicate melts: an experimental study at high viscosities. Journal of Geophysical Research 100:4215-4229

Lejeune AM, Bottinga Y, Trull TW, Richet P (1999) Rheology of bubble-bearing magmas. Earth and Planetary Science Letters 166:71- 84

Llewellin EW, Mader HM, Wilson SDR (2002a) The constitutive equation and flow dynamics of bubbly magmas. Geophysical Research Letters 29(24) doi:10.1029/2002GL015697

Llewellin EW, Mader HM, Wilson SDR (2002b) The rheology of a bubbly liquid. Proceedings of the Royal Society of London Series A-Mathematical Physical and Engineering Sciences 458(2020):987-1016

Llewellin EW, Manga M (2005) Bubble suspension rheology and implications for conduit flow. Journal of Volcanology & Geothermal Research 143:205-217

Manga M, Loewenberg M (2001) Viscosity of magmas containing highly deformable bubbles. Journal of Volcanology & Geothermal Research 105:19-24

Mangan MT, Cashman KV, Newman S (1993) Vesiculation of basaltic magma during eruption. Geology 21(2):157-160

Mangan MT, Cashman KV (1996) The structure of basaltic scoria and reticulite and inferences for vesiculation, foam formation, and fragmentation in lava fountains. Journal of Volcanology and Geothermal Research 73:1-18

Marchetti E, Ripepe M (2005) Stability of the seismic source during effusive and explosive activity at Stromboli Volcano. Geophysical Research Letters 32(3) doi:10.1029/2004GL021406

Marsh BD (1981) On the crystallinity, probability of occurrence, and rheology of lava and magma. Contributions to Mineralogy and Petrology 78:85-98

Mastin L, Christiansen B, Thornber C, Lowenstern JB, Beeson MH (2004) What makes hydromagmatic eruptions violent? Some insights from Keanakako'i Ash, Kilauea Volcano, Hawai'i. Journal of Volcanology and Geothermal Research 137:15-31

McGetchin T, Chouet BA (1979) Energy Budget of the Volcano Stromboli, Italy. Geophysical Research Letters 6(4):317-319

Métrich N, Bertagnini A, Landi P, Rosi M (2001) Crystallization driven by decompression and water loss at Stromboli Volcano (Aeolian Islands, Italy). Journal of Petrology 42:1471-1490

Monaco C, Catalano S, Cocina O, De Guidi G, Ferlito C, Gresta, S, Musumeci C, Tortorici L (2005) Tectonic control on the eruptive dynamics at Mt. Etna Volcano (Sicily) during the 2001 and 2002-2003 eruptions. Journal of Volcanology and Geothermal Research 144:211-233

Neri M, Acocella V, Behncke B, Maiolino V, Ursino A, Velardita R (2005) Contrasting triggering mechanisms of the 2001 and 2002-2003 eruptions of Mount Etna (Italy). Journal of Volcanology and Geothermal Research 144:235-255

Pal R (2003) Rheological behavior of bubble-bearing magmas. Earth and Planetary Science Letters 207(1-4):165-179

Parfitt EA, Wilson L (1995) Explosive volcanic eruptions - IX. The transition between Hawaiian-style lava fountaining and Strombolian explosive activity. Geophysical Journal International 121:226-232

Parfitt EA (2004) A discussion of the mechanisms of explosive basaltic eruptions. Journal of Volcanology and Geothermal Research 134(1-2):77-107

Pasquare, G; Francalanci, L; Garduno, V H; Tibaldi, A (1993) Structure and geologic evolution of the Stromboli Volcano, Aeolian Islands, Italy. Acta Vulcanologica 3:79-89

Patrick M, Harris AJL, Ripepe M, Dehn J, Rothery DA, Calvari S (in press) Strombolian explosive styles and source conditions: Insights from thermal (FLIR) video. Bulletin of Volcanology

Phan-Thien N, Pham DC (1997) Differential multiphase models for polydispersed suspensions and particulate solids. Journal of non-Newtonian Fluid Mechanics 72:305-318

Pinkerton H, Stevenson RJ (1992) Methods of determining the rheological properties of magmas at sub-liquidus temperatures. Journal of Volcanology and Geothermal Research 53(1-4):47-66

Polacci M, Pioli L, Rosi M (2003) The Plinian phase of the Campanian Ignimbrite eruption (Phlegrean Fields, Italy): evidence from density measurements and textural characterization of pumice. Bulletin of Volcanology 65:418-432

Polacci M, Corsaro RA, Andronico D (2006) Coupled textural and compositional characterization of basaltic scoria: Insights into the transition from Strombolian to fire fountain activity at Mount Etna, Italy. Geology 34(3):201-204

Pyle DM (1989) The thickness, volume and grain-size of tephra fall deposits. Bulletin of Volcanology 51:1-15

Pyle DM (1998) Forecasting sizes and repose times of future extreme volcanic events. Geology 26: 367-370

Ripepe M, Rossi M, Saccorotti G (1993) Image-processing of explosive activity at Stromboli. Journal of Volcanology and Geothermal Research 54(3-4):335-351

Ripepe M, Gordeev E (1999) Gas bubble dynamics model for shallow volcanic tremor at Stromboli. Journal of Geophysical Research-Solid Earth 104:10639-10654

Ripepe M, Coltelli M, Privitera E, Gresta S, Moretti M, Piccinini D (2001a) Seismic and infrasonic evidences for an impulsive source of the shallow volcanic tremor at Mt. Etna, Italy. Geophysical Research Letters 28:1071-1074

Ripepe M, Ciliberto S, Della Schiava M (2001b) Time constraints for modeling source dynamics of volcanic explosions at Stromboli. Journal of Geophysical Research 106:8713–8727

Ripepe M, Harris AJL, Carniel R (2002) Thermal, seismic and infrasonic evidences of variable degassing rates at Stromboli volcano. Journal of Volcanology and Geothermal Research 118(3-4):285-297

Ripepe M, Marchetti E (2002) Array tracking of infrasonic sources at Stromboli volcano. Geophysical Research Letters 29(22) doi:10.1029/2002GL015452

Ripepe M, Marchetti E, Ulivieri G, Harris A, Dehn J, Burton M, Caltabiano T, Salerno G (2005a) Effusive to explosive transition during the 2003 eruption of Stromboli volcano. Geology 33(5):341-344

Ripepe M, Harris AJL, Marchetti E (2005b) Coupled thermal oscillations in explosive activity at different craters of Stromboli volcano. Geophysical Research Letters 32. doi: 10.1029/ 2005GL022711

Romano R, Sturiale C (1982) The historical eruptions of Mt. Etna. Memorie della Societe Geologica Italiana 23:75-97

Rosi M (1980) The island of Stromboli. Rendiconti della Società Italiana di Mineralogia e Petrologia 36:1-24

Rosi M, Bertagnini A, Landi P (2000) Onset of the persistent activity at Stromboli Volcano (Italy). Bulletin of Volcanology 62:294-300

Rosi M, Bertagnini A, Harris AJL, Pioli L, Pistolesi M, Ripepe M (2006) A case history of paroxysmal explosion at Stromboli: Timing and dynamics of the April 5, 2003 event. Earth and Planetary Science Letters 243:594-606

Rothery DA, Francis PW, Wood CA (1988) Volcano monitoring using short wavelength infrared data from satellites. Journal of Geophysical Research 93:7993-8008

Rothery DA, Coltelli M, Pirie D, Wooster MJ, Wright R (2001) Documenting surface magmatic activity at Mount Etna using ASTR remote sensing. Bulletin of Volcanology 63:387-397

Sable JE, Houghton BF, Wilson CJN, Carey, RJ (in press) Complex proximal sedimentation from plinian plumes: the example of Tarawera 1886. Bulletin of Volcanology

Sahagian DL, Proussevitch AA (1998) 3D particle size distributions from 2D observations - stereology for natural applications. Journal of Volcanology and Geothermal Research 84:173-196

Schiano P, Clocchiatti R, Ottolini L, Sbrana A (2004) The relationship between potassic, calc-alkaline and Na-alkaline magmatism in South Italy volcanoes: A melt inclusion approach. Earth and Planetary Science Letters 220(1-2):121-137

Seyfried R, Freundt A (2000) Experiments on conduit flow and eruption behavior of basaltic volcanic eruptions. Journal of Geophysical Research-Solid Earth 105:23727-23740

Shaw H (1972) Viscosities of magmatic silicate liquids: an empirical method of prediction. American Journal of Science 272:870-893

Sornette D, Knopoff L, Kagan YY, Vanneste C (1996) Rank-ordering statistics of extreme events; application to the distribution of large earthquakes. Journal of Geophysical Research 101:13883-13893

Sparks RSJ (1978) The dynamics of bubble formation and growth in magmas: a review and analysis. Journal of Volcanology and Geothermal Research 3:1-37

Spera FJ (2000) Physical Properties of Magma. In Sigurdsson (ed) Encyclopedia of Volcanoes:171-190

Stevenson DS, Blake S (1998) Modelling the dynamics and thermodynamics of volcanic degassing. Bulletin of Volcanology 60:307- 317

Swanson DA, Duffield, WA, Jackson DB, Peterson DW (1979) Chronological narrative of the 1969-71 Mauna Ulu eruption of Kilauea Volcano, Hawaii. USGS Professional Paper 1056, 55pp.

Taddeucci J, Pompilio M, Scarlato P (2004) Conduit processes during the July-August 2001 explosive activity of Mt. Etna (Italy): inferences from glass chemistry and crystal size distribution of ash particles. Journal of Volcanology & Geothermal Research 137:33-54

Thordarson T, Self S, Óskarsson N, Hulsebosch T (1996) Sulfur, chlorine, and fluorine degassing and atmospheric loading by the 1783–1784 AD Laki (Skaftár Fires) eruption in Iceland. Bulletin of Volcanology 58:205–225

Tibaldi A (2001) Multiple sector collapses at Stromboli volcano, Italy: how they work. Bulletin of Volcanology 63(2-3):112-125

Tibaldi A (2003) Influence of cone morphology on dykes, Stromboli, Italy. Journal of Volcanology and Geothermal Research 126(1-2):79-95

Tilling RI, Christiansen RL, Duffield WA, Endo ET, Holcomb RT, Koyanagi RY, Peterson DW, Unger JD (1987) The 1972-1974 Mauna Ulu eruption, Kilauea Volcano; an example of quasi-steady-state magma transfer Volcanism in Hawaii. USGS Professional Paper 1350:405-409

Tinti S, Pagnoni G, Zaniboni F, Bortolucci E (2003) Tsunami generation in Stromboli island and impact on the south-east Tyrrhenian coasts. Natural Hazards and Earth System Sciences 3: 299–309

Vergniolle S, Jaupart C (1986) Separated two-phase flow and basaltic eruptions. Journal of Geophysical Research 91:12842-12860

Wadge G, Walker GPL, Guest, JE (1975) The output of Etna volcano. Nature 255: 385-387

Wadge G (1981) The variation of magma discharge during basaltic eruptions. Journal of Volcanology and Geothermal Research 11:139-168

Walker GPL (1973) Explosive volcanic eruptions - a new classification scheme. Geologische Rundschau 62:431-446

Washington HS (1917) Persistence of vents at Stromboli and its bearing on volcanic mechanism. Bulletin of the Geological Society of America 28:249-278

Wentworth CK, MacDonald GA (1953) Structures and forms of basaltic rocks in Hawaii. USGS Bulletin 994:1-98

Wilson L (1980) Relationships between pressure, volatile content and ejecta velocity in three types of volcanic explosion. Journal of Volcanology and Geothermal Research 8:297-313

Wright R, Blake S, Harris, AJL, Rothery DA (2001) A simple explanation for the space-based calculation of lava eruption rates. Earth and Planetary Science Letters 192:223-233